IDENTIFICATION AND CHARACTERIZATION OF MICROFIBERS IN WASTEWATER DISCHARGING INTO LAKE ERIE

Blane Houck

A Thesis

Submitted to the Graduate College of Bowling Green
State University in partial fulfillment of
the requirements for the degree of

MASTER OF SCIENCE

May 2019

Committee:

John Farver, Advisor

Ganming Liu

Jeffrey Snyder

ABSTRACT

John Farver, Advisor

The presence of microplastic fibers (MPFs) among freshwater systems is an increasing concern in the context of global freshwater potability due to their persistence, potential toxicity, and ubiquity among the natural environment. These MPFs are described as being filamentous microplastic particles (MPPs) that are released into the natural environment through byproducts of wastewater treatment plants (WWTPs) or effluent discharged from combined sewer overflow (CSO) events. The primary purpose of this study is to develop a reproducible method of extracting, quantifying, and chemically characterizing MPFs among wastewater, CSO, and sludge cake samples. The influent, effluent, and sludge cake samples from three different WWTPs that discharge into Lake Erie were analyzed for the presence of MPFs. Additionally, CSO outfalls (located in Bowling Green and Cleveland, OH) were analyzed for the presence of MPFs during CSO events. Laboratory processing of a given sample involved density separation within a sediment-microplastic isolation unit (SMIU), organic matter digestion of the SMIU's supernatant, vacuum filtration of the digested solution, extraction of MPFs from the vacuum filter onto microscope slides and capturing images of MPFs on microscope slides using a polarized light microscope (PLM). MPFs among images were counted using an ImageJ macro designed to count asbestos fibers. An adjusted macro was used to identify MPPs among images. MPFs among all effluent samples were counted both manually and with ImageJ. Raman spectra of MPFs and standard plastic materials were obtained via Raman spectroscopy. Using the Spectral ID software, spectra of the analyzed MPFs were matched to spectra of the analyzed

standard plastic materials within a specified degree of certainty. Comparing ImageJ's counts to manual counts of MPFs among effluent samples revealed a linear relationship between the two groups (r-squared equals 0.6969). The comparison of MPFs in effluent samples to MPFs in influent samples showed a decrease of 85-94% with effluent samples yielding average MPFs values of 152-255 fibers/liter for the different WWTPs. Background amounts of MPFs were determined through processing deionized (DI) water. Through analysis, it was demonstrated that the atmosphere was the largest source of MPFs to the DI water samples. Analysis of effluent discharged from CSOs located in Bowling Green and Cleveland, OH revealed an average of 648 MPFs and 1401 MPPs contained within a given liter of CSO effluent, respectively. Raman analysis revealed that greater than 99-percent of the identified MPFs were composed of polyester. These results suggest that clothes washing activities are in fact contributing MPFs to WWTPs and that MPPs were released from the analyzed CSOs during discharge events. However, a given WWTP may be able to reduce its MPF emissions by adopting treatment regimens similar to those implemented by the BG WWTP. Moreover, the presence of environmental background amounts of MPFs suggests that atmospheric concentrations of MPFs may be more significant than previously thought. Furthermore, the results and methods of this study may be used to establish reproducible methods of analyzing MPFs discharging from potential sources into Lake Erie.

ACKNOWLEDGMENTS

The authors wish to thank the Ohio Lake Erie Commission (LEPF 522-2017). We would also like to thank Douglas Clark (of the Bowling Green Wastewater Treatment Plant), Chris McGibbeny and Mark Stoffan (of the Bay View Wastewater Treatment Plant), and Mike Ulatowski (of the North East Ohio Regional Sewer District) for their continued technical support and assistance. Dr. Ganming Liu and Dr. Jeffrey Snyder are thanked for their contributions. Additionally, the Center for Photochemical Sciences at Bowling Green State University is thanked for allowing open use of their Raman spectrometer.

TABLE OF CONTENTS

LIST OF FIGURES

LIST OF TABLES

CHAPTER I. INTRODUCTION

1.1 Background

The usage of plastics as raw materials for the production of consumer products is relatively new (Derraik, 2002). Dating back to around 60-70 years ago, the plastics industry became established within the context of global trade (Chidambarampadmavathy et al., 2017). Plastics are chosen as production materials because they are lightweight, durable, and inexpensive (Joseph et al., 2016). Due to their durability, plastics may resist degradation once in the natural environment (Moore, 2008). Now, more than ever, plastic products are rapidly being produced, utilized, and discarded in such a fashion that plastic debris have begun to accumulate among notable marine and freshwater systems (Baldwin et al., 2016). More than 300 million tons of plastic products are produced annually, and about half of this amount is expected to be directly released into the natural environment (Mason et al., 2016; Zhan et al., 2015). This may be attributed to the fact that it is much cheaper for manufacturers to create new plastic products than reprocess and recycle old plastic materials (Cooper and Corcoran, 2010). The inevitable result being the accumulation of plastic debris among marine environments.

The term “plastic debris” is dynamic in that it carries a different meaning depending upon the recipient of the term. This is because “plastic debris” may be sub-categorized depending upon its source, size, or structural morphology. Macroplastics, for instance, refers to plastic debris that are greater than 5 millimeters in diameter (Laforsch et al., 2017). These plastics are usually distinguishable with the naked eye and can include an array of objects ranging from bottle caps to grocery store bags. On the other hand, microplastic particles (MPPs) refers to particulate plastic matter that is less than 5 millimeters in diameter (Tsang et al., 2017). MPPs may be further classified as being primary or secondary in nature depending upon their source of

origination. The principal source of primary MPPs within the natural environment is thought to be from the usage of personal hygiene products containing microbeads, such as soaps or exfoliates. These primary MPPs and macroplastic products may remain in the natural environment for extended periods of time where they may succumb to various degradation processes and fragmentation. Secondary MPPs are those that are produced from the mechanized breakdown of preexisting plastic materials (Van Wezel et al., 2016). Additionally, primary or secondary MPPs may be further categorized as being particulates, foams, or fibers depending upon their observed structural morphology (Rochman et al., 2015).

1.2 Thermoplastics

The term 'polymer' is often used to describe molecular compounds that consist of repeating, chain-like sequences of anatomical units. Because plastic molecules are primarily composed of carbon and hydrogen atoms, plastic polymers are known to consist of many hydrocarbon-based molecules bound together in a repeating sequence. Thermoplastics refers to a particular subset of plastic polymers that become malleable when heated to temperatures of up to 400 °C, and harden when cooled to lower temperatures (Saini and Shenoy, 1985). This process of heating and cool hardening can be continuously repeated. Thus, thermoplastic products are widely implemented in the manufacturing of textiles and other materials because they can be conformed to a number of shapes and sizes (Napper and Thompson, 2016).

1.3 Importance of Microplastic Fibers

The vast majority of plastic debris studies are primarily concerned with analyzing the spatial distribution of macroplastics and MPPs among marine sediments, whereas few plastic studies are concerned with the analysis of microplastic fibers (MPF) among marine environments. (Hidalgo-Ruz et al., 2012). Given their small diameter and cylindrical shape,

studying MPFs has proven to be extremely difficult because they can easily pass through meshed sieves (Pirc et al., 2016). Additionally, potential sources of MPFs are not yet fully understood which adds to the difficulty of selecting potential sample locations. Although, the principal source of environmental MPFs is considered to be effluent from wastewater treatment plants (WWTPs) and clothes washing activities (Andrady, 2017).

During a single machine wash, nylon or acrylic clothing materials can shed up to 700,000 MPFs (Napper and Thompson, 2016). These fibers typically range from 10-50 μm in diameter and are usually between 0.5-5 cm in length (Bagaev et al., 2017). Once washed, MPFs emitted from clothing products are directed to the nearest WWTP via domestic drainage conduits. Upon arrival to a WWTP, MPFs may be removed from municipal wastewater through various stages of filtration and settling before being discharged into local aquatic environments (Mason et al., 2016). Settling is arguably the most effective MPF removal method (Mason et al., 2016; Mintenig et al., 2017). Using this method, modern WWTPs can reportedly sequester up to 99% of received MPFs in sludge cake (Ziajahromi et al., 2016). Although, a 1% MPF emittance value is still significant given the large quantities of wastewater that most WWTPs process on any given day (Napper and Thompson, 2016; Shen et al., 2015). Using estimates of MPPs released from over 30,000 WWTP facilities, Mason et al. (2016) calculated that an average of 13 billion MPPs are released into US waterways per day via wastewater (Mason et al., 2016).

Once present in the aquatic environment, microplastics can become degraded through exposure to physical forces, such as wind and wave action, and insolation that is within the ultraviolet (UV) spectrum (Andrady, 2017). Persistent organic pollutants (POPs), such as polychlorinated biphenyls (PCBs) or polycyclic aromatic hydrocarbons (PAHs), are known to partition well to MPF surfaces (Devriese et al., 2017). If ingested by a mammalian host, POPs

can cause a number of side effects and adverse reactions such as the formation of cancer, immunosuppression, and central nervous system (CNS) disruptions (Carpenter, 2011). Moreover, MPFs are known to often include a variety of additive compounds within their chemical matrix that may be harmful to most organisms. This is especially true of MPFs originating from clothing materials, as most textile fabrics are associated with certain additive compounds (such as fire retardants) that enhance a particular trait of a given polymer (Kim et al., 2019). Many additives associated with polymers are known to be carcinogens and endocrine disrupters (Kumar, 2018). Such findings are of concern because environmental MPFs have regular interactions with biological entities.

Because of their small diameters and fibrous shape, MPFs bear a striking resemblance to the prey items of benthic macroinvertebrates and larval organisms (Collard, Gilbert, Eppe, Parmentier, & Das, 2015; Steer, Cole, Thompson, & Lindeque, 2017). If ingested, a given MPF may remain inert within an organism's gastrointestinal (GI) tract, or be translocated to other organs, depending upon its size (Wright and Kelly, 2017). Thus, an organism may experience physiological side effects (such as gut blockages, artificial satiation, multiorgan stress, and behavioral changes) upon ingestion of MPFs (Steer et al., 2017). Additionally, recent studies have shown that MPFs are capable of being transferred among marine food webs through trophic interactions (Pracheil et al., 2016; Rochman et al., 2015; Setälä, Fleming, & Lehtiniemi, 2013). As reported by Collard et al. (2015), planktivorous fish species sampled from European seas showed signs of MPF accumulation among GI tissues. It was speculated that the analyzed MPFs were first ingested by planktonic organisms, and those planktonic organisms containing MPFs within their GI tracts were subsequently ingested by the sampled fish species (Collard et al., 2015). Therefore, it is possible for human subjects to acquire MPFs through similar trophic

exchanges. Due to the fact that Lake Erie annually generates more than $8 billion in revenue from tourist activities, and provides more than 11 million people with a source of freshwater, potential contaminants that may degrade the quality of this natural resource should be minimized (Sekaluvu et al., 2017; Watson et al. 2016). Thus, it is the goal of this study that these findings may contribute to the limited knowledge base surrounding the impacts of MPFs discharging into Lake Erie.

1.4 General Wastewater Treatment Plant Model

A given WWTP receives wastewater from both domestic and stormwater inputs as influent. Specifically, wastewater is defined as water that has been anthropogenically altered to an unpotable state (Lutchmiah, Verliefde, Roest, Rietveld, & Cornelissen, 2014). A given WWTP is responsible for processing wastewater into water that is either potable or capable of being returned to the natural environment. Wastewater coming into a WWTP is defined as influent, and treated wastewater leaving a WWTP is defined as effluent. Before wastewater can be classified as being treated effluent, it must go through several treatment stages. These treatment stages can be defined as primary, secondary, or tertiary based upon the degree of treatment (Mason et al., 2016). Primary treatment of wastewater typically involves the removal of particulates from wastewater through the usage of fine-bar screens and settling tanks. Fine-bar screens consist of a mesh with small openings that preclude the passage of particles with a larger area than the area of the openings. Settling tanks (or clarifiers) use the force of gravity to remove dense particles from wastewater by allowing gravity to draw suspended particles down to the bottom of the settling tanks (Asadi, Verma, Yang, & Mejabi, 2017). These processes result in the formation of sludge cake on the surface of fine-bar screens and at the bottom of settling tanks. This sludge cake must be periodically removed and treated to prevent build up. Sludge cake

treatment is focused on the removal of water and microbes through digestion, pressing, incineration, and drying (Christensen, Keiding, Nielsen, & Jørgensen, 2015). Once treated, sludge cake may be returned to the natural environment through practical applications (such as being used as a fertilizer or soil amendment).

Secondary treatment of wastewater may involve aeration, disinfection, and further clarification (or settling). Aeration is accomplished by supplying aerobic microbes, oxygen, and flocculants to wastewater. Aerobic microbes act to degrade organic compounds within wastewater through the process of aerobic respiration. Once degraded, organic compounds are effectively removed from the system. Flocculants, on the other hand, are designed to chemically adhere to particles suspended within wastewater (Asadi et al., 2017). Once particles are attached to flocculants, they may be easily removed from wastewater. Disinfection of wastewater can be accomplished through the addition of chlorine to wastewater or exposing wastewater to UV radiation. Both chlorine and UV disinfection involve the breakdown of proteins and deoxyribonucleic acid (DNA) among microbial cells and viruses. Further treatment of wastewater, other than the previously described processes, is considered to be a tertiary treatment (Mason et al., 2016). Typically, a given WWTP will choose to operate by a treatment regime that is fitting for the needs of the area being serviced (Figure 1).

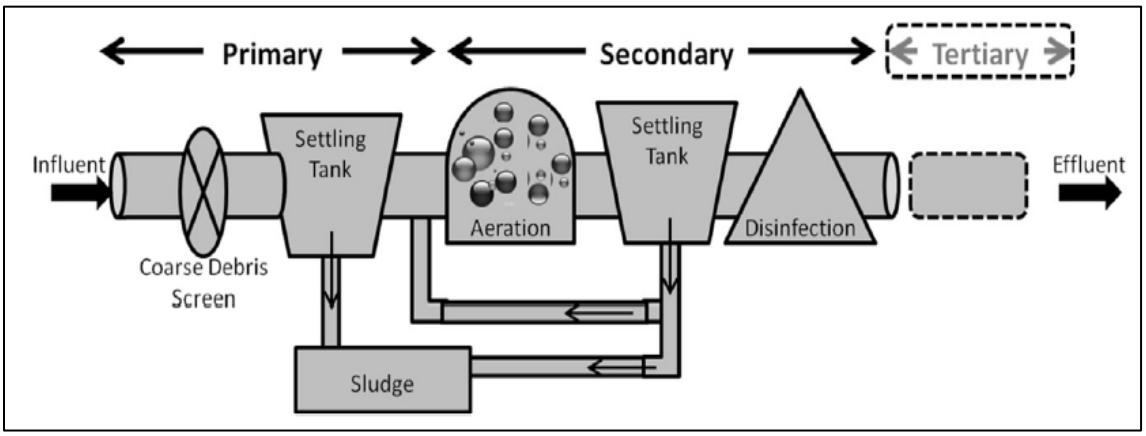

Figure 1. General WWTP Model. Showing a generalized treatment regime that is implemented by most wastewater treatment plants (Mason et al., 2016).

1.5 Research Objectives

The primary goal of this research was to develop a reproducible method of quantifying MPFs among influent, effluent, sludge cake, and combined sewer overflow samples. Secondarily, this research sought to determine differences in MPF concentrations between samples of influent and samples of effluent gathered from three different wastewater treatment plants of differing treatment capacities. Branching from this objective, a third goal was to determine if changes in MPF concentrations between samples of influent and samples of effluent differed when gathered under “high flow” and “normal flow” conditions. Additionally, this research focused on determining background amounts of MPFs. Also, a goal was to chemically characterize a subsection of MPFs gathered randomly from all sample types. Finally, the overarching objective of this study was to quantify total MPF outputs from the analyzed sources.

CHAPTER II. METHODS

2.1 General Approach

The methods employed in this study largely relied upon the methodological approach outlined by the National Oceanic and Atmospheric Administration's (NOAA) Marine Debris Program, which is primarily concerned with the analysis of microplastics among water samples (Masura et al., 2015). The methods outlined by this program were adapted to analyze microplastic fibers (MPFs) among samples collected from wastewater treatment plants (WWTPs) and combined sewer overflow (CSO) events. Laboratory processing of all sample types involved the use of a zinc chloride density separation fluid (1.5 g/mL), a sediment-microplastic isolation unit (SMIU), an organic matter digestion phase, and a vacuum filtration phase. Through the use of an ultrasonic, filter membranes associated with vacuum filtration were further processed to allow for the isolation of MPFs onto microscope slides. Images of MPFs were captured via a petrographic microscope equipped with a polarizing lens and a mounted camera. With appropriate plugins, the captured images were processed using ImageJ in order to quantify the number MPFs present among each sample type. In addition, MPFs associated with all effluent samples were manually counted. Manual counts of MPFs among effluent samples were cross-referenced with ImageJ's counts of MPFs to determine ImageJ's counting accuracy. Chemical characterization of MPFs was achieved through the use of Raman spectroscopy and the Spectral ID software.

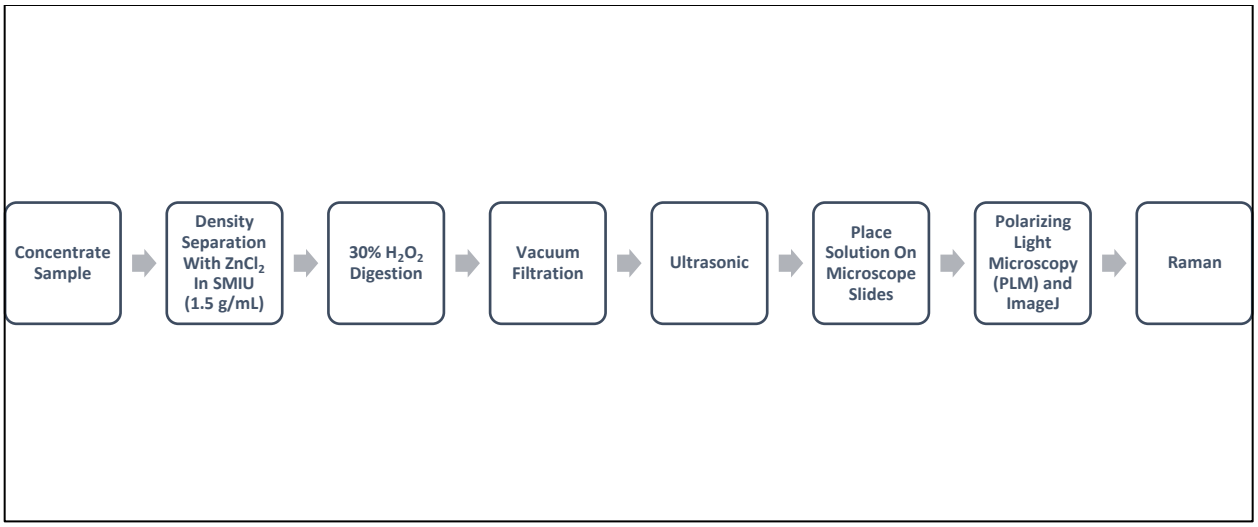

Figure 2. Methods Flow Chart. Shows a flow chart of processing for wastewater, CSO, or sludge cake samples.

2.2 Study Areas

Samples of wastewater were collected from three WWTPs that release effluent into Lake Erie. The Bowling Green (BG) WWTP (located in Bowling Green, OH) experienced an average daily flow rate of 24.96 million liters per day (MLD) during 2018. Specifically, the BG WWTP is considered to be a tertiary treatment plant where influent is first processed through a fine-bar screen and then processed through two clarifiers before being independently processed by six different aeration tanks. Subsequent to aeration, wastewater is then processed through two final clarifiers and is then processed through a cloth media filtration device. The cloth media filtration system acts to filter wastewater through a porous media (with pore spaces of 5-microns). As the wastewater flows through the cloth media filtration device, particulates with a diameter greater than 5-microns are precluded from passing through the media. Wastewater that is processed through the cloth media filtration device is then exited from the device as effluent. Finally, wastewater is subjected to ultraviolet (UV) disinfection before being discharged from the BG WWTP as effluent directly outside of the facility (Figure 3). Effluent from the BG WWTP drains

into a ditch, known as Poe Ditch, that runs parallel to East Poe Road (located in Bowling Green, OH). Poe Ditch is directly connected to the Portage River, which flows into Lake Erie.

The treatment schematics of the Bay View (BV) WWTP (located in Toledo, OH) and the Southern Cleveland (Southerly) WWTP (located in Cleveland, OH) are similar where the only difference between these two secondary treatment facilities is their average daily flow rates. The BV WWTP also implements grease skimming tanks to treat wastewater, whereas the Southern Cleveland WWTP does not. The BV WWTP experienced an average daily flow rate of 273 MLD and the Southern Cleveland WWTP experienced an average daily flow rate of 418.9 MLD in 2018. For both treatment plants, influent is first processed through a fine-bar screen before being processed through primary aeration tanks. Wastewater is then processed through an initial settling tank, a second aeration tank, and a final settling tank. Wastewater is then chlorinated before being discharged as effluent from the facilities. For the Bay View WWTP, wastewater is discharged directly into the Maumee River (Figure 3). For the Southern Cleveland WWTP, wastewater is discharged directly into the Cuyahoga River (Figure 4). Both rivers flow into Lake Erie.

A given WWTP can only process a certain volume of wastewater before it's systems risk potential failure. Given that WWTPs receive wastewater inputs from domestic and stormwater inputs, a WWTP will divert influent from its facility to a nearby combined sewer overflow during heavy rain events to prevent potential overload of the WWTP systems. Samples of wastewater were gathered from a CSO located in Bowling Green, OH and from a CSO located in Cleveland, OH during heavy rain events (Figures 3 and 4). Effluent from the BG CSO discharges into a ditch that is directly adjacent to, and runs parallel to, East Poe Road (located in Bowling Green, OH). The CSO located in Cleveland, OH (referred to as the Forest City CSO or CSO

Outfall #201) is located within the property boundaries of the Forest City Yacht Club, and the effluent of this CSO discharges directly into Lake Erie.

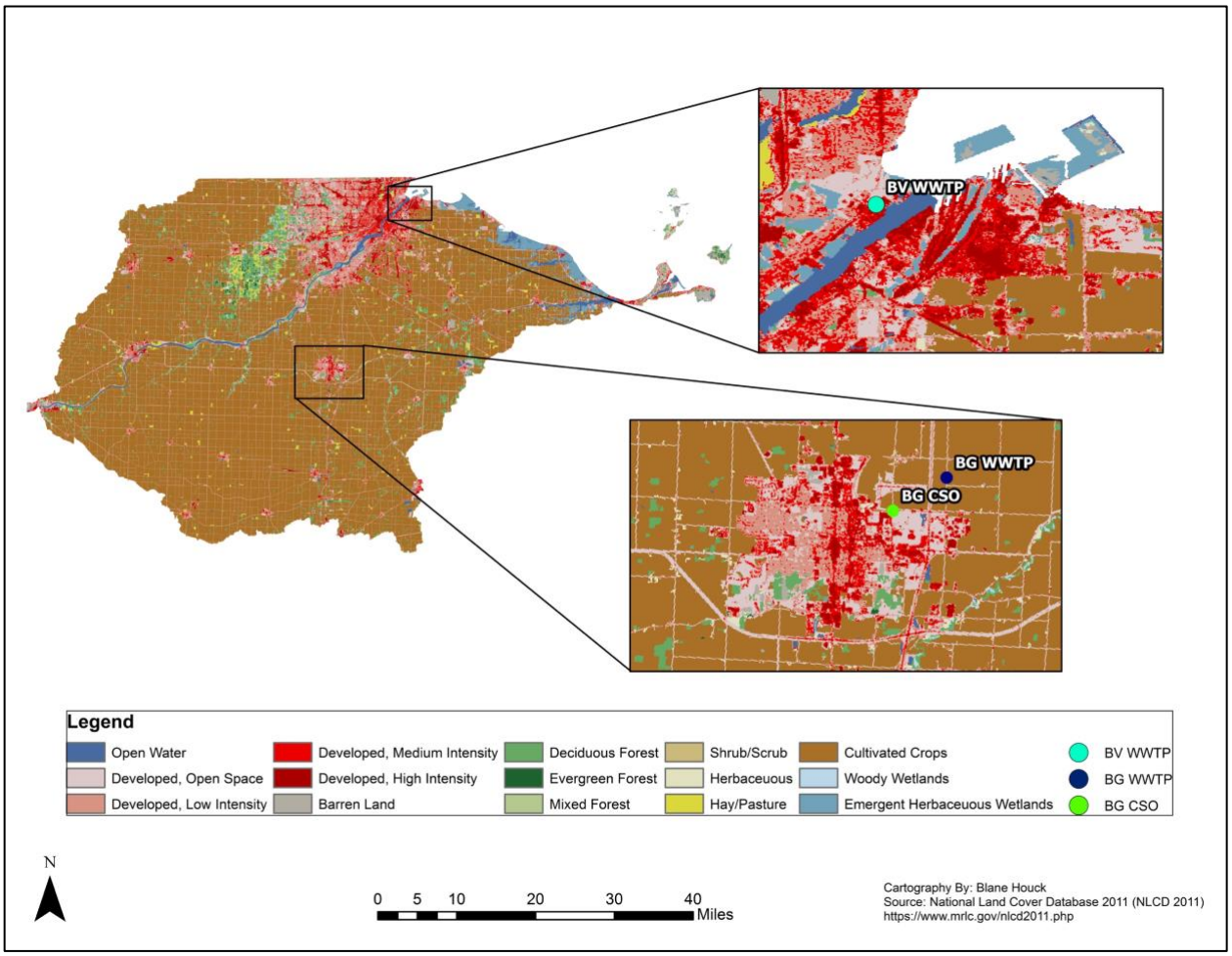

Figure 3. Bowling Green and Bay View Study Areas. Showing the location of the Bowling Green (BG) wastewater treatment plant (WWTP), the BG combined sewer overflow (CSO), and the Bay View (BV) WWTP in relation to surrounding land cover (NLCD 2011). The watershed is delineated based upon the boundaries of the Lower Maumee watershed and the Cedar-Portage watershed. Effluent from the BG WWTP is discharged into a ditch that runs parallel to East Poe Road, which is the first road directly north of the WWTP. Effluent from the BV WWTP is discharged into the Maumee River, which is depicted as "open water" and is directly adjacent to the BV WWTP.

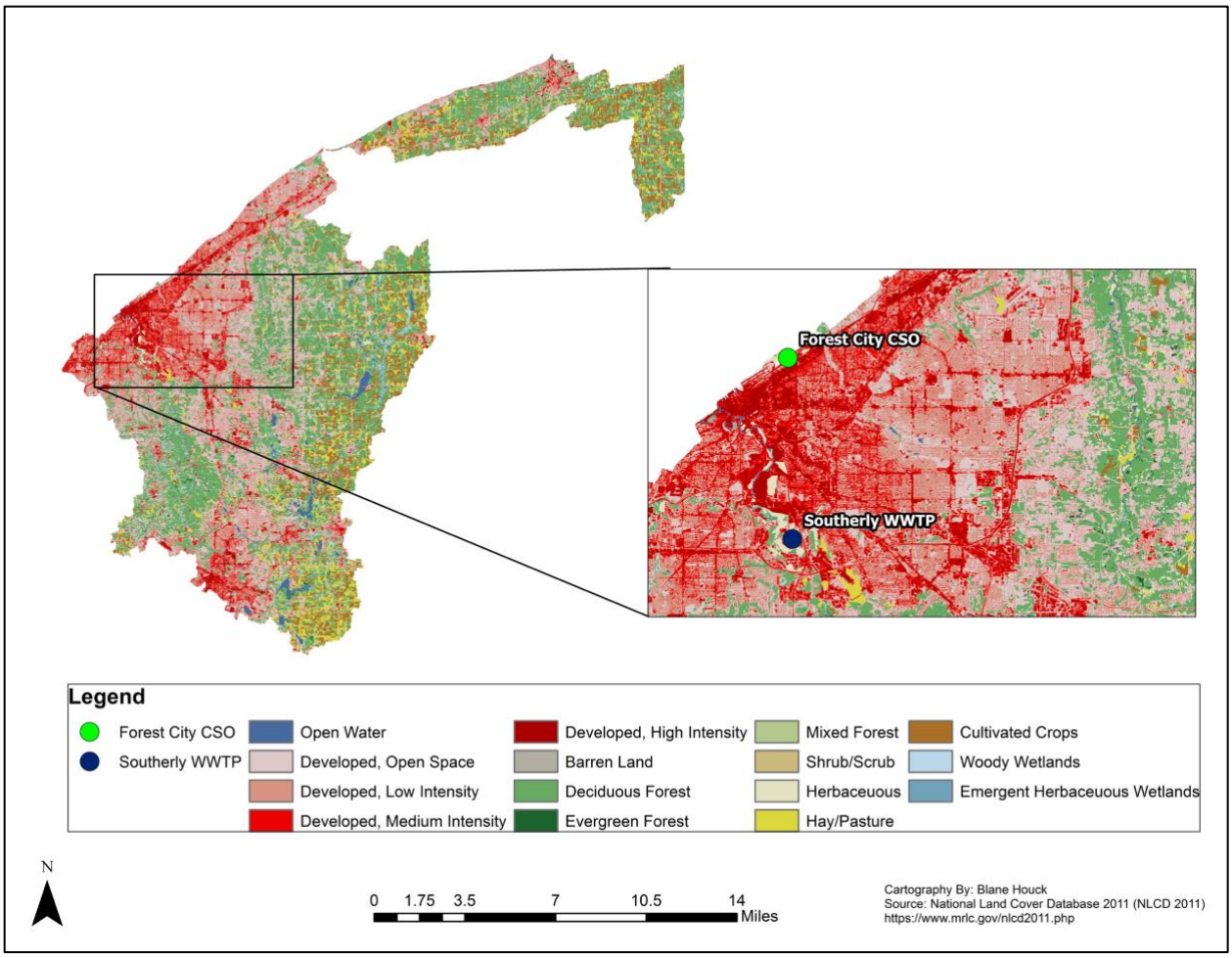

Figure 4. Southerly Study Area. Showing the location of Southern Cleveland (Southerly) wastewater treatment plant (WWTP) in relation to surrounding land cover (NLCD 2011). The watershed is delineated based upon the boundaries of the Cuyahoga River watershed and the Lake Erie watershed. Effluent from the Southerly WWTP is discharged into the Cuyahoga River, which is depicted as winding "open water" body directly adjacent to the Southerly WWTP.

2.3 Field Methods

WWTP operators must analyze influent, effluent, and sludge cake for the presence of various biological and contaminant hazards at least once per day. Usually, operators collect composite samples of influent, effluent, and sludge cake in excess. Thus, left-over composite samples were obtained in cooperation with the sampling regimes of WWTP operators. Composite samples of both influent and effluent were stored by WWTP operators in 50 to100-

gallon tanks. These tanks were shaken for one minute to homogenize the wastewater. Once homogenized, composite samples of both influent and effluent were then separately transferred to 1-liter high-density Polyethylene (HDPE) bottles. During a sample collection, between 1-3 liters of both influent and effluent were collected at a time. Composite samples of sludge cake were stored by WWTP operators in sample bags. During a sample collection, between 10-20 grams of composite sludge cake was transferred from the sample bags into HDPE jars. All samples of influent, effluent, and sludge cake were then immediately placed in a container (such as a cooler) for transport to the laboratory. Upon arrival to the laboratory, samples were refrigerated until further processing.

Water samples were collected from the surface and the base (or depth) of CSO outflows. Grab samples from surface waters of CSO outflows were gathered using a long-arm sample dipper and transferred to 1-liter HDPE bottles (Figure D3 in Appendix D). During a sample collection, between 1-2 liters of surfaces samples were collected at a time. Grab samples from the bottom-most portion of CSO outflows were gathered using a 2-liter horizontal water sampler (Figure D2 in Appendix D). The 2-liter horizontal water sampler was set in the open position and was lowered to the bottom section of CSO outflows using an attached rope. Once the 2-liter horizontal water sampler was submerged at the bottommost section of a CSO outflow, the water sampler was closed at depth (using a traveling weight to activate a spring mechanism) and was brought back to the surface using an attached rope. Water samples contained within the water sampler and HDPE bottles were stored in a container (such as a cooler) for transport back to the laboratory. Upon arrival to the laboratory, the 2-liter horizontal water sampler was opened, and its contents were transferred into two separate 1-liter HDPE containers. All of the samples were then refrigerated until further processing.

2.4 Cleaning Process

The process for cleaning lab equipment was largely adapted from the cleaning process outlined by the National Oceanic and Atmospheric Administration's (NOAA) Marine Debris Program where dish soap and distilled water was used to clean and rinse all lab equipment (Masura et al., 2015). For this project, 10 to 20- milliliter of dish soap was first applied to the inner and outer surfaces of all lab equipment. The applied dish soap was then thoroughly rinsed off with running tap water. Following, all lab equipment and was thoroughly rinsed off with ethyl alcohol, and the ethyl alcohol was rinsed off with deionized (DI) water using an LDPE squirt bottle. All lab equipment was left to dry in the open air upon being rinsed with DI water. Prior to 7/26/18, all lab equipment was left to dry on paper towels. Subsequent to 7/26/18, all lab equipment was left to dry on a metal drying rack. All lab equipment was cleaned using this process directly after being used.

2.5 Construction of the Sediment-microplastic Isolation Unit

Similar to Coppock et al. (2017), a sediment-microplastic isolation unit (SMIU) was constructed to facilitate density separation of wastewater, CSO and, SC samples in a localized manner (Figure D1 in Appendix D). Clear polyvinyl chloride (PVC) tubing, with a diameter of 2.5-inches, was cut into 6-inch (length) sections. Within a fume hood, the sections of PVC tubing were then secured to the bottom and top openings (2.5-inches in diameter) of a ball valve using PVC primer and PVC cement. A 12-inch by 12-inch PVC plate was then gathered. PVC primer and PVC cement were then used to secure an exposed section of PVC tubing, that is attached to the ball valve, to the middle of the PVC plate. Following this, the constructed apparatus remained undisturbed for 24 hours (Coppock, Cole, Lindeque, Queirós, & Galloway, 2017).

2.6 Density Separation

Every polymer has a specific density, and hence, a given polymer will float if it is put into a solution that has a higher density than its own. Conversely, a given polymer will sink if it is put into a solution that has a lower density than its own. Using this simple model, a fluid with a higher density than most MPFs was prepared to allow separation between MPFs and unwanted materials (such as detritus and heavy organic compounds). Most microplastic studies conducted within the U.S. are concerned with the occurrence of MPPs among beached sediments (Hidalgo-Ruz et al., 2012). MPPs within this type of environment typically exhibit density values ranging from 0.9-1.1 g/mL (Figure 5). Thus, many studies have opted to use a sodium chloride (NaCl) solution as an inexpensive and non-toxic density separator with a maximum achievable density of around 1.2 g/mL. However, most MPFs associated with clothing fabrics have densities of around 1.4 g/mL, which exceeds the maximum density of NaCl in water (Napper and Thompson, 2016). Thus, a different solute that allows for a greater maximum achievable density in water must be used to prepare a solution with a density that is greater than the average density of most MPFs. Some studies have opted to use sodium iodide (NaI) as a means of density separation because it has a maximum density of 1.8 g/mL in water. However, the continual use of this compound has proven to be uneconomical without accounting for the reuse and recycling of used NaI (Kedzierski, Le Tilly, César, Sire, & Bruzaud, 2017). Thus, zinc chloride ($ZnCl_2$) was used as a density separator in this study because it allows for a maximum density of 1.7 g/mL in water, and it is a much cheaper alternative to NaI.

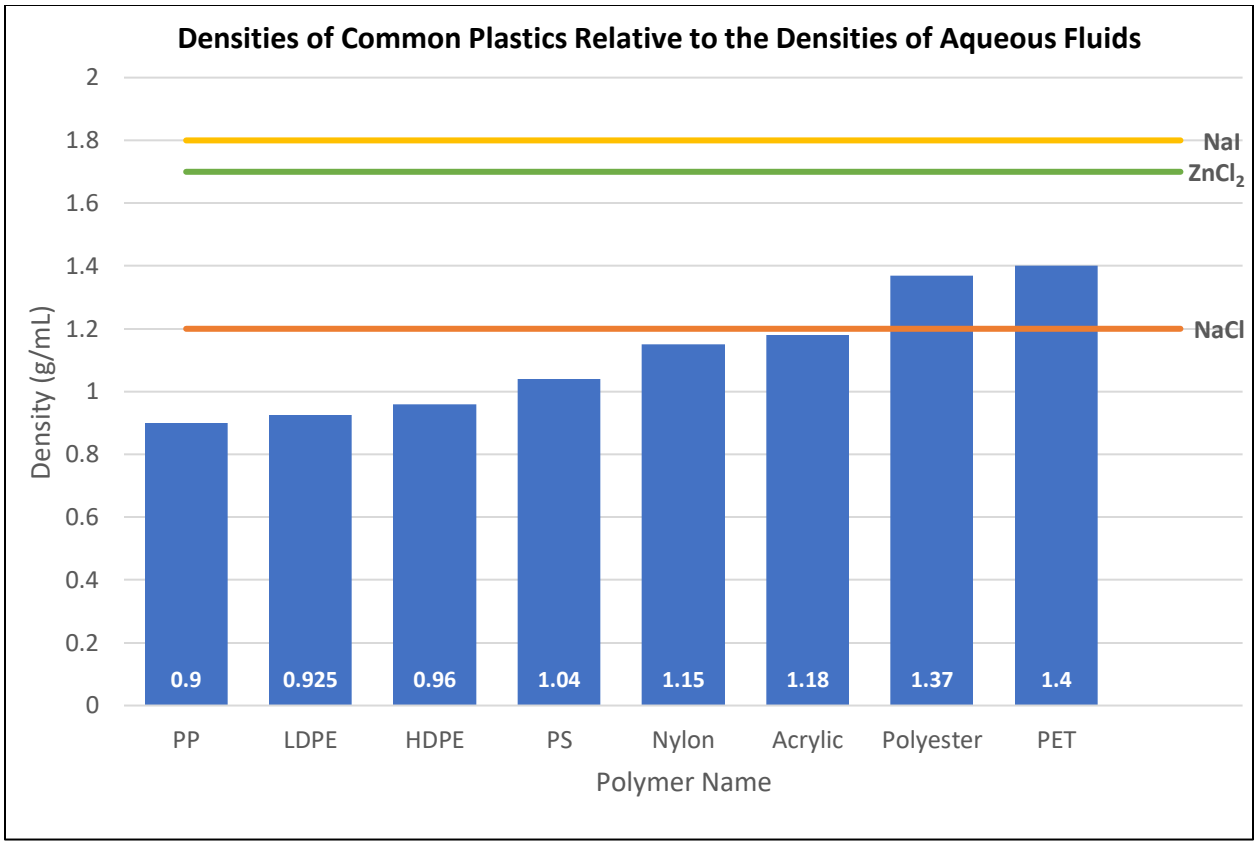

Figure 5. Density of Plastics and Solutes. Shows the densities of common plastics relative to the maximum densities of different solutes. The identified polymers are polypropylene (PP), low-density polyethylene (LDPE), high-density polyethylene (HDPE), polystyrene (PS), nylon, acrylic, polyester, and polyethylene-terephthalate (or polyester; PET).

2.7 Sample Preparation

Given that all wastewater and CSO samples were stored in 1-liter increments, 1-liter of a given wastewater or CSO sample was processed at a time. The first step to sample processing was the concentration of samples. A given wastewater or CSO sample was first transferred from its respective sample container into a 1000-milliliter glass beaker. The sample container was then rinsed with DI water, and the container's contents were added to the beaker. The glass beaker containing the wastewater or CSO sample was then placed onto a hot plate, and the hot plate was set to 200-degrees Celsius. This caused the sample to reach its boiling point where evaporation of the wastewater or CSO sample could occur. Once the sample had achieved a volume of 450-

milliliters, the beaker was removed from the hotplate and was allowed to cool at room temperature for 10-30 minutes. A magnetic stir bar was then dropped into the beaker, and the beaker was placed onto a magnetic stirrer set to 100-RPM. At a separate station, a 1000-milliliter wide mouth HDPE jar was weighed using a 200-gram scale. The weight of the jar was then zeroed to the scale. Increments of zinc chloride were then poured into the jar, and the weight of the zinc chloride was noted. Because the limit of the scale was 200-grams, only 50-100 grams of zinc chloride was measured at any given time. The jar containing the zinc chloride was then brought over to the wastewater or CSO sample, and the zinc chloride was added to the sample. This process was repeated until the wastewater or CSO sample contained a total of 675-grams of zinc chloride. Given that the initial volume of the wastewater or CSO sample was measured to be 450-milliliters, the addition of 675-grams of zinc chloride to the wastewater or CSO sample allowed for the solution to achieve a density of 1.5 grams per milliliter with a total volume of 700-milliliters. This solution, and its associated magnetic stir bar, was then added to the SMIU with the ball valve in the open position. The beaker was then rinsed with DI water, and the contents of the beaker were then added to the SMIU. The top opening of the SMIU was then covered with aluminum foil. The SMIU was then placed onto a magnetic stirrer set to 600-RPM. After 10-minutes, the SMIU was removed from the magnetic stirrer, and the solution within the SMIU was allowed to settle for 24-hours.

Upon settling, the ball valve was closed. This effectively separated the top section of the sample from the bottom section of the sample. The top section of the sample, or supernatant, was then placed into a 1000-milliliter beaker. DI water was used to rinse the top section of the SMIU. The DI water used to rinse the top section of the SMIU was added to the 1000-milliliter glass beaker containing the supernatant. Depending upon the fouling of the supernatant, 100 to 500-

milliliters of hydrogen peroxide (30% H_2O_2; Fisher Scientific) was added to the supernatant solution. The beaker containing the supernatant and H_2O_2 was then covered with aluminum foil, and the solution was allowed to react for 24-hours.

A vacuum filter flask was equipped with a borosilicate glass funnel and base where a 47-millimeter quartz filter paper (with pore spaces of 1.6 μm) was inserted between the funnel and base (Laforsch et al., 2017). The funnel and base were held together with an anodized aluminum spring clamp. Vacuum tubing, attached to a vacuum pump, was attached to the vacuum filter flask. The supernatant and the H_2O_2 solution were added to the vacuum filter funnel, and the vacuum pump was turned on. Upon filtration of the solution, the sides of the vacuum filter funnel were rinsed with DI water. Upon rinsing, the vacuum pump was turned off, and the vacuum filtration assembly was disassembled. Using a pair of tweezers, the quartz filter paper was transferred to a 100-milliliter glass beaker. Between 10 to 20-milliliters of ethyl alcohol (99 % C_2H_6O; Fisher Scientific) was added to the beaker. The beaker was then covered with aluminum foil, and the ethyl alcohol was allowed to react with the filter paper for 24 hours.

After 24-hours, the 100-milliliter beaker (containing the quartz filter and ethyl alcohol) was placed into an ultrasonic bath (Branson) for ten minutes. After ten minutes, the beaker was removed from the ultrasonic bath. Using tweezers, the filter paper was carefully removed from the solution. DI water was used as needed to transfer remaining particulates from the filter paper to the solution within the 100-milliliter beaker. The contents of the beaker were then transferred onto microscope slides within a fume hood. For samples processed prior to 7/26/18, microscope slides and dishes were placed atop sheets of paper towels with the fume hood door left open at all times. For samples processed subsequent to 7/26/18, microscope slides were placed atop non-stick pans, and cleaned dishes were left to dry on a metal drying rack. Additionally, the fume

hood door was kept in the closed position at all times except for when samples were transferred onto microscope slides within the fume hood. Sludge cake samples were processed in the same way as wastewater and CSO samples. However, solutions of zinc chloride (with densities of 1.5 grams per milliliter) were used to density separate 1-gram aliquots sludge cake housed within SMIUs.

A sub-experiment was conducted with a third aliquot of the sludge cake collected from the Southerly WWTP on 7/26/18 where the sample was allowed to react with 300 to 350-milliliters of H_2O_2 while stirred at 200-RPM for 12-hours subsequent to the density separation step and prior to the vacuum filtration step (Figure 15). This resulted in a semi-clear solution. However, further inspection of images related to this sample processing revealed similar amounts of organic contents to samples processed using the regular sludge cake protocol. Thus, this was the only sample of sludge cake that was processed in this way.

2.8 Blank Sample Processing

DI water samples served as sample blanks where DI water was processed in the same fashion as wastewater and CSO samples. This was done to determine possible background contamination of MPFs associated with the utilized sample media or the environment. DI water was gathered from a tap, and the processing of DI water samples occurred in the exact same manner as the processing of wastewater and CSO samples (as outlined above). Prior to 7/26/18, two DI water blanks were processed to assess any background amounts of MPFs. MPFs identified among these two DI water samples were counted via the MPF ImageJ macro and manual counts. Manual counts and ImageJ counts of MPFs among these two DI water samples were averaged. If MPFs were identified among a given sample (processed prior to 7/26/18) via ImageJ counts, the average ImageJ counts of MPFs among the two DI water samples were used

as a basis for background contamination for the given sample. If MPFs were identified among a given sample (processed prior 7/26/18) via manual counts, the average manual counts of MPFs among the two DI water samples were used as a basis for background contamination among the given sample.

Subsequent to 7/26/18, a given DI water sample was processed along with each sample batch where a sample batch was defined as a collection of samples. MPFs identified among DI water samples ran subsequent to 7/26/18 were counted via the MPF ImageJ macro and manual counts. If MPFs were identified among a given sample (processed subsequent to 7/26/18) via ImageJ counts, ImageJ counts of MPFs among the DI water sample that was prepared along with the given sample was used as a basis for background contamination of MPFs. If MPFs were identified among a given sample (processed subsequent to 7/26/18) via manual counts, manual counts of MPFs among the DI water sample that was prepared along with the given sample was used as a basis for background contamination of MPFs.

The proposed sources of MPFs associated with background contamination were the utilized DI water, quartz filter papers, HDPE sample containers, and the atmosphere. To assess any amounts of MPFs among the DI water, 2-liters of DI water were gathered from a tap and placed directly into a 2000-milliliter beaker. Within a fume hood, the beaker containing the DI water was placed onto a hot plate set to 200-degrees Celsius. The DI water within the beaker was then allowed to evaporate until the DI water reached a total volume of around 50-milliliter. The DI water was then transferred onto clean microscope slides. To assess any amounts of MPFs associated with the quartz filter, a 100-milliliter beaker was filled with 20-milliliters of ethyl alcohol. Following, a quartz filter was placed into the beaker. The filter was allowed to remain submerged within the ethyl alcohol for 24-hours. Following, the 100-milliliter beaker containing

the ethyl alcohol and the filter paper was placed into an ultrasonic, and the timer was set to 10-minutes. After 10-minutes, the ethyl alcohol was transferred onto clean microscope slides within a fume hood. DI water, within a LDPE squirt bottle, was used to transfer any remaining particulates from the filter paper to the microscope slides. To assess any amounts of MPFs among the HDPE sample bottles, two 1-liter HDPE sample bottles were each filled with DI water from a tap. The sample bottles containing the DI water were then shaken for 10-minutes. Within a fume hood, the beaker containing the DI water originating from the HDPE sample bottles was placed onto a hot plate set to 200-degrees Celsius. The DI water within the beaker was then allowed to evaporate until the DI water reached a total volume of around 50-milliliters. The DI water was then transferred onto clean microscope slides. Samples of the proposed sources of background contamination were processed prior to 7/26/18. Thus, microscope slides were stored in an open fume hood where paper towels were used as a drying surface for microscope slides and dishes.

2.9 Image Processing and Manual Counts of MPFs

Images of MPFs on microscope slides were captured using a polarizing light microscope (PLM) at a magnification of 50x. This microscope was equipped with a cross-polar lens and a mounted camera. Pictures were captured anytime a particle exhibiting birefringence came into view. For images related to the 6/12/18 sample collection, however, images of the entire microscope slides were captured. Identification of MPFs among images captured from wastewater, CSO, and SC samples was achieved using an ImageJ macro organically developed for counting asbestos fibers (Cho, Yoon, Han, & Kim, 2011). This macro, termed the MPF ImageJ macro, first utilized a built-in function within ImageJ to “invert” the images. Next, the built-in “Subtract Background” function was used with a “rolling ball radius” of 50-pixels. For

further processing, the images were then converted into 8-bit images. Using the "Auto-Local Threshold" plugin, the threshold of each pixel among each image was tabulated within a 10-pixel radius based upon the characteristics of surrounding pixels. Next, the "Dilate" plugin was used to widen pixels. Finally, ImageJ's built-in "Analyze Particles" functionality was used to analyze particles with a size ranging from 50 to 5000-pixels and a circularity ranging from 0.00 to 0.33 (Cho et al., 2011). For datasets where the majority of MPPs among images exhibited a particulate morphology, an adjusted macro was used where the maximum entropy option for "Auto-Local Threshold" was chosen and circularity was adjusted to range from 0.00 to 0.28. In addition, MPFs among all effluent samples were manually counted. Any particulate that displayed birefringence, and was of a fibrous morphology, was counted manually among each image of the effluent samples.

2.10 Implementation of Raman Spectroscopy and Spectral ID

The chemical composition of a material is comparable to a fingerprint that can be cross-referenced and matched to a given array of materials among a database that exhibit similar chemical traits. Fourier-transform Infrared spectroscopy (FTIR) and Raman spectroscopy are both methods that rely upon transferring the vibrational frequencies among chemical bonds of a given material into spectral data (Osayemwenre et al., 2018). However, FTIR requires a much greater surface area of a given material to obtain a spectral signature than that of Raman spectroscopy. In fact, Raman spectroscopy can obtain a spectral signature over a surface area of just a few microns. Given that MPFs are measured to be microns in diameter, Raman spectroscopy is a better choice for chemically characterizing MPFs than FTIR. Spectral data of a given material, obtained using Raman spectroscopy, results in a curve that can be matched to the

spectral curve of a known compound. Thus, allowing for the identification of a given material within a certain degree of likelihood.

MPFs were chosen for Raman analysis based upon their birefringent colors where birefringence is defined as a material's ability to refract (or propagate) light when subjected to a polarizing lens (Shchepanskyi et al., 2017). MPFs of representative color types (white, blue, red, and yellow) were isolated onto microscope slides. The MPFs were analyzed using a Renshaw inVia Reflex Raman spectrometer equipped with a Leica microscope housed in the Photochemical Sciences Center at BGSU. The exciting source was a 785 nm diode laser operating at around 50-megawatts power. Calibration was done using a static spectral acquisition on a high purity silicon standard. The analysis was done in confocal mode, yielding a high spatial resolution of < 3μm. The laser was guided to the desired MPFs using an attached USB camera at an objective of 50x. Spectra were collected over the range of 100 cm^{-1} to 4000 cm^{-1} with an exposure time of 60 seconds. In an attempt to improve the signal to noise ratio, the number of accumulations was set to four. All spectral data were normalized using the "smooth" and "subtract baseline" plug-ins included in Wire 3.2's software.

Many spectral libraries commercially available do not include Raman data for polymers commonly associated with MPFs. Thus, the spectra of the unknown MPFs were matched to reference spectra using an in-home spectral library and the "Spectral ID" software (Collard et al., 2015). The in-home spectral library included High-Density Polyethylene (HDPE), Polypropylene (PP), Nylon, Polytetrafluoroethylene (PTFE), Acrylic, Polyester, Low-Density Polyethylene (LDPE), Polyvinyl Chloride (PVC), Polystyrene (PS), and Cellulose. Raman spectra of reference standards were obtained from one-eighth inch diameter plastic pellets with each individual pellet being comprised of either HDPE, PP, Nylon, PTFE, or Acrylic (U.S. Plastics). Additional Raman

standards were prepared from a polyester film (U.S. Plastics), a LDPE film (U.S. Plastics), PVC piping (U.S. Plastics), polystyrene microparticles (Sigma-Aldrich), and a cellulose microcrystalline powder (Arcos Organics). The PVC standard was prepared by cutting a leftover section of the PVC piping, used to construct the SMIU, with a 0.5-inch diameter hole saw. A Raman spectra of a quartz filter paper (Whatman) was also gathered.

Raman spectra of the reference standards were acquired over the same conditions as the unknown MPFs. These spectra were grouped into a custom library in Spectral ID. With the custom, in-home library selected as the primary reference source in the library selector, Spectral ID was able to determine the degree of best fit between the Raman spectra of unknown MPFs and the Raman spectra of reference standards using the Euclidian Distance algorithm. The best possible match determinable from this formula would yield a distance value of zero. The worst possible match determinable from this formula would yield a distance value of 1.41421. Spectral ID categorizes the Euclidian distance differences between the spectra contained within the library and the spectra of unknown MPFs as "quality" values. Given the limits of the Euclidian distance algorithm, obtained quality values were converted into percentages of best fit. Spectral searches with the lowest "quality" values and the highest percentages of best fit were chosen as the best potential matches.

CHAPTER III. RESULTS

3.1 Introduction to Results

MPFs among all processed samples were counted via the MPF ImageJ macro unless otherwise stated. All samples experienced some degrees of MPF bundling (where several MPFs were observed to be tangled together in a ball; Figure 7), MPF twisting (where MPFs were contorted at one or more sections; Figure 7), and non-linear (or bent) MPFs (Figure 8). These three variables are likely to interfere with ImageJ's MPF counting capabilities. In some cases, however, the program was unable to count linear MPFs under pristine conditions (Figure 6). Heavy concentrations of organic matter were known to obscure MPFs, causing some MPFs to be uncounted, or partially counted, by the MPF ImageJ macro (Figure 9). For these described reasons, both manual and ImageJ counts of MPFs were obtained for effluent samples. Figures 6-9 show exaggerated examples of issues with ImageJ. Background MPFs are described as being MPFs that are not native to a given sample. Background MPFs were identified by processing DI water samples in the same way as wastewater or CSO samples (as outlined above). MPFs identified among DI water samples served as a proxy for background contamination of MPFs. Possible sources of background contamination were investigated. Using Raman spectroscopy, and the Spectral ID software, the chemical composition of MPFs were equated to the chemical composition of standard plastic materials within a calculated degree of likelihood.

Figure 6. Linear Fiber Example. Shows an image of a MPF obtained from the first aliquot sample of effluent collected from the BG WWTP on 9/25/18 under cross-polarized light (left) and its associated output image obtained via the MPF ImageJ macro (right). No MPFs were identified by the ImageJ MPF macro.

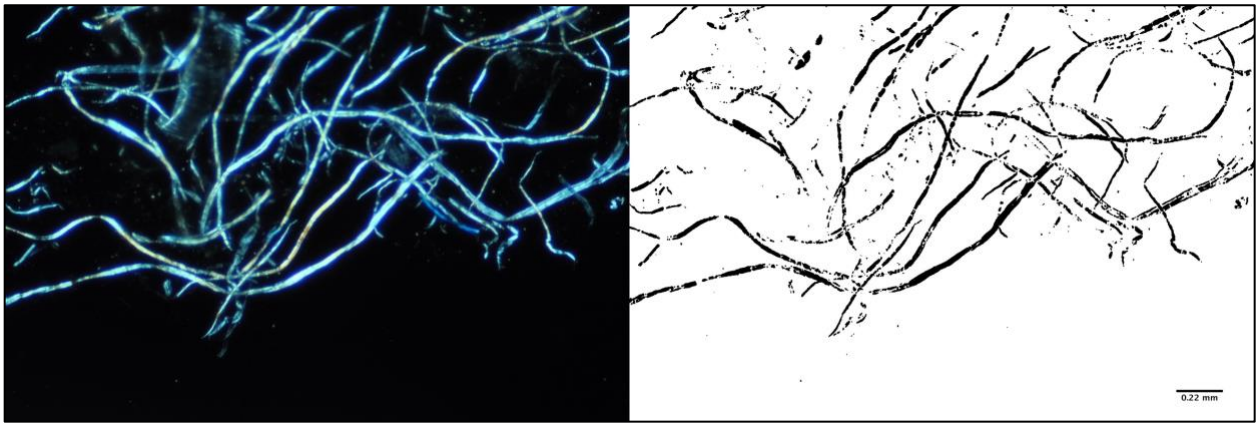

Figure 7. Fiber Bundle Example. Shows an image of a bundle of MPFs obtained from influent collected from the BV WWTP on 4/30/18 under cross-polarized light (left) and its associated output image obtained via the MPF ImageJ macro (right). No MPFs were identified by the ImageJ MPF macro.

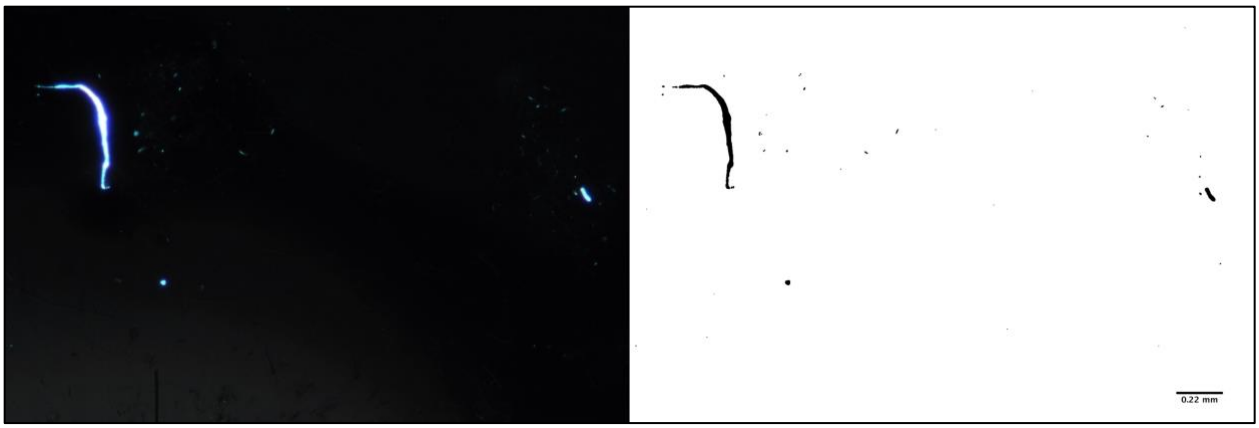

Figure 8. Curved Fiber Example. Shows an image of a bent MPF and a linear MPF obtained from influent collected from the BV WWTP on 4/30/18 under cross-polarized light (left) and its associated output image obtained via the MPF ImageJ macro (right). No MPFs were identified by the ImageJ MPF macro.

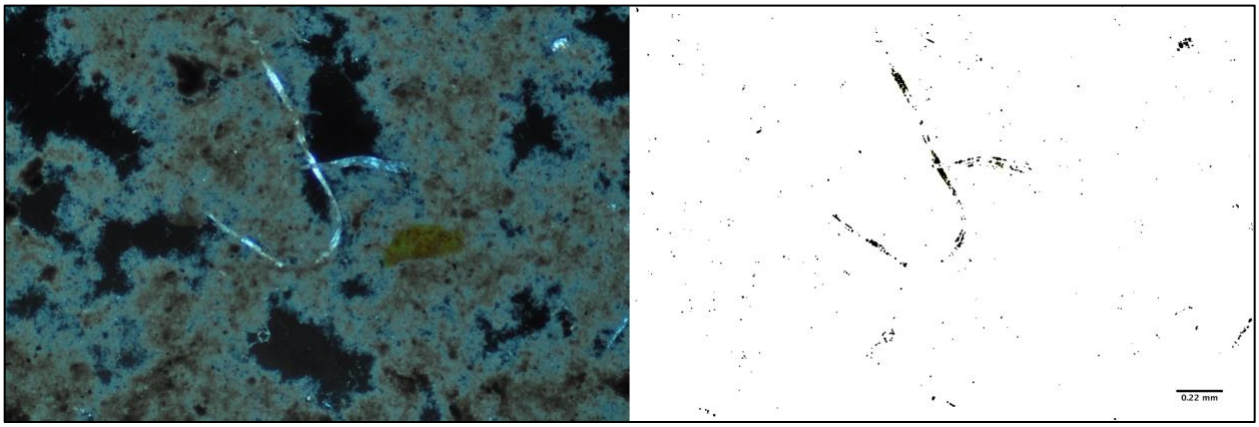

Figure 9. Fibers and Organics. Shows an image of MPFs obscured by organic matter obtained from effluent collected from the BG WWTP on 9/25/18 under cross-polarized light (left) and its associated output image obtained via the MPF ImageJ macro (right). Four MPFs, highlighted in yellow, were "identified" by the ImageJ MPF macro. The four "identified MPFs" represent sections of the same MPF.

3.2 Bivariant Analysis of Manual and ImageJ MPF Counts

An error analysis of ImageJ's capability of accurately counting MPFs was conducted by comparing ImageJ's MPF counts among effluent samples to manual counts of MPFs for the same effluent samples. Comparing manual counts of MPFs for effluent samples to ImageJ's

counts of MPFs for effluent samples showed a linear regression with an r-squared value of 0.6969 (Figure 10). As displayed within Figure 10, a one-to-one linear regression shows the trendline for a scenario where there was total agreement between manual and ImageJ counts. As observed in Figure 10, the trendline of manual MPF counts versus ImageJ MPF counts among effluent samples does not stray far from an idealized one-to-one trendline. Given the time constraints and overall feasibility associated with manually counting MPFs, this analysis reveals ImageJ to be a rapid and reliable method of quantifying MPFs.

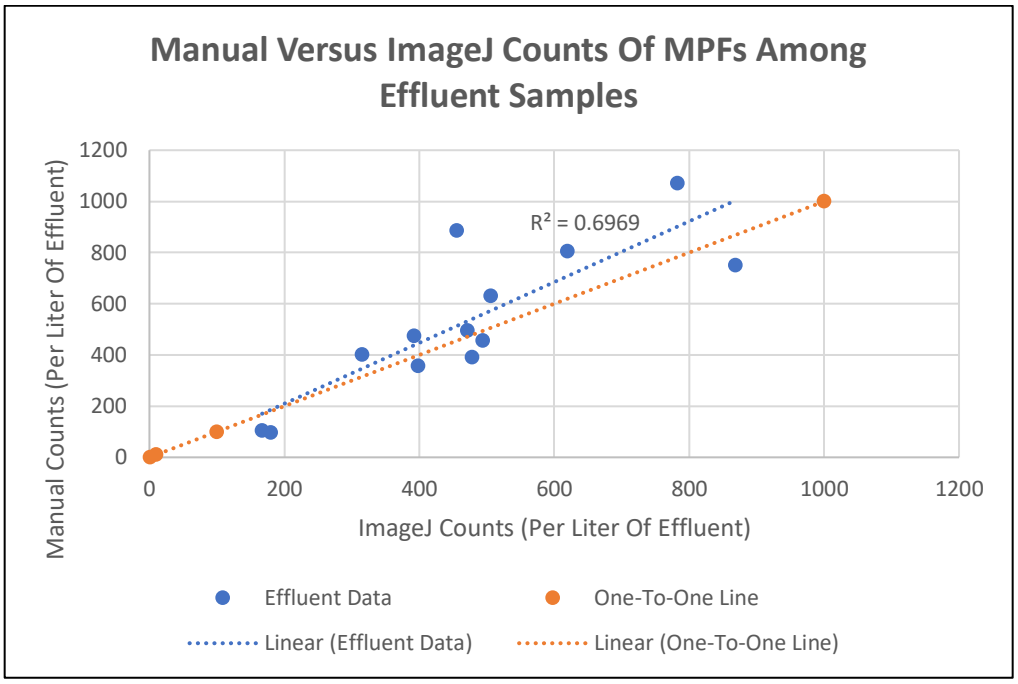

Figure 10. Manual Versus ImageJ Fiber Counts. Comparison of manual MPF counts among effluent samples to ImageJ's counts of MPFs among the same effluent samples. Each data point is representative of MPF counts found among a single effluent sample, gathered from a single day.

Table 1. Ratios of Manual to ImageJ Fiber Counts.

WWTP Location and Sample Date	ImageJ Counts	Manual Counts	ImageJ Counts/Manual Counts
BV (4/30/18)	783	1070	0.731775701
BV (5/21/18)	620	805	0.770186335
BV (6/12/18)	869	751	1.157123835
BV (9/10/18) #1	472	496	0.951612903
BV (9/10/18) #2	494	457	1.080962801
BG (7/9/18)	456	886	0.514672686
BG (9/25/18) #1	180	97	1.855670103
BG (9/25/18) #2	167	105	1.59047619
BG (12/5/18) #1	393	473	0.830866808
BG (12/5/18) #2	316	402	0.786069652
South (7/26/18) #1	506	631	0.801901743
South (7/26/18) #2	399	358	1.11452514
South (11/10/18)	479	391	1.225063939

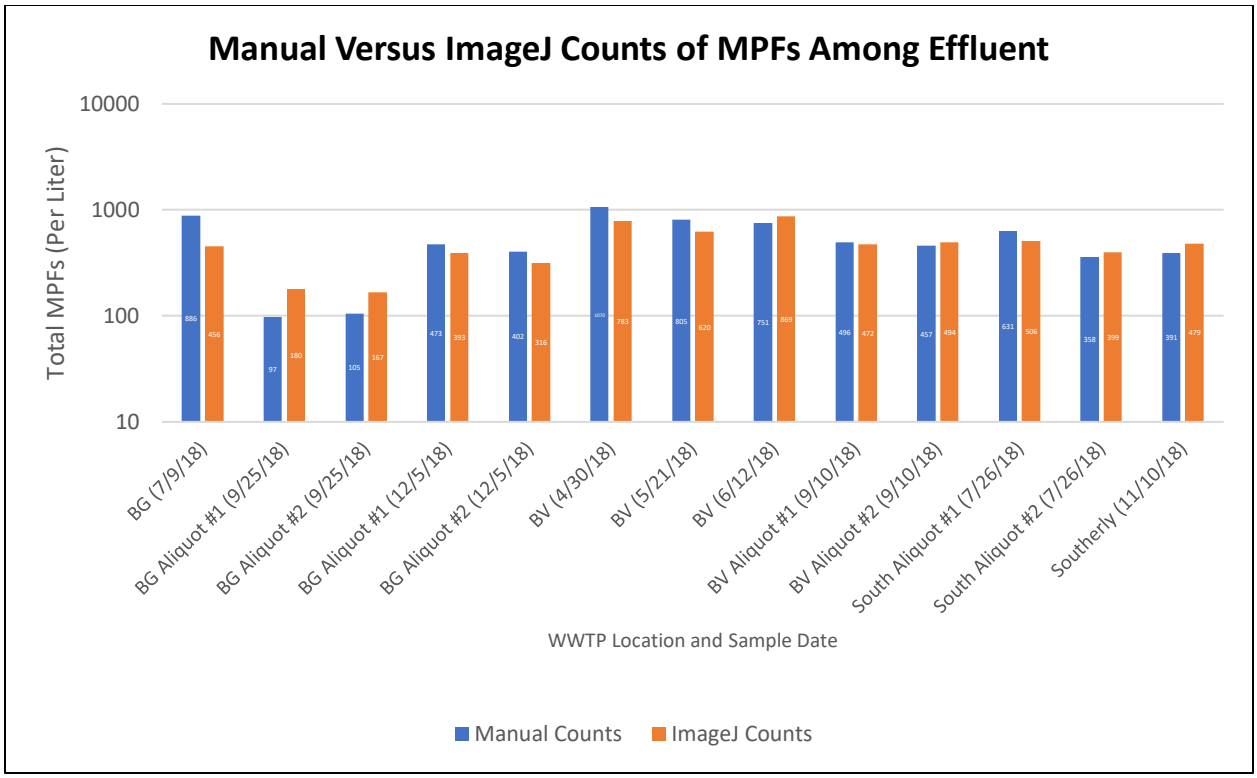

Figure 11. Comparison Between Manual and ImageJ Fiber Counts. Graphicly describes the relationship between manual and ImageJ counts of MPFs among samples of effluent gathered from a given WWTP on a given day. Samples were gathered from the Bowling Green (BG), Bay View (BV), and Southern Cleveland (South) WWTPs. Note that the primary y-axis is on a logarithmic scale (see Table 1).

A two-tailed paired t-test, with a threshold value of 0.05, revealed that some samples shared a significant difference between manual and ImageJ counts of MPFs among each image. In other cases, however, there was no significant difference between manual and ImageJ counts of MPFs among each image. The number of pictures processed did not have an effect on the existence of a significant difference between manual and ImageJ counts. This is illustrated in tables A1-A13 (in Appendix A) where fluctuating image amounts produces varying degrees of significance among manual and ImageJ counts. For example, Tables A4 and A5 (in Appendix A) show that no significant difference exists between manual and ImageJ counts with 238 and 224 images processed, respectively. However, Tables A7 and A8 (in Appendix A) show that a

significant difference exists among manual and ImageJ counts with 198 and 203 images processed, respectively. Percent matching varied with the number of pictures taken of "blank space". ImageJ and manual counts were in agreement that no MPFs were present in instances where pictures were absent of MPFs, particulates, or organic matter. This occurrence led to "inflated" percent matching values among some sample batches (Tables A1, A4, and A10 in Appendix A). In all cases, except for MPFs identified among the effluent of the BV WWTP on 4/30/18 and the BG WWTP on 7/9/18 (Tables A1 and A4 in Appendix A), manual counts of MPFs among each image showed a lower standard deviation than ImageJ counts of MPFs amongst each image.

3.3 Comparison of MPF Counts Between Influent and Effluent Samples

In this section, the reported MPF counts among influent and effluent samples were all determined via MPF ImageJ macro. Organic matter was present in all analyzed samples. MPFs associated with background contamination among influent samples were determined from independently processing DI water samples and counting MPFs associated with DI water samples via the MPF ImageJ macro. Background MPFs associated with the sample dates 4/30/18, 5/21/18, and 6/12/18, 7/9/18, and 7/26/18 represent the average of two independently processed DI water samples with MPFs counted via the MPF ImageJ macro. Background MPFs associated with the sample dates 9/10/18, 9/25/18, 11/10/18, and 12/5/18 were counted via the MPF ImageJ macro where a DI water sample was independently processed along with the influent samples of those sample dates (Figures 12, 13, and 14). Background amounts of MPFs were subtracted from influent and effluent values when determining reductions in MPF from the influent to the effluent. The term "high flow" is a categorical nomenclature used by WWTP

operates to describe increased amounts of flow within a given WWTP. “Normal flow” refers to flow within a given WWTP that is typically experienced on a day-to-day basis.

With regards to the Bay View WWTP, the second and third aliquots pertaining to the sample date of 9/10/18 (with respective MPF counts of 564 and 531) experienced extremely high amounts of organic matter (Figure 12). So much so, that the majority of present MPFs were obscured by the heavy organics in these samples. Thus, these two samples can be seen as outliers relative to the first aliquot of 9/10/18 (with 1713 MPF counts) and are not included in the calculations of percent reduction in MPFs from the influent to the effluent (Figure 12). Pertaining to samples gathered from the BV WWTP on 12/5/18, organics were extremely high for the first aliquot (with 900 MPF counts) but were seemingly nonexistent for the second aliquot (with 2137 MPF counts).

With regards to the BV WWTP, “normal flow” days were experienced on 4/30/18, 5/21/18, and 6/12/18 and “high flow” was experience on 9/10/18. Under “normal flow” conditions, there was a consistent reduction in MPFs between influent and effluent samples gathered from the BV WWTP on the same days (Figure 12). On 4/30/18, 4829 MPFs were counted among an influent sample and 438 MPFs were counted among an effluent sample. This represents a 90.91-percent decrease in MPFs between the influent and effluent on this “normal flow” day. On 5/21/18, 4761 MPFs were counted among an influent sample and 274 MPFs were counted among an effluent sample. This represents a 94.25-percent decrease in MPFs between the influent and effluent on this “normal flow” day. On 6/12/18, 6341 MPFs were counted among an influent sample and 505 MPFs were counted among an effluent sample. This represents a 92.04-percent decrease in MPFs between the influent and effluent on this “normal flow” day. Under “high flow” conditions, the first aliquot of influent gathered from the BV

WWTP on 9/10/18 contained 1605 MPFs. The first and second aliquots of effluent gathered from the BV WWTP on 9/10/18 contained 364 and 386 MPFs, respectively. This represents a 77.32-percent reduction in MPFs between the first aliquot of influent and the first aliquot of effluent on this “high flow” day. This also represents a 75.95-percent reduction in MPFs between the first aliquot of influent and the second aliquot of effluent on this same “high flow” day. Based upon this data, there is a less reduction in MPFs from the influent to the effluent on “high flow” days than “normal flow” days at the BV WWTP (Figure 12).

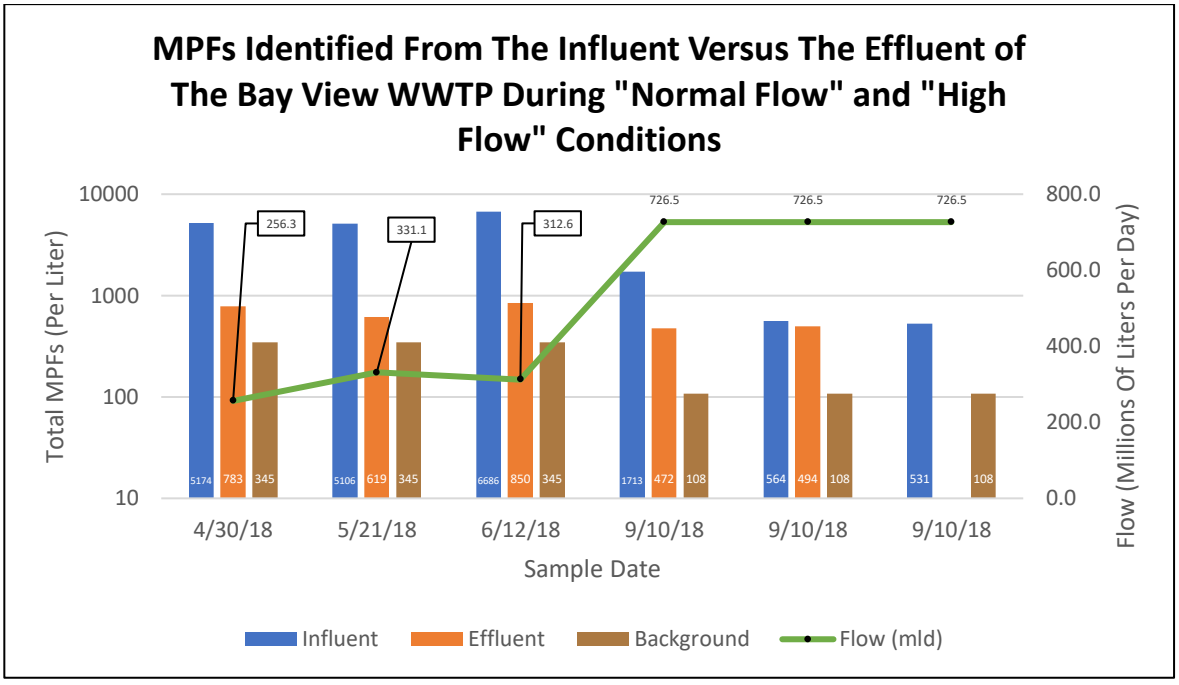

Figure 12. Fibers from the Bay View WWTP. Shows the comparison of MPF counts (done via the MPF ImageJ macro) among influent and effluent samples gathered from the Bay View WWTP under “normal flow” and “high flow” conditions. “Normal flow” days were experienced on 4/30/18, 5/21/18, and 6/12/18. “High flow” was experience on 9/10/18. Samples gathered on 9/10/18 represent multiple aliquots of the same sample day. Each data point represents MPFs counted among a single sample. Note that the primary y-axis is on a logarithmic scale. High organics among the second and third aliquot of influent on 9/10/18 obscured MPFs.

With regards to the Bowling Green (BG) WWTP, “normal flow” days were observed on 7/9/18 and 12/5/18. “High flow” was observed on 9/25/18. On 7/9/18, 8408 MPFs were counted

among an influent sample and 98 MPFs were counted among an effluent sample. This represents a 98.83-percent decrease in MPFs between the influent and effluent on this “normal flow” day. On 12/5/18, 2835 MPFs were counted among an influent sample. The first and second aliquots of effluent gathered from the BG WWTP on 12/5/18 contained 214 and 291 MPFs, respectively. This represents a 92.5-percent reduction in MPFs between the analyzed influent sample and the first aliquot of effluent on this “normal flow” day. This also represents an 89.74-percent reduction in MPFs between the analyzed influent sample and the second aliquot of effluent on this same “normal flow” day. The first and second aliquots of influent gathered from the BG WWTP on 9/25/18 contained 875 and 792 MPFs, respectively. Additionally, the first and second aliquots of effluent gathered from the BG WWTP on 9/25/18 contained 59 and 72 MPFs, respectively. This represents a 93.3-percent reduction in MPFs between the first aliquot of influent and the first aliquot of effluent, a 91.78-percent reduction in MPFs between the first aliquot of influent and the second aliquot of effluent, a 92.55-percent reduction in MPFs between the second aliquot of influent and the first aliquot of effluent, and a 90.91-percent reduction in MPFs between the second aliquot of influent and the second aliquot of effluent on this “high flow” day. Based upon this data there is less reduction in MPFs from the influent to the effluent on “high flow” days than “normal flow” days at the BG WWTP (Figure 13).

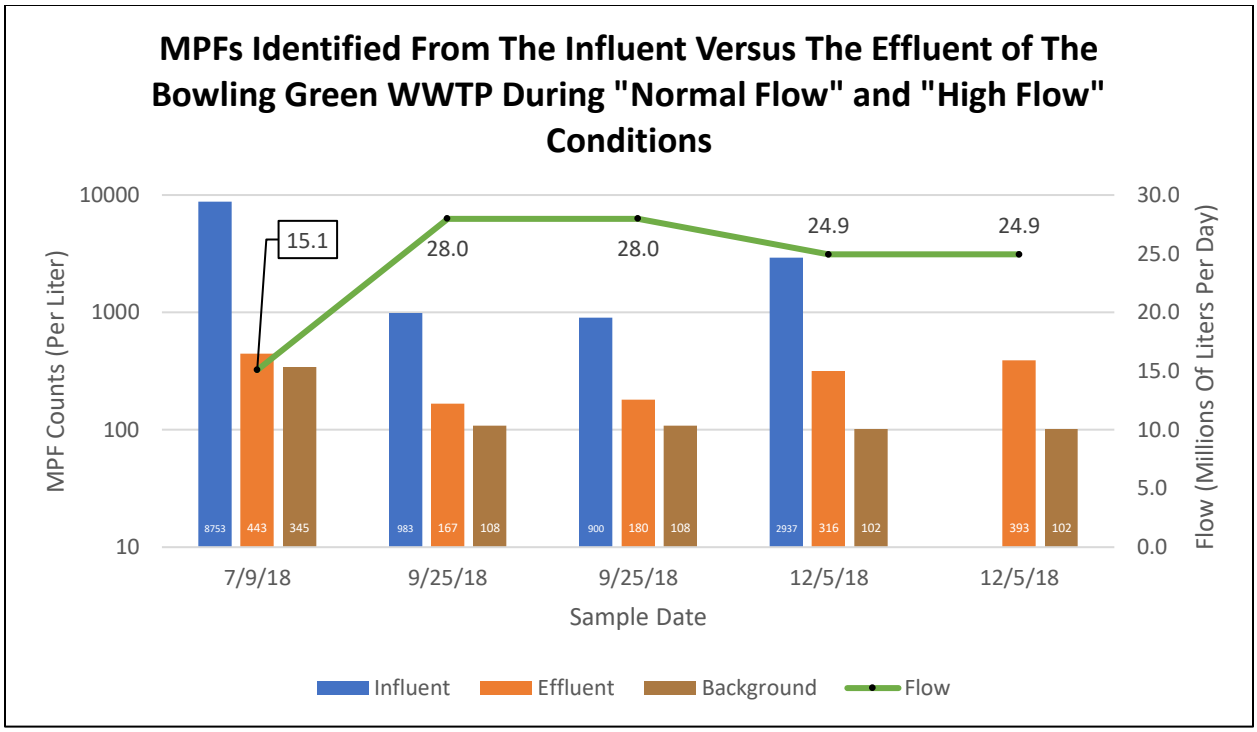

Figure 13. Fibers from the Bowling Green WWTP. Shows the comparison of MPF counts (done via the MPF ImageJ macro) among influent and effluent samples gathered from the Bowling Green WWTP under "normal flow" and "high flow" conditions. "Normal flow" days were experienced on 7/9/18 and 12/5/18. "High flow" was experience on 9/25/18. Samples gathered on 9/25/18 and 12/5/18 represent multiple aliquots of the same sample day. Each data point represents MPFs counted among a single sample. Note that the primary y-axis is on a logarithmic scale. Only one sample of influent was gathered on 12/5/18.

With regards to the Southern Cleveland (Southerly) WWTP, samples were only gathered under "normal flow" conditions. The first and second aliquots of both influent and effluent gathered from the Southern Cleveland WWTP on 7/26/18 were independently processed by two different researchers. Thus, only the first aliquot of influent and effluent was used to calculate reductions in MPFs from the influent to the effluent. The first aliquot of influent gathered from the Southern Cleveland WWTP on 7/26/18 contained 567 MPFs. The first aliquot of effluent gathered from the Southern Cleveland WWTP on this same day contained 153 MPFs. This represents a 73.02-percent decrease in MPF counts between the first aliquot of influent gathered on 7/26/18 and the first aliquot of effluent gathered on this same day. The analyzed sample of

influent gathered on 11/10/18 contained 1627 MPF, and the analyzed sample of effluent gathered on this same day contained 316 MPFs. This represents an 80.58-percent decrease in MPFs between the analyzed influent and effluent pertaining to the sample date of 11/10/18. There is great similarity between the percent reduction in MPFs among the first aliquots of influent and effluent gathered on 7/26/18 and the analyzed influent and effluent samples gathered on 11/10/18 (Figure 14).

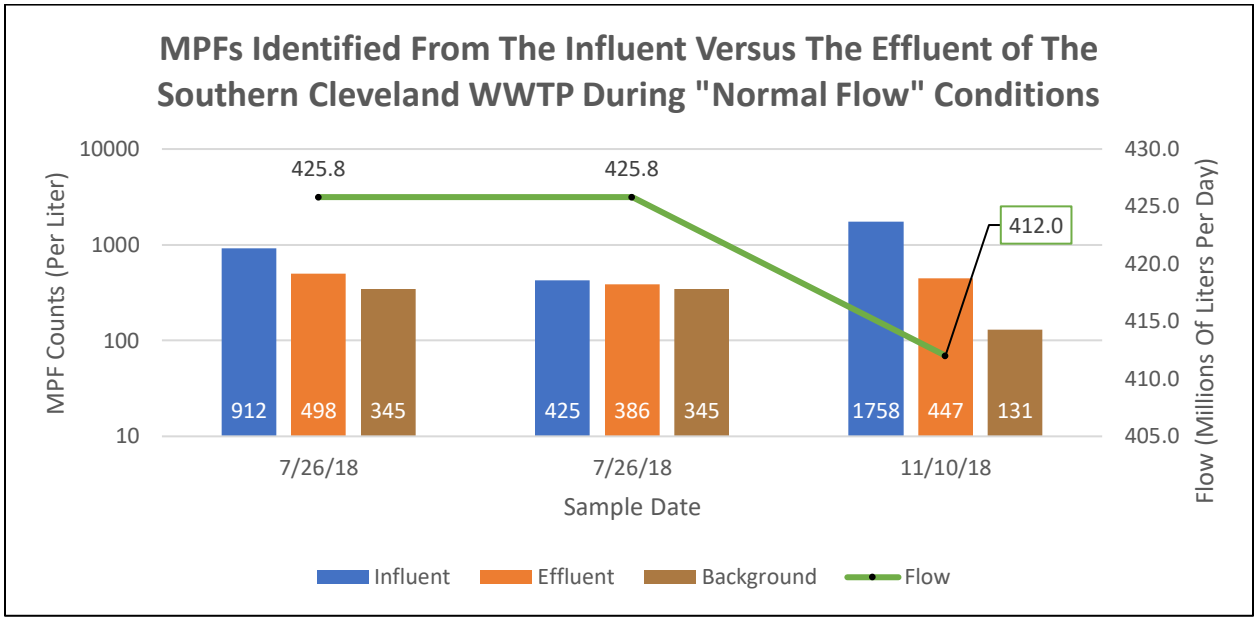

Figure 14. Fibers from the Southerly WWTP. Shows the comparison of MPF counts (done via the MPF ImageJ macro) among influent and effluent samples gathered from the Southern Cleveland (Southerly) WWTP under "normal flow" conditions. Samples gathered on 7/26/18 represent multiple aliquots of the same sample day. However, the second aliquots of influent and effluent gathered on 7/26/18 were processed by a separate researcher. Each data point represents MPFs counted among a single sample. Note that the primary y-axis is on a logarithmic scale.

Of the three studied WWTPs, the Bowling Green WWTP had the highest reduction in MPFs between influent and effluent samples under "normal flow" conditions with an average reduction of 93.67-percent. The Bay View WWTP had the second highest reduction in MPFs between influent and effluent samples under "normal flow" conditions with an average reduction of 92.4-percent. The Southern Cleveland WWTP had the lowest reduction in MPFs between

influent and effluent samples under “normal flow” conditions with an average reduction of 76.8-percent.

Table 2. Reduction in Background Corrected MPF Counts from Influent to Effluent.

WWTP Name	Sample Date	Flow Conditions	Influent MPF Counts	Effluent MPF Counts	Percent Reduction	Average Percent Reduction
BV WWTP	4/30/18	Normal	4829	438	90.91	92.4
	5/21/18	Normal	4761	274	94.25	
	6/12/18	Normal	6341	505	92.04	
	9/10/18	High	1605	364	77.32	76.64
				386	75.95	
BG WWTP	7/9/18	Normal	8408	98	98.83	93.67
	12/5/18	Normal	2835	214	92.5	
				291	89.74	
	9/25/18	High	875	59	92.1	92.1
			792	72		
Southerly WWTP	7/26/18	Normal	567	153	73.02	76.8
	11/10/18	Normal	1627	316	80.58	

3.4 Identification of MPFs in Sludge Cake

There is high variability in MPF counts among sludge cake aliquots pertaining to the same given collection days. The first aliquot of sludge cake processed from the Bowling Green WWTP, associated with the sample date of 7/9/18, contained 784 MPFs per gram of sludge cake. The second aliquot of sludge cake processed from the Bowling Green WWTP of the same sample date contained 2156 MPFs. This represents a factor of 3 difference in MPF counts among these two aliquots. The first aliquot of sludge cake processed from the Bay View WWTP, associated with the sample date of 4/30/18, contained 4203 MPFs. The second aliquot of sludge cake processed from the Bay View WWTP of the same sample date contained 424 MPFs. This represents a factor of 10 difference in MPF counts among these two aliquots. The first aliquot of sludge cake processed from the Bay View WWTP, associated with the sample date of 5/21/18,

contained 2662 MPFs. The second aliquot of sludge cake processed from the Bay View WWTP of the same sample date contained 1372 MPFs. This represents a factor of 2 difference in MPF counts among these two aliquots. The first aliquot of sludge cake processed from the Bay View WWTP, associated with the sample date of 6/12/18, contained 633 MPFs. The second aliquot of sludge cake processed from the Bay View WWTP of the same sample date contained 886 MPFs. This represents a factor of 1.4 difference in MPF counts among these two aliquots. The first aliquot of sludge cake processed from the Southern Cleveland WWTP, associated with the sample date of 7/26/18, contained 1524 MPFs. The third aliquot of sludge cake processed from the Southern Cleveland WWTP of the same sample date contained 2894 MPFs. This represents a factor of 2 difference in MPF counts among these two aliquots. The first aliquot of sludge cake processed from the Bay View WWTP, associated with the sample date of 9/10/18, contained 1286 MPFs. The second aliquot of sludge cake processed from the Bay View WWTP of the same sample date contained 634 MPFs. The third aliquot of sludge cake processed from the Bay View WWTP of the same sample date contained 435 MPFs. MPF counts among these aliquots differed by a factor of 3 (Figure 15).

MPFs associated with background contamination among sludge cake samples were determined from independently processing DI water samples and counting MPFs associated with DI water sample via the MPF ImageJ macro. Background MPFs associated with the sample dates 4/30/18, 5/21/18, 6/12/18, 7/9/18, and 7/26/18 represent the average of two independently processed DI water samples with MPFs counted via the MPF ImageJ macro. This average being 345 MPFs. Background MPFs associated with the 9/10/18 sample date were determined from a DI water sample that was independently processed along with the SC sample of that sample date (Figure 15). The MPF ImageJ macro revealed there to be 108 MPFs among this DI water sample.

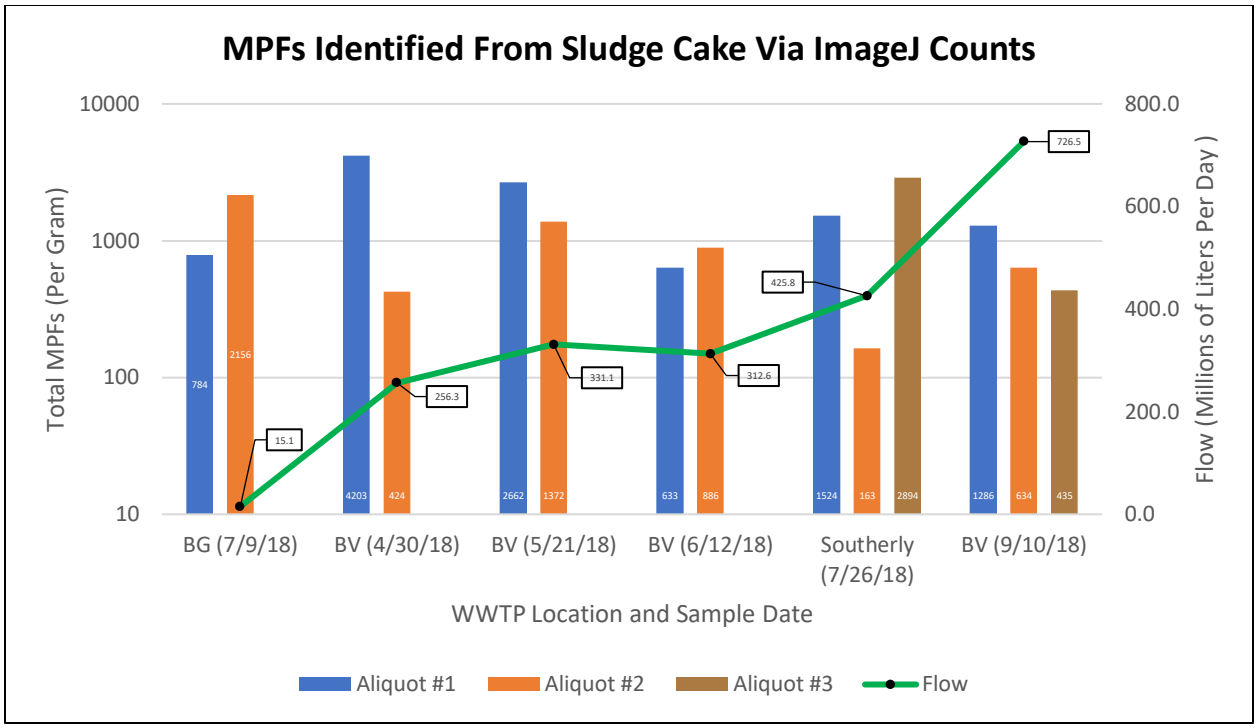

Figure 15. Fibers Among Sludge Cake. Shows the comparison of MPF counts (done via the MPF ImageJ macro) among aliquots of sludge cake gathered from the Bowling Green (BG) WWTP, the Bay View (BV) WWTP, and the Southern Cleveland (Southerly) WWTP. Each data point represents MPFs counted among a single sample. Note that the primary y-axis is on a logarithmic scale.

3.5 Analysis of Microplastics in CSO Samples

MPPs identified among CSO samples obtained from the BG CSO outfall were primarily fibrous in nature. Thus, the same ImageJ macro used to identify MPFs among wastewater and sludge cake samples was used to identify MPFs among CSO samples obtained from the BG CSO outfall (Figure 15). This same macro was also used to identify MPFs among the Forest City CSO outfall (CSO outfall #201) under "inactive" conditions, as most of the identified plastics within this particular sample batch were determined to be fibrous in nature (Figure 17). Most of the microplastics identified among CSO outfall #201 during "active" conditions on 11/18/18 were of a particulate morphology. Thus, an adjusted ImageJ macro was used to identify these MPPs (see methods section). CSO samples were collected from the Bowling Green (BG) CSO outfall

during rain events where 3.94-centimeters of precipitation was experienced on 6/27/18 and 1.93-centimeters of precipitation was experienced on 9/8/18.

On 6/27/18, an average of 678 MPFs per liter was found among surface samples of the BG CSO outfall. On this same day, an average of 618 MPFs was found among samples collected from the bottom-most portion of the CSO outfall. Because the average number of MPFs found among surface and depth samples gathered on 6/27/18 was greater than the proposed amount of background contamination of MPFs to the samples (345), it can be said that MPFs were discharged from this CSO outflow as a function of precipitation on 6/27/18. On 9/9/18, 194 MPFs were found among a surface sample of the BG CSO outfall. On this same day, 222 MPFs were found among a depth sample of the BG CSO outfall. Because the number of MPFs found among surface and depth samples gathered on 9/9/18 was less than the proposed amount of background contamination of MPF to the samples (295), it can be said that no MPFs were detected from this CSO outflow as a function of precipitation on 9/9/18 (Figure 16).

A surface sample of CSO outfall #201 revealed there to be 220 MPFs per liter on 8/8/18. Furthermore, an average of 231 MPFs was found among depth samples of CSO #201 on 8/8/18. Because the number of MPFs found among surface and depth samples gathered on 8/8/18 was less than the proposed amount of background contamination of MPF to the samples (295), it can be said that no MPFs were detected from this CSO outflow under “inactive” conditions (Figure 18). Samples collected from CSO outfall #201 during an “active” event showed an average of 1940 MPPs among surface samples and an average of 861 MPPs among depth samples. Given that MPPs were identified among CSO outfall #201 during “active conditions, and no MPFs or MPPs were said to be discharged from CSO outfall #201 during “inactive” conditions, it can be

said that MPPs were in fact discharged from CSO outfall #201 during "active" conditions on 11/18/18 (Figures 17 and 18).

Background MPFs associated with all CSO samples were determined from independently processing DI water samples and counting MPFs associated with DI water samples via the MPF ImageJ macro. Background MPFs associated with the 6/27/18 sample date represent the average of two independently processed DI water samples with MPFs counted via the MPF ImageJ macro. Background MPFs associated with the sample dates 8/8/18 and 9/9/18 were determined from DI water samples that were independently processed along with the associated CSO samples of those sample dates.

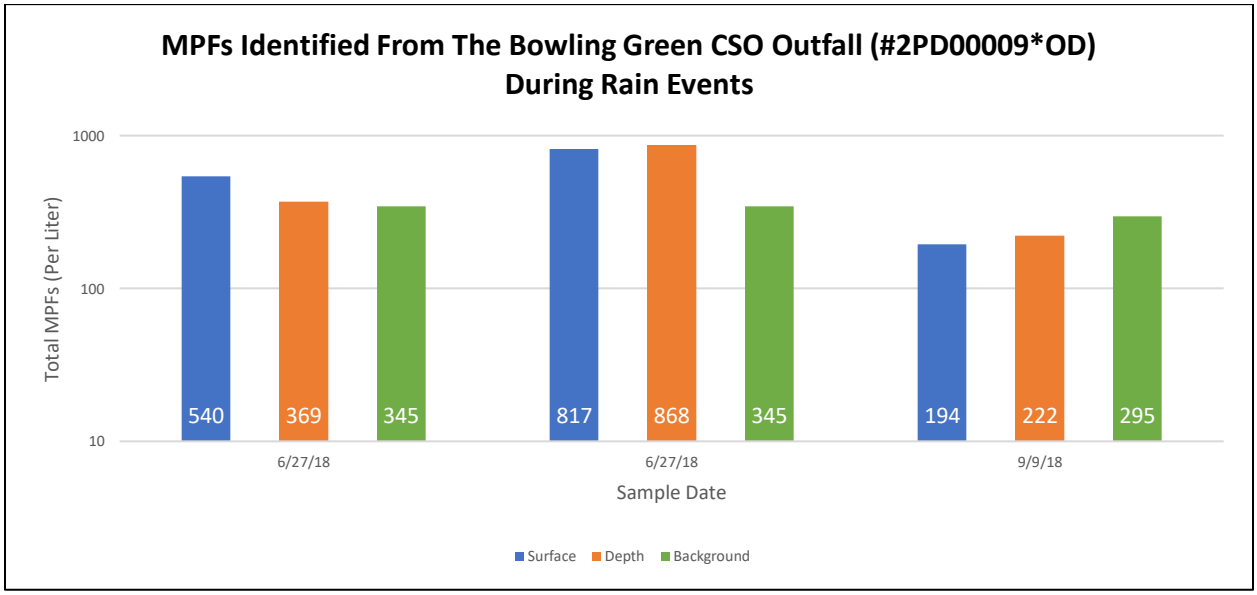

Figure 16. Fibers from BG CSO. Shows the total amounts of MPFs (identified via ImageJ counts) among the Bowling Green CSO outfall (#2PD00009*OD; located in Bowling Green, OH). Note that the primary y-axis is displayed on a logarithmic scale.

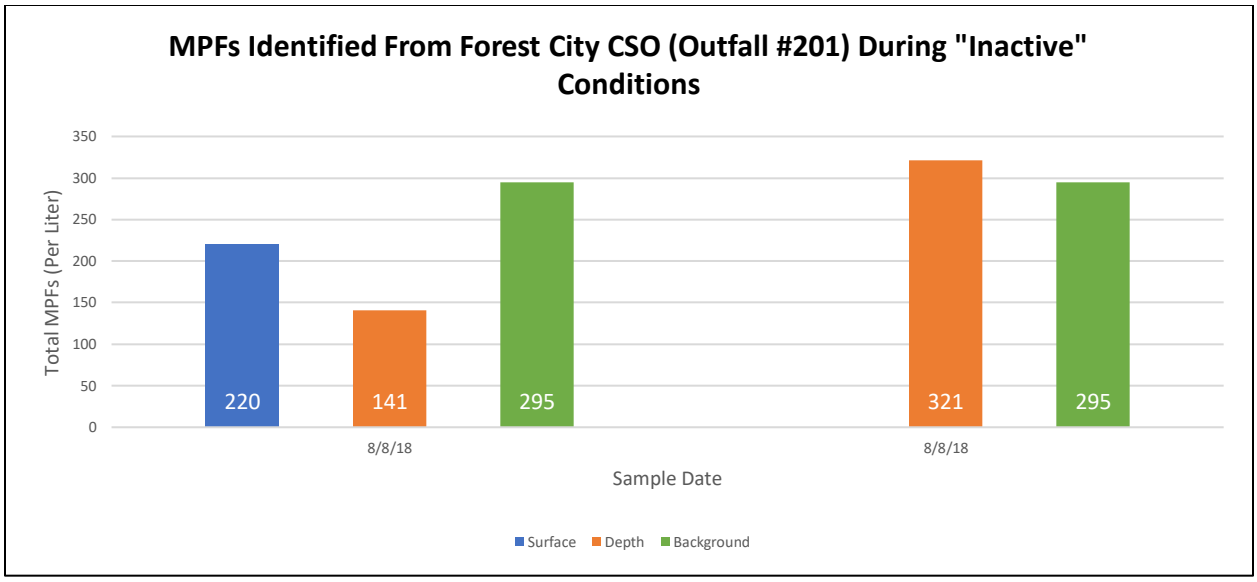

Figure 17. Fibers from Inactive Forest City CSO. Shows the total amounts of MPFs (identified via ImageJ counts) among CSO outfall #201 (located near the Forest City Yacht club in Cleveland, OH) during "inactive" conditions and MPFs associated with background contamination (identified via ImageJ counts). Several aliquots of samples were gathered from the depth of the CSO.

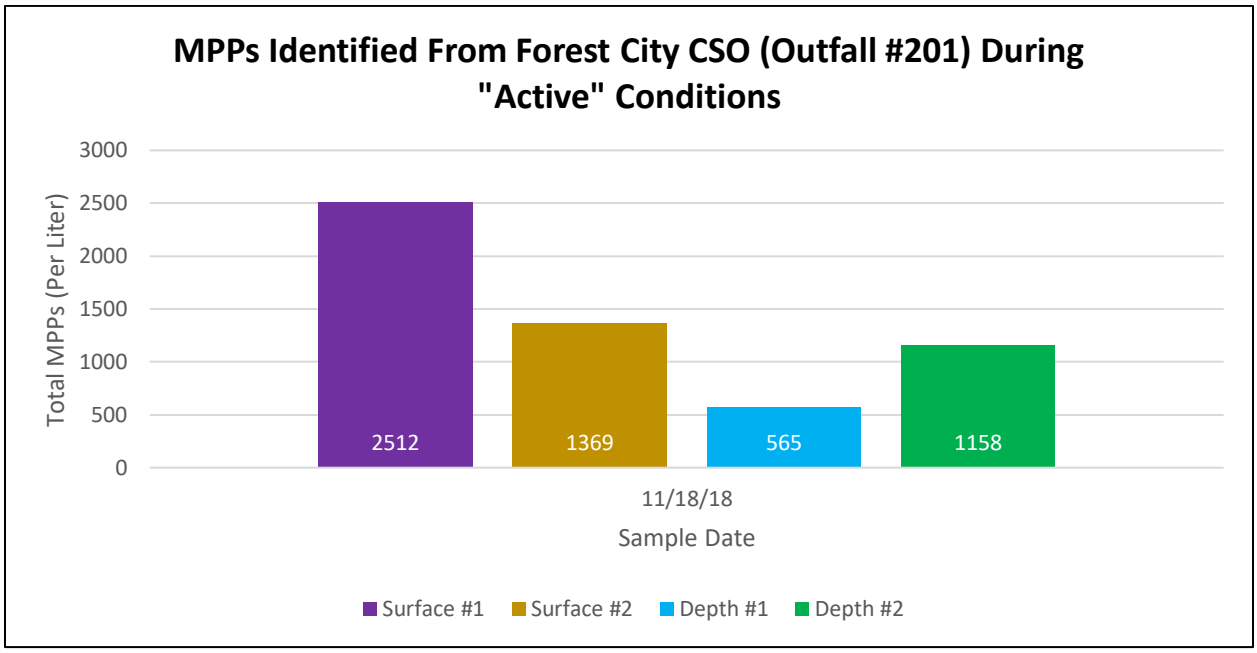

Figure 18. Fibers from Active Forest City CSO. Shows the total amount of MPPs (identified via ImageJ counts) among CSO outfall #201 (located near the Forest City Yacht club in Cleveland, OH) and MPFs associated with background contamination (identified via ImageJ counts). Several aliquots of samples were gathered from the top and bottom sections of the CSO outflow.

3.6 MPFs From Potential Background Contamination Sources

The analysis of MPFs among the proposed sources of background contamination revealed there to be background amounts of MPFs. The average counts of MPFs among two liters of DI water revealed there to be 82.5 MPFs per liter using the MPF ImageJ macro. The average MPF counts of two liters of DI water placed within two separate HDPE sample bottles revealed there to be an average of 88.5 MPFs per liter using the MPF ImageJ macro. Of the analyzed sampling media, the quartz filter paper was determined to be associated with the highest amount of MPFs with a total of 245 MPFs identified via MPF ImageJ macro (Figure 19). Cleaning 30.72 square-inches of microscope slides and placing them directly into an open fume hood for 24-hours revealed there to be around 4 MPFs per square inch of the analyzed microscope slides. MPF counts were done via the MPF ImageJ macro. The processing of samples associated with proposed sources of environmental background contamination was done prior to 7/26/18. Thus, microscope slides were stored in an open fume hood where paper towels were used as a drying surface for microscope slides and dishes. Furthermore, background contamination of MPFs associated with these samples (determined from the average number of ImageJ counts of MPFs among two independently processed DI water samples) was determined to be 345 MPFs (Figure 19).

MPFs associated with environmental background contamination can be determined from MPFs counted among the DI water samples processed in the same way as wastewater samples. Prior to 7/26/18, MPFs associated with background contamination were determined from the average MPF counts found among two independently processed DI water samples where paper towels were used as a drying surface with the fume-hood door open. Subsequent to 7/26/18, a DI water sample was run with each sample batch and metal drying racks were used as drying

surfaces with the fume-hood door closed. Manual MPF counts of the two DI water samples run before 7/26/18 revealed an average of 255 MPFs per liter of DI water. Manual counts of DI water samples run after 7/26/18 revealed 93, 62, and 99 MPFs per liter of DI water with an average of 84.66 MPFs per DI water blank. Comparing the average number of MPFs found among DI water blanks processed prior to 7/26/18 with the average number of MPFs found among DI water blanks processed subsequent to 7/26/18 revealed a reduction in MPFs by a factor of 1.5.

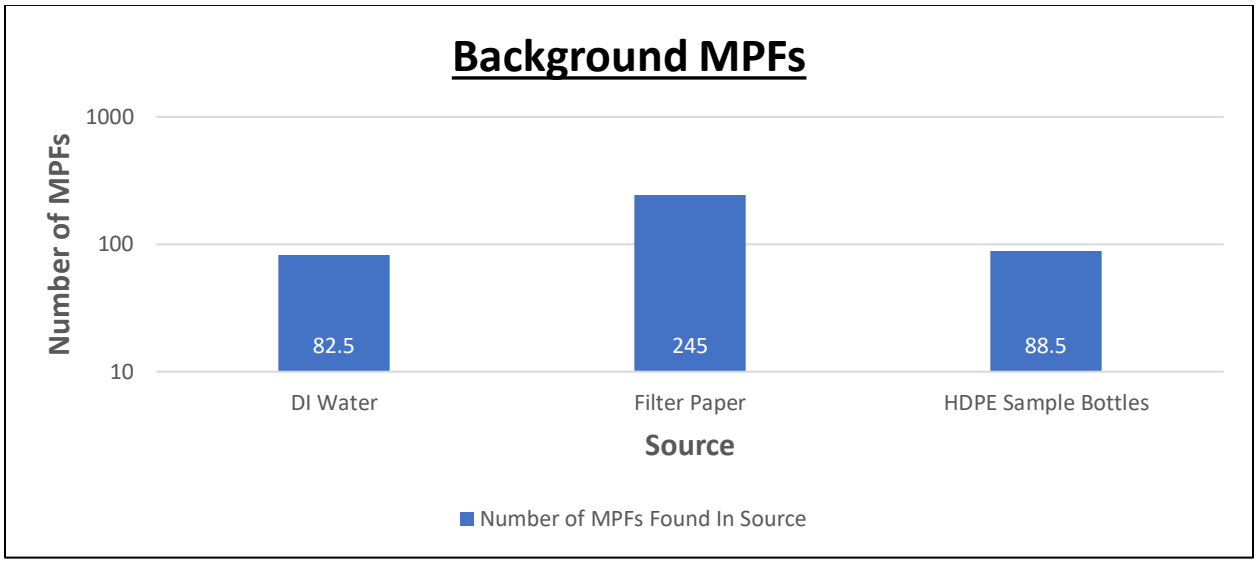

Figure 19. Potential Sources of Background Fibers. Shows MPFs identified via ImageJ counts among sample processing media. Note that the primary Y-axis is displayed on a logarithmic scale. Standard error was applied to the total counts.

3.7 Chemical Characterization of MPFs

To remain unbiased, unknown MPFs were randomly selected from the entire population of identified MPFs. MPFs were chosen for Raman analysis based upon their birefringent colors where representative MPFs were selected of each color type. All analyzed white and blue MPFs were determined to be composed of polyester (Table 2). All analyzed red MPFs were determined

to be composed of the quartz filter paper. All analyzed yellow MPFs were determined to be composed of cellulose (Table 2). Note that percent best-fit, which is based upon the Euclidian distance algorithm, is related to the degree of similarity between the whole curve of an unknown sample and the whole curve of a known standard. Quality values represent the output comparison of the Euclidian distance between the spectral curves of known polymers to the spectral curves of unknown MPFs. The best match from this comparison would yield a "quality" value of zero, and the worst possible match would yield a "quality" value of 1.41421 (outlined above). Given that greater than 99-percent of MPFs found among all sample types exhibit a white birefringence, and that all of the analyzed MPFs with a white birefringence were determined to be polyester, it was determined that greater than 99-percent of all of the analyzed MPFs are composed polyester (Figure B28 in Appendix B).

Table 3. Spectral ID Results.

Unknown MPF ID and Color	MPF Type	Quality	Percent Best Fit
Unknown MPF #1 (White)	Polyester	0.0814801	94.23847236
Unknown MPF #2 (White)	Polyester	0.0820567	94.19770048
Unknown MPF #3 (White)	Polyester	0.0757741	94.64194851
Unknown MPF #4 (White)	Polyester	0.0819229	94.2071616
Unknown MPF #5 (White)	Polyester	0.0706929	95.00124451
Unknown MPF #6 (White)	Polyester	0.0655517	95.36478317
Unknown MPF #7 (White)	Polyester	0.0636144	95.50177131
Unknown MPF #8 (White)	Polyester	0.064317	95.45208986
Unknown MPF #9 (White)	Polyester	0.143167	89.87653885
Unknown MPF #10 (White)	Polyester	0.132061	90.66185361
Unknown MPF #11 (White)	Polyester	0.143409	89.85942682
Unknown MPF #12 (White)	Polyester	0.141967	89.96139187
Unknown MPF #13 (White)	Polyester	0.147556	89.5661889
Unknown MPF #14 (Blue)	Polyester	0.0762532	94.60807094
Unknown MPF #15 (Blue)	Polyester	0.0638651	95.4840441
Unknown MPF #16 (Blue)	Polyester	0.0628244	95.55763288
Unknown MPF #17 (Red)	Quartz Filter	0.152764	89.19792676
Unknown MPF #18 (Red)	Quartz Filter	0.190808	86.50780294
Unknown MPF #19 (Red)	Quartz Filter	0.0875182	93.81151314
Unknown MPF #20 (Yellow/Orange)	Cellulose	0.177848	87.42421564
Unknown MPF #21 (Yellow/Orange)	Cellulose	0.236482	83.2781553
Unknown MPF #22 (Yellow/Orange)	Cellulose	0.108301	92.34194356

Table 4. Total Analysis of Fiber Compositions.

Type	Number Identified	Percent Of Total MPFs
Polyester	55487	99.912
Quartz Filter	16	0.029
Cellulose	33	0.059

CHAPTER IV. DISCUSSION

The foremost goal of this research was to develop a reproducible method of quantifying microplastic fibers (MPFs) among wastewater, combined sewer overflow (CSO) effluent, and sludge cake samples. As compiled by Mason et al. (2016), five separate studies were reported to use similar methods of quantifying microplastics among wastewater effluent. A common element of these five studies is that they all opted to filter wastewater through sieves (with the finest mesh sizes ranging from 1.2 to 300-microns). Subsequent to sieving, microplastics were manually quantified via microscopy (Mason et al., 2016). The results of these studies indicate that there is a direct relationship between the mesh size of a sieve used to filter wastewater and the number of microplastics quantified. Thus, it can be stated that the likelihood of capturing MPPs on a given sieve is inversely proportional to the sieve's mesh size. For studies that reported low quantifications of MPPs among wastewater, it is possible that the utilized mesh size was too coarse.

As one of the five studies reported by Mason et al. (2016), Martin and Eizhvertina (2014) was shown to have identified an average of 32.91 MPFs among 2-liters of effluent collected from WWTPs located in the greater New York region. This was achieved via filtering the 2-liters of effluent through a sieve (with a mesh size of 1.2 micrometers) and analyzing residual MPFs contained on the sieve (Mason et al., 2016). The mesh size of the sieve utilized by Martin and Eizhvertina (2014) to filter effluent is very similar to the pore space diameter of the quartz filter paper used to filter wastewater collected from the Bowling Green (BG) WWTP, the Bay View (BV) WWTP, and the Southern Cleveland WWTP. However, there is an order of magnitude difference between the MPF counts outlined by Martin and Eizhvertina (2014) and counts of MPFs among samples of effluent collected from the BG WWTP, the BV WWTP, and the

Southern Cleveland WWTP (even when accounting for background contamination of MPFs). The order of magnitude difference in MPF counts could be an indication that operator bias plays a large role in obtaining highly precise counts of MPFs among wastewater samples. This is further demonstrated where two aliquots of the same composite sample of effluent (collected from the Southern Cleveland WWTP on 7/26/18) showed an order of magnitude difference in MPFs counts when independently processed by two different researchers, Blane Houck and a Bowling Green State University undergraduate student, and accounting for background contamination of MPFs to the samples (Figure 14). However, there is consistency in MPF counts (as described by the analytics of this thesis) when aliquots of the same sample of wastewater are processed by the same researcher. Therefore, trends in MPF counts among different samples of wastewater can be seen as being valid as long as samples are processed by the same researcher. Slight alterations in the processing of samples by different researchers may produce differences in MPF counts among aliquots of the same sample of wastewater, but the resulting data should see the same general trends as long as these researchers are consistent in their methods. Nonetheless, further analysis of operator bias regarding differences in MPF counts between samples processed in the same manner (but by different researchers) is required to determine the reproducibility of these methods in gaining highly precise counts of MPFs among wastewater.

Given that a linear relationship exists between manual and ImageJ counts of MPFs among effluent samples (r-squared equals 0.6969), ImageJ can be used as a reliable measure of obtaining accurate MPF counts. An r-squared value of 0.6969 indicates that a given ImageJ count can be reliably related to a given manual count around 70-percent of the time. On the other hand, this value also indicates that this same relationship will not hold around 30-percent of the time. Additionally, a one-to-one linear regression displayed through the data of manual to

ImageJ counts of MPFs among effluent shows little disagreement between manual and ImageJ counts when MPF counts are less than 600 per liter of effluent (Figure 10). When MPF counts among effluent samples becomes greater than 600 MPFs per liter, the relationship of manual to ImageJ counts becomes further separated from the one-to-one regression line. This can be interpreted as ImageJ's MPF counts becoming less reliable when there is a higher density of MPFs per a given liter of effluent. Nonetheless, the relationship of manual to ImageJ counts of MPFs among effluent samples is not too far from a one-to-one relationship between manual and ImageJ counts. Thus, ImageJ's counts of MPFs can be described as being reliable. There were some instances where ImageJ could not count MPFs that are non-linear, discern between multiple birefringent sections of the same MPF, or count MPFs among images containing high amounts of organic matter. As opposed to ImageJ counts, lower standard deviations in MPF counts among images exist for manual counts. However, given the time constraints associated with manually counting fibers, it is much quicker (and more efficient) to use ImageJ as a means of counting MPFs among samples.

Samples of sludge cake contained the highest amounts of organic matter and represent a heterogeneous mixture. As such, sludge cake samples yielded the greatest heterogeneity in MPF counts among aliquots of the same samples. To obtain extremely precise MPF counts, a given aliquot of sludge cake would need to be subjected to multiple phases of organic matter digestion. However, even if MPFs were completely unobstructed by organic matter among sludge cake samples, MPF counts among a given aliquot of sludge cake cannot serve as a representative of MPFs among a given sample of sludge cake. Unlike wastewater, sludge cake is not homogenized via WWTP processes into composite samples. Although a 70-percent reliability in ImageJ's MPF counts among effluent samples was observed, this same reliability may not be observed for

ImageJ's ability to count MPFs among different sample types. Further analysis of ImageJ's ability to count MPFs among a larger sample size of different sample types (influent, effluent, sludge cake, and CSO samples) is required to reliably discern ImageJ's error in counting MPFs among different sample types.

MPFs were found to be present among the effluent of the BG CSO outflow during rain events, and MPPs were found to be present among CSO outflow #201 during "active" conditions. Given the fact that the BG CSO outflow is predominantly surrounded by agricultural lands, it is possible that sludge cake applied to these agricultural lands would contain some amounts of MPFs. Given this scenario, MPFs would travel with runoff (from precipitation) into nearby drainage conduits leading to the BG CSO outflow. MPFs were determined to be present among the effluent of the BG CSO outflow, as the amount of MPFs identified among this CSO outflow was greater than the proposed amount of background MPFs. On the other hand, samples taken from CSO outfall #201 during "inactive" conditions showed MPF counts among surface and depth samples that were less than the proposed amount of background MPFs across all aliquots. Thus, it can be stated that no MPFs were detected among CSO outfall #201 during "inactive" conditions. However, a significant amount of MPPs were identified among CSO outfall #201 during "active" conditions. Given the fact that CSO outfall #201 is predominantly surrounded by impervious surfaces (characterized by residential and commercial land use), it is possible that MPPs found among CSO #201 during "active" conditions are the result of plastics discarded inland. In this theoretical model, plastics discarded inland would be subjected to environmental erosional processes (either wind or UV erosion) and would become degraded over time. Thus, giving rise to MPPs. Again, because the landscape surrounding CSO outfall #201 is predominantly characterized by impervious surfaces, precipitation would immediately runoff to

CSO outfall #201. Consequently, causing MPPs (degraded from larger pieces of plastic) to be washed from inland locations to the CSO outfall. Because microplastics are light and have a high surface area, it is also possible that MPFs and MPPs identified among the CSO samples arrived to the CSOs via heavy winds (Andrady, 2017). This idea is further confirmed through the identification of MPFs among deionized (DI) water samples processed in the same manner as wastewater, CSO, and sludge cake samples.

Of the analyzed "normal flow" days, the BG WWTP had the greatest average reduction in MPFs from the influent to the effluent. This, in part, could be due to the BG WWTP's treatment regime. In comparison to the BV WWTP and the Southern Cleveland WWTP, the BG WWTP is the only treatment plant to utilize a cloth media filtration system. This system utilizes large discs comprised of a proprietary cloth media. Influent is directed to the discs within a large housing and is then directed through the cloth media discs via vacuum filtration. The pore spaces of the proprietary cloth media discs are around 5-microns in diameter. Because of these small openings, large particles are precluded from transferring through the cloth media discs. Influent directed through the discs is then discharged from the cloth media filtration system as effluent. Although the cloth media filtration system is likely one of the reasons why the BG WWTP experiences the greatest reduction in MPFs from the influent to the effluent of the three WWTPs, further analyzation of the cloth media filtration system's capacity for reducing MPFs is required.

The BV WWTP had the second highest average reduction in MPFs from the influent to the effluent under "normal flow" conditions, while the Southern Cleveland WWTP had the lowest average reduction in MPFs of the three WWTPs. The BV WWTP and the Southern Cleveland WWTP have similar regimens for the treatment of wastewater, but the BV WWTP has a much larger average reduction in MPFs from the influent to the effluent than the Southern

Cleveland WWTP. This is likely due to the fact that the Southern Cleveland WWTP experiences a much higher flow rate than the BV WWTP. As demonstrated, there was a lower reduction in MPF counts from the influent to the effluent of the BV WWTP and the BG WWTP during "high flow" conditions than during "normal flow" conditions. In essence, this serves as an indication that these WWTPs were less effective at removing MPFs from wastewater during "high flow" conditions. It is known that a system with higher flow has more energy to move larger (and more) particles than a system with lower flow. In fact, a study conducted by Fornari et al. (2016) showed that increased turbulence to a sustained homogeneous isotropic solution caused reduced settling of fine-sized rigid microspheres by 6 to 60-percent (Fornari, Picano, Sardina, & Brandt, 2016). Thus, it is entirely possible that increased flow to a given WWTP will cause more turbulence among treatment plant processes. Thereby, allowing MPFs to bypass certain treatment processes (like those associated with settling) via increased suspension within flow columns before being discharged among effluent. This would also explain why the BV WWTP has a higher reduction in MPFs from the influent to the effluent than the Southern Cleveland WWTP, given that the only real difference between these two WWTPs is that the Southern Cleveland WWTP experiences much greater flow on average than the BV WWTP.

Although the Bay View WWTP had a greater reduction in MPFs from its influent to its effluent than the Southern Cleveland WWTP, the Bay View WWTP had a much higher proposed emittance of MPFs than the Southern Cleveland WWTP. As shown, the Southern Cleveland WWTP experienced much lower MPF counts among influent than the Bay View WWTP. It can then be stated that inputs of MPFs to the Bay View WWTP are much greater than that of the Southern Cleveland WWTP. This is most likely due to the fact that wastewater inputs to the Bay View WWTP primarily originate from residential land-use sources. Whereas, inputs to the

Southern Cleveland WWTP primarily originate from industrial land-use sources. Because residential sources of wastewater include clothes washing activities, it is logical that a given WWTP whose sources of wastewater primarily originate from residential sources would experience higher fiber counts among influent and effluent samples than a given WWTP whose sources of wastewater primarily originate from industrial sources. The Bowling Green WWTP experienced the lowest average emittance of MPFs, it is the most efficient at removing MPFs from its influent to its effluent, and it experiences the lowest flow rate of the analyzed WWTPs.

Background amounts of MPFs were found to be present among DI water samples processed in the same way as wastewater, CSO, and sludge cake samples. It was proposed that MPFs associated with background contamination originated from either the external environment, the utilized DI water, the quartz filter papers, or the HDPE sample bottles. Analysis of MPFs associated with the DI water, the quartz filter papers, and the HDPE sample bottles revealed MPF counts among these sample media were less than the proposed amount of background MPFs associated with DI water samples that were processed in the same way as wastewater, CSO, and sludge cake samples. In some cases, the amount of MPFs identified among a given sample was less than the amount of MPFs identified among a given DI water sample processed along with the given sample. This was the case for CSO samples gathered from the BG CSO on 9/9/18. Given cases such as these, it can then be said that no MPFs were inherently present among these media and that the contribution of background MPFs to the DI water samples from these sample media is minimal. It is hypothesized, however, that MPFs associated with background contamination primarily originated from the atmosphere. This statement was reinforced by the fact that MPFs were shown to be present on microscope slides subsequent to being cleaned and left in a fume hood (with the door open) overnight. Leaving the

fume hood door closed showed a significant reduction in background MPFs among DI water samples, but background amounts of MPFs still remained. As highlighted by Dris et al. (2016), a significant portion of microplastics among the natural environment were shown to be associated with atmospheric fallout where 2 to 355 particles were captured from the atmosphere per square-meter per day (Dris, Gasperi, Saad, Mirande, & Tassin, 2016). As such, the results of this study are further reinforced by the fact that MPFs were shown to be present on clean microscope slides within a fume hood. Therefore, the portion of MPFs among the atmospheric sector of the natural environment may be more significant than previously thought.

Upon inspection of MPFs among images, it is apparent that greater than 99-percent of the identified MPFs exhibit a white birefringence. The Raman spectra of 13 MPFs with a white birefringence, selected from the total population of MPFs identified among all sample types (n=55,536), showed great similarity to the Raman spectra of the identified Polyester standard. Spectral ID revealed percent matchings of the Raman spectra of the 13 white MPFs to the Raman spectra of the Polyester standard ranged from 89.86-percent to 95.50-percent. Given the fact that all 13 of the MPFs with a white birefringence were matched to polyester, it is reasonable to predict that the entire population of MPFs with a white birefringence are primarily composed of polyester. The same phenomenon was observed for MPFs with a blue birefringence where the Raman spectra of 3 MPFs with a blue birefringence were matched to the Raman spectra of Polyester with Spectral ID percent matchings ranging from 94.61-percent to 95.56-percent. The Raman spectra of 3 MPFs with a red birefringence were matched to the Raman spectra of a quartz filter standard (used for vacuum filtration) with Spectral ID percent matching ranging from 86.50-percent to 93.81-percent. The Raman spectra of 3 MPFs with a yellow birefringence were matched to the Raman spectra of a cellulose standard with Spectral ID percent matching

ranging from 83.28-percent to 92.34-percent. Because all of the identified MPFs with a red birefringence were matched to a quartz filter paper standard, and all of the identified MPFs with a yellow birefringence were matched to a cellulose standard, it is reasonable to predict that the entire population of red MPFs (n=16) and yellow MPFs (n=33) are primarily composed of quartz filter paper and cellulose, respectively. To confirm these results, further analyzation of the material composition of MPFs (via Raman spectroscopy) is required.

When considering the number of MPFs identified among effluent samples gathered under "normal" flow and "high" flow conditions, and background contamination of MPFs to samples, no notable differences in MPF counts was observed. Thus, average flow rates among WWTPs can be used to determine MPF outputs during a given year. During the year of 2018, the Bay View WWTP experienced an average daily flow rate of 273 million liters per day (MLD), the Bowling Green WWTP experienced an average daily flow rate of 24.96 MLD, and the Southern Cleveland WWTP experienced an average daily flow rate of 418.9 MLD. Total amounts of MPFs found to be present among samples of effluent were corrected for background contamination of MPFs to the samples. An average of 393 MPFs, 147 MPFs, and 170 MPFs per liter was identified among samples of effluent collected from the Bay View WWTP, the Bowling Green WWTP, and the Southern Cleveland WWTP, respectively. It can then be stated that (during the year of 2018) an average of $3.92*10^{13}$ MPFs, $1.34*10^{12}$ MPFs, and $2.60*10^{13}$ MPFs were discharged as effluent per year from the Bay View WWTP, the Bowling Green WWTP, and the Southern Cleveland WWTP, respectively.

Without knowing the specific amounts of wastewater discharged from CSO outflows during CSO events, it is hard to accurately assess the total amounts of MPFs discharged from CSOs. Due to the heterogeneity of sludge cake, it is also difficult to assess the total amounts of

MPFs contained within sludge cake. Nonetheless, this work shows that WWTP effluent, CSO effluent, sludge cake, and the atmosphere are significant sources of MPFs to the natural environment. The presence of MPFs among the natural environment is significant due to the potential interaction of MPFs and biological entities. Microplastics have been shown to readily adsorb persistent organic pollutants (POPs), which pose many health risks (such as cancer, immunosuppression, and neurological disruption) to biological entities upon ingestion (Andrady, 2017). The work of this thesis did not specifically analyze for the adsorption of POPs to MPFs. However, given the research conducted by Andrady et al. (2017), it is plausible that POPs were adsorbed to the analyzed MPFs. Future studies should be conducted to confirm the notion that POPs were adsorbed to MPFs found among effluent samples of the analyzed WWTPs. Additionally, this study only analyzed potential sources of MPFs to Lake Erie. It did not analyze the traveling distances of MPFs from the potential sources MPFs into the natural environment. A study conducted by Chubarenko et al. (2016) showed that the residence time of polyester microplastic fibers among a physical model (designed to replicate the environmental conditions of the euphotic zone of a given marine environment) was around 6 to 8-months (Chubarenko, Bagaev, Zobkov, & Esiukova, 2016). This study also proposed that the residence time of polyethylene microbeads among this same environment to be around 10 to 12-years (Chubarenko et al., 2016). Thus, it can be said that there is an inverse relationship between the surface area of a given microplastic particle and its residence time among the euphotic zone of a marine environment. Specifically, it was proposed that a given microplastic particle with a large surface area would have more available binding sites for organic matter than a microplastic particle with a lower surface area. Thus, a given microplastic particle bound to high amounts of organic matter would be heavier and sink more rapidly than a given microplastic particle with a lower amount

of organic matter. Given that WWTP and CSO effluent is known to contain high amounts of organic matter, it is likely that organic matter will readily be attached to MPFs found among WWTP effluent. In which case, these MPFs would either sink to the bottom of a given marine environment in accordance with the flow conditions of the given marine environment or remain suspended in the euphotic zone of a given marine environment for 6 to 8-months. Nonetheless, additional work is required to analyze the mobility of MPFs discharging from the proposed sources to marine environments.

Currently, there are no environmental restrictions regarding the discharge of MPFs into Lake Erie. Given the sheer amounts of MPFs proposed to be discharging from the analyzed sources, and the potential health risks that MPFs pose to biological entities, environmental agencies should begin to discuss regulations on the direct release of MPFs into Lake Erie. These regulations may include restrictions on the number of MPFs allowed to be contained within a given liter of WWTP or CSO effluent discharging into Lake Erie. By implementing and enforcing such regulations in a timely manner, the impact of environmental MPFs could be minimized before the presence of MPFs among the natural environment becomes a known environmental concern.

CHAPTER V. CONCLUSION

Given the strong linear relationship between manual and ImageJ counts of MPFs, the methods utilized by this study to analyze MPFs among potential sources was determined to be successful. Although the standard deviation of MPF counts among each image of effluent samples was lower for manual counts than for ImageJ counts, the automated counting of MPFs using ImageJ was substantially more time efficient and applicable to samples with large quantities of MPFs. Through image analysis, it was discovered that the effluent of the Bowling Green CSO outfall contained a significant portion of MPFs, while the effluent of CSO outfall #201 contained a significant portion of microplastic particles (MPPs). Differences in the morphologies of microplastics identified among samples collected from these two CSOs is most likely related to land cover and land use surrounding the outfalls. Given that a significant portion of MPFs were identified among sludge cake samples, CSOs located near agricultural land use where sludge cake is applied (such as the BG CSO) may contain large quantities of MPFs in comparison to a CSO that is located near an industrial land use.

In comparison to the Bay View and the Southern Cleveland WWTPs, the Bowling Green (BG) WWTP saw the greatest reduction in MPFs from its influent to its effluent. This could be due to the fact that the BG WWTP experiences the lowest flow rate of the three analyzed WWTPs, and that the BG WWTP utilizes a cloth media filtration system. Additionally, it was discovered that the BV and BG WWTPs were less efficient at removing MPFs from their influent to their effluent under “high” flow conditions. In this case, it was proposed that higher flow rates among WWTPs will lead to a decreased capacity for MPF sequestration. Thus, the BG WWTP had the lowest proposed average daily emittance of MPFs among the analyzed WWTPs. Background amounts of MPFs were found to be present among deionized (DI) water samples.

After individually analyzing the utilized sample processing media, it was determined that the atmosphere was the largest contributor of background MPFs to the samples. Given the proposed amounts of background MPFs, the methodologies utilized within this study may not be reproducible. This is further demonstrated by the fact that different aliquots of the same wastewater sample processed independently by two separate researchers (Blane Houck and an undergraduate researcher) saw an order of magnitude difference in MPF counts (Figure 14). Further work should be done to determine if the methodologies used in this study yield consistent results, among aliquots of the same sample processed by separate researchers. Background amounts of MPFs may be reduced by processing samples in a positive-pressure fume hood (a fume hood that does not draw in air from the external environment) or in a "clean lab" (a room designed to reduce airborne contaminants).

Raman analysis revealed that greater than 99-percent of all the analyzed MPFs were composed of polyester. This fits the described model that clothes washing activities are the primary source of MPFs to WWTPs and CSOs. Although, only a small subset of MPFs were analyzed (n=22) relative to the entire population of identified MPFs (n=55,536). Thus, further Raman analysis of MPFs needs to be conducted to satisfy this claim. Given the proposed amounts of MPFs discharging into the environment from the analyzed sample types, and the potential health impacts of MPFs to biological entities, the impact of MPFs discharging into the natural environment may be more significant than previously thought. Future studies should act to determine the fate and mobility of MPFs discharging from WWTPs into the environment. This would allow for a greater understanding of the environmental health implications associated with MPFs. Future studies should also consider MPFs or MPPs discharging from other sources (such as runoff from impervious surfaces).

REFERENCES

Andrady, A. L. (2017). The plastic in microplastics: A review. *Marine Pollution Bulletin*, *119*(1), 12–22. https://doi.org/10.1016/j.marpolbul.2017.01.082

Asadi, A., Verma, A., Yang, K., & Mejabi, B. (2017). Wastewater treatment aeration process optimization: A data mining approach. *Journal of Environmental Management*, *203*, 630–639. https://doi.org/10.1016/j.jenvman.2016.07.047

Bagaev, A., Mizyuk, A., Chubarenko, I., Isachenko, I., & Khatmullina, L. (2017). Anthropogenic fibres in the Baltic Sea water column: Field data, laboratory and numerical testing of their motion. *Science of the total environment*. https://doi.org/10.1016//j.scitotenv.2017.04.185

Baldwin, A. K., Corsi, S. R., De Cicco, L. A., Lenaker, P. L., Lutz, M. A., Sullivan, D. J., & Richards, K. D. (2016). Organic contaminants in Great Lakes tributaries: Prevalence and potential aquatic toxicity. *Science of the Total Environment*, *554–555*, 42–52. https://doi.org/10.1016/j.scitotenv.2016.02.137

Carpenter, D. (2011). Health effects of persistent organic pollutants: The challenge for the Pacific Basin and for the world. *Reviews on environmental health*, *26*, 61–69.

Chidambarampadmavathy, K., Karthikeyan, O. P., & Heimann, K. (2017). Sustainable bio-plastic production through landfill methane recycling. *Renewable & Sustainable Energy Reviews*, *71*, 555–562. https://doi.org/10.1016/j.rser.2016.12.083

Cho, M.-O., Yoon, S., Han, H., & Kim, J. K. (2011). Automated counting of airborne asbestos fibers by a high-throughput microscopy (HTM) method. *Sensors (Basel, Switzerland)*, *11*(7), 7231–7242. https://doi.org/10.3390/s110707231

Christensen, M. L., Keiding, K., Nielsen, P. H., & Jørgensen, M. K. (2015). Dewatering in biological wastewater treatment: A review. *Water Research*, *82*, 14–24.

https://doi.org/10.1016/j.watres.2015.04.019

Chubarenko, I., Bagaev, A., Zobkov, M., & Esiukova, E. (2016). On some physical and dynamical properties of microplastic particles in marine environment. *Marine Pollution Bulletin*, *108*(1), 105–112. https://doi.org/10.1016/j.marpolbul.2016.04.048

Collard, F., Gilbert, B., Eppe, G., Parmentier, E., & Das, K. (2015). Detection of Anthropogenic Particles in Fish Stomachs: An Isolation Method Adapted to Identification by Raman Spectroscopy. *Archives of Environmental Contamination and Toxicology*, *69*(3), 331–339. https://doi.org/10.1007/s00244-015-0221-0

Cooper, D. A., & Corcoran, P. L. (2010). Effects of mechanical and chemical processes on the degradation of plastic beach debris on the island of Kauai, Hawaii. *Marine Pollution Bulletin*, *60*(5), 650–654. https://doi.org/10.1016/j.marpolbul.2009.12.026

Coppock, R. L., Cole, M., Lindeque, P. K., Queirós, A. M., & Galloway, T. S. (2017). A small-scale, portable method for extracting microplastics from marine sediments. *Environmental Pollution*, *230*, 829–837. https://doi.org/10.1016/j.envpol.2017.07.017

Derraik, J. G. B. (2002). The pollution of the marine environment by plastic debris: a review. *Marine Pollution Bulletin*, *44*(9), 842.

Devriese, L. I., De Witte, B., Vethaak, A. D., Hostens, K., & Leslie, H. A. (2017). Bioaccumulation of PCBs from microplastics in Norway lobster (Nephrops norvegicus): An experimental study. *Chemosphere*, *186*, 10–16. https://doi.org/10.1016/j.chemosphere.2017.07.121

Dris, R., Gasperi, J., Saad, M., Mirande, C., & Tassin, B. (2016). Synthetic fibers in atmospheric fallout: A source of microplastics in the environment? *Marine Pollution Bulletin*, *104*(1), 290–293. https://doi.org/10.1016/j.marpolbul.2016.01.006

Fornari, W., Picano, F., Sardina, G., & Brandt, L. (2016). Reduced particle settling speed in turbulence. *Journal of Fluid Mechanics*, *808*, 153–167. https://doi.org/10.1017/jfm.2016.648

Hidalgo-Ruz, V., Gutow, L., Thompson, R. C., & Thiel, M. (2012). Microplastics in the Marine Environment: A Review of the Methods Used for Identification and Quantification. *Environmental Science & Technology*, *46*(6), 3060–3075. https://doi.org/10.1021/es2031505

Homer, C.G., Dewitz, J., Yang, L., Jin, S., Danielson, P., Xian, Coulston, J., Herold, N., Wickham, J. and K. Megown. 2015. Completion of the 2011 National Land Cover Database for the conterminous United States – representing a decade of land cover change information, *Photogrammetric Engineering and Remote Sensing, Vol. 81*, 345-353.

Joseph, N., Kumar, A., Majgi, S. M., Kumar, G. S., & Prahalad, R. B. Y. (2016). Usage of Plastic Bags and Health Hazards: A Study to Assess Awareness Level and Perception about Legislation Among a Small Population of Mangalore City. *Journal Of Clinical And Diagnostic Research: JCDR*, *10*(4), LM01-LM4. https://doi.org/10.7860/JCDR/2016/16245.7529

Kedzierski, M., Le Tilly, V., César, G., Sire, O., & Bruzaud, S. (2017). Efficient microplastics extraction from sand. A cost effective methodology based on sodium iodide recycling. *Marine Pollution Bulletin*, *115*(1–2), 120–129. https://doi.org/10.1016/j.marpolbul.2016.12.002

Kim, J.-H., Kwon, D.-J., Shin, P.-S., Baek, Y.-M., Park, H.-S., DeVries, K. L., & Park, J.-M. (2019). The evaluation of the interfacial and flame retardant properties of glass fiber/unsaturated polyester composites with ammonium dihydrogen phosphate. *Composites*

Part B: Engineering, *167*, 221–230. https://doi.org/10.1016/j.compositesb.2018.12.032

Kumar, P. (2018). Role of Plastics on Human Health. *The Indian Journal of Pediatrics*, *85*(5), 384–389. https://doi.org/10.1007/S12098-017-2595-7

Laforsch, C., Imhof, H. K., Rusek, J., Thiel, M., & Wolinska, J. (2017). Do microplastic particles affect Daphnia magna at the morphological, life history and molecular level? *PLoS ONE*, *12*(11), 1–20. https://doi.org/10.1371/journal.pone.0187590

Lutchmiah, K., Verliefde, A. R. D., Roest, K., Rietveld, L. C., & Cornelissen, E. R. (2014). Forward osmosis for application in wastewater treatment: A review. *Water Research*, *58*, 179–197. https://doi.org/10.1016/j.watres.2014.03.045

Mason, S. A., Garneau, D., Sutton, R., Chu, Y., Ehmann, K., Barnes, J., … Rogers, D. L. (2016). Microplastic pollution is widely detected in US municipal wastewater treatment plant effluent. *Environmental Pollution*, *218*, 1045–1054. https://doi.org/10.1016/j.envpol.2016.08.056

Mintenig, S. M., Int-Veen, I., Löder, M. G. J., Primpke, S., & Gerdts, G. (2017). Identification of microplastic in effluents of waste water treatment plants using focal plane array-based micro-Fourier-transform infrared imaging. *Water Research*, *108*, 365–372. https://doi.org/10.1016/j.watres.2016.11.015

Moore, C. J. (2008). Synthetic polymers in the marine environment: A rapidly increasing, long-term threat. *Environmental Research*, *108*(2), 131–139. https://doi.org/10.1016//j.envres.2008.07.025

Napper, I. E., & Thompson, R. C. (2016). Release of synthetic microplastic plastic fibres from domestic washing machines: Effects of fabric type and washing conditions. *Marine Pollution Bulletin*, *112*(1–2), 39–45. https://doi.org/10.1016/j.marpolbul.2016.09.025

Pirc, U., Vidmar, M., Mozer, A., & Kržan, A. (2016). Emissions of microplastic fibers from microfiber fleece during domestic washing. *Environmental Science & Pollution Research*, *23*(21), 22206–22211.

Pracheil, B., Marshall Adams, S., Bevelhimer, M., Fortner, A., Greeley, M., Murphy, C., … Peterson, M. (2016). Relating fish health and reproductive metrics to contaminant bioaccumulation at the Tennessee Valley Authority Kingston coal ash spill site. *Ecotoxicology*, *25*(6), 1136–1149.

Rochman, C. M., Tahir, A., Williams, S. L., Baxa, D. V, Lam, R., Miller, J. T., … Teh, S. J. (2015). Anthropogenic debris in seafood: Plastic debris and fibers from textiles in fish and bivalves sold for human consumption. *Scientific Reports*, 14340. https://doi.org/10.1038/srep14340

Saini, D. R., & Shenoy, A. V. (1985). Melt Rheology of Some Specialty Polymers. *Journal of Elastomers & Plastics*, *17*(3), 189–217. https://doi.org/10.1177/009524438501700305

Sekaluvu, L., Zhang, L., & Gitau, M. (2018). Evaluation of constraints to water quality improvements in the Western Lake Erie Basin. *Journal of Environmental Management*, *205*, 85–98. https://doi.org/10.1016/j.jenvman.2017.09.063

Setälä, O., Fleming, V., & Lehtiniemi, M. (2013). Ingestion and transfer of microplastics in the planktonic food web. *Environmental pollution (Barking, Essex : 1987)*, *185C*, 77–83.

Shen, Y., Linville, J. L., Urgun-Demirtas, M., Mintz, M. M., & Snyder, S. W. (2015). An overview of biogas production and utilization at full-scale wastewater treatment plants (WWTPs) in the United States: Challenges and opportunities towards energy-neutral WWTPs. *Renewable & Sustainable Energy Reviews*, *50*, 346–362. https://doi.org/10.1016/j.rser.2015.04.129

Steer, M., Cole, M., Thompson, R. C., & Lindeque, P. K. (2017). Microplastic ingestion in fish larvae in the western English Channel. *Environmental Pollution*. https://doi.org/10.1016/j.envpol.2017.03.062

Tsang, Y. Y., Mak, C. W., Liebich, C., Lam, S. W., Sze, E. T. P., & Chan, K. M. (2017). Microplastic pollution in the marine waters and sediments of Hong Kong. *Marine Pollution Bulletin*, *115*(1–2), 20–28. https://doi.org/10.1016/j.marpolbul.2016.11.003

van Wezel, A., Caris, I., & Kools, S. A. E. (2016). Release of primary microplastics from consumer products to wastewater in the Netherlands. *Environmental Toxicology And Chemistry*, *35*(7), 1627–1631. https://doi.org/10.1002/etc.3316

Watson, S. B., Miller, C., Arhonditsis, G., Boyer, G. L., Carmichael, W., Charlton, M. N., … Wilhelm, S. W. (2016). The re-eutrophication of Lake Erie: Harmful algal blooms and hypoxia. *Harmful algae*, *56*, 44–66. https://doi.org/10.1016/j.hal.2016.04.010

Wright, S. L., & Kelly, F. J. (2017). Plastic and Human Health: A Micro Issue? *Environmental Science and Technology*. https://doi.org/10.1021/acs.est.7b00423

Zhang, K., Gong, W., Lv, J., Xiong, X., & Wu, C. (2015). Accumulation of floating microplastics behind the Three Gorges Dam. *Environmental Pollution*, *204*, 117–123. https://doi.org/10.1016/j.envpol.2015.04.023

Ziajahromi, S., Neale, P. A., & Leusch, F. D. L. (2016). Wastewater treatment plant effluent as a source of microplastics: review of the fate, chemical interactions and potential risks to aquatic organisms. *Water Science & Technology*, *74*(10), 2253–2269.

APPENDIX A. TABLES OF IMAGEJ AND MANUAL COUNTS OF MPFS

This appendix contains a series of tables that present the comparison of ImageJ counts via the MPF ImageJ macro to manual counts of MPFs for samples of effluent. The mean and standard deviation values represent the average number of MPFs counted among each image and the deviation of MPFs counted among each image, respectively. A two-tailed paired t-test, with a threshold value of 0.05, was used to determine if a significant difference existed between ImageJ and manual counts. A "percent matching" value was used to depict the number of instances where ImageJ counts were equal to manual counts for each image relative to the total number of images.

Table A1. Shows a comparison of the ImageJ MPF counts to the manual MPF counts for a liter of effluent collected from the Bay View WWTP on 4/30/18.

	Image J Counts	**Manual Counts**
Sum	783.000	1070.000
Mean (MPFs/Picture)	3.000	4.100
Standard Deviation (MPFs/Picture)	3.427	5.886
Number of Pictures	261.000	
t	3.198	
Degrees of Freedom	260.000	
Statistical Difference?	Yes	
P-Value	0.0016	
Standard Error or Difference	0.344	
Percent Matching	15.3256705	

Table A2. Shows a comparison of the ImageJ MPF counts to the manual MPF counts for a liter of effluent collected from the Bay View WWTP on 5/21/18.

	Image J Counts	**Manual Counts**
Sum	620.000	805.000
Mean (MPFs/Picture)	1.086	1.410
Standard Deviation (MPFs/Picture)	1.839	1.227
Number of Pictures	571.000	
t	4.1176	
Degrees of Freedom	570.000	
Statistical Difference?	Yes	
P-Value	< 0.0001	
Standard Error or Difference	0.079	
Percent Matching	29.07	

Table A3. Shows a comparison of the ImageJ MPF counts to the manual MPF counts for a liter of effluent collected from the Bay View WWTP on 6/12/18.

	Image J Counts	**Manual Counts**
Sum	869.000	751.000
Mean (MPFs/Picture)	0.655	0.566
Standard Deviation (MPFs/Picture)	2.457	0.913
Number of Pictures	1327	
t	1.4021	
Degrees of Freedom	1326	
Statistical Difference?	No	
P-Value	0.1611	
Standard Error or Difference	0.063	
Percent Matching	65.34	

Table A4. Shows a comparison of the ImageJ MPF counts to the manual MPF counts for a liter of effluent collected from the Bay View WWTP on 9/10/18. This represents the first aliquot from this sample date.

	Image J Counts	**Manual Counts**
Sum	472.000	496.000
Mean (MPFs/Picture)	2.000	2.102
Standard Deviation (MPFs/Picture)	1.643	1.288
Number of Pictures	238	
t	0.2653	
Degrees of Freedom	237	
Statistical Difference?	No	
P-Value	0.791	
Standard Error or Difference	0.127	
Percent Matching	32.35	

Table A5. Shows a comparison of the ImageJ MPF counts to the manual MPF counts for a liter of effluent collected from the Bay View WWTP on 9/10/18. This represents the second aliquot from this sample date.

	Image J Counts	**Manual Counts**
Sum	494.000	457.000
Mean (MPFs/Picture)	2.205	2.040
Standard Deviation (MPFs/Picture)	1.996	1.418
Number of Pictures	224	
t	1.3472	
Degrees of Freedom	223	
Statistical Difference?	No	
P-Value	0.1793	
Standard Error or Difference	0.123	
Percent Matching	31.25	

Table A6. Shows a comparison of the ImageJ MPF counts to the manual MPF counts for a liter of effluent collected from the Bowling Green WWTP on 7/9/18.

	Image J Counts	**Manual Counts**
Sum	456.000	886.000
Mean (MPFs/Picture)	0.656	1.275
Standard Deviation (MPFs/Picture)	1.327	1.620
Number of Pictures	695	
t	9.8735	
Degrees of Freedom	694	
Statistical Difference?	Yes	
P-Value	< 0.0001	
Standard Error or Difference	0.063	
Percent Matching	48.49	

Table A7. Shows a comparison of the ImageJ MPF counts to the manual MPF counts for a liter of effluent collected from the Bowling Green WWTP on 9/25/18. This represents the first aliquot from this sample date.

	ImageJ Counts	**Manual Counts**
Sum	180.000	97.000
Mean (MPFs/Picture)	2.769	1.492
Standard Deviation (MPFs/Picture)	2.603	0.954
Number of Pictures	65	
t	3.6082	
Degrees of Freedom	64	
Statistical Difference?	Yes	
P-Value	0.0006	
Standard Error or Difference	0.354	
Percent Matching	23.08	

Table A8. Shows a comparison of the ImageJ MPF counts to the manual MPF counts for a liter of effluent collected from the Bowling Green WWTP on 9/25/18. This represents the second aliquot from this sample date.

	Image J Counts	**Manual Counts**
Sum	167.000	105.000
Mean (MPFs/Picture)	1.988	1.250
Standard Deviation (MPFs/Picture)	2.114	0.726
Number of Pictures	84	
t	3.361	
Degrees of Freedom	83	
Statistical Difference?	Yes	
P-Value	0.0012	
Standard Error or Difference	0.22	
Percent Matching	34.52	

Table A9. Shows a comparison of the ImageJ MPF counts to the manual MPF counts for a liter of effluent collected from the Bowling Green WWTP on 12/5/18. This represents the first aliquot from this sample date.

	Image J Counts	**Manual Counts**
Sum	393.000	473.000
Mean (MPFs/Picture)	1.975	2.377
Standard Deviation (MPFs/Picture)	2.407	1.753
Number of Pictures	199	
t	2.3657	
Degrees of Freedom	198	
Statistical Difference?	Yes	
P-Value	0.019	
Standard Error or Difference	0.17	
Percent Matching	25.13	

Table A10. Shows a comparison of the ImageJ MPF counts to the manual MPF counts for a liter of effluent collected from the Bowling Green WWTP on 12/5/18. This represents the second aliquot from this sample date.

	Image J Counts	**Manual Counts**
Sum	316.000	402.000
Mean (MPFs/Picture)	1.557	1.980
Standard Deviation (MPFs/Picture)	1.935	1.772
Number of Pictures	203	
t	2.9006	
Degrees of Freedom	202	
Statistical Difference?	Yes	
P-Value	0.0041	
Standard Error or Difference	0.127	
Percent Matching	29.06	

Table A11. Shows a comparison of the ImageJ MPF counts to the manual MPF counts for a liter of effluent collected from the Southern Cleveland WWTP on 7/26/18. This represents the first aliquot from this sample date.

	Image J Counts	**Manual Counts**
Sum	506.000	631.000
Mean (MPFs/Picture)	1.020	1.272
Standard Deviation (MPFs/Picture)	1.934	1.081
Number of Pictures	496	
t	2.8502	
Degrees of Freedom	495	
Statistical Difference?	Yes	
P-Value	0.0046	
Standard Error or Difference	0.088	
Percent Matching	34.68	

Table A12. Shows a comparison of the ImageJ MPF counts to the manual MPF counts for a liter of effluent collected from the Southern Cleveland WWTP on 7/26/18. This represents the second aliquot from this sample date.

	Image J Counts	**Manual Counts**
Sum	399.000	358.000
Mean (MPFs/Picture)	0.819	0.735
Standard Deviation (MPFs/Picture)	1.638	0.842
Number of Pictures	487	
t	1.1423	
Degrees of Freedom	486	
Statistical Difference?	No	
P-Value	0.2539	
Standard Error or Difference	0.074	
Percent Matching	51.95	

Table A13. Shows a comparison of the ImageJ MPF counts to the manual MPF counts for a liter of effluent collected from the Southern Cleveland WWTP on 11/10/18.

	Image J Counts	**Manual Counts**
Sum	479	391
Mean (MPFs/Picture)	3.303	2.697
Standard Deviation (MPFs/Picture)	4.147	3.644
Number of Pictures	145	
t	2.2271	
Degrees of Freedom	144	
Statistical Difference?	Yes	
P-Value	0.0275	
Standard Error or Difference	0.273	
Percent Matching	25.52	

APPENDIX B. RAMAN SHIFTS

This appendix contains a series of figures showing the Raman spectra of MPFs (unknown in their compositions) and the Raman spectra of plastic materials (known in their compositions). Raman shifts were gathered over a range of one-hundred to four-thousand inverse centimeters. The color of a given MPF refers to its observed birefringent color.

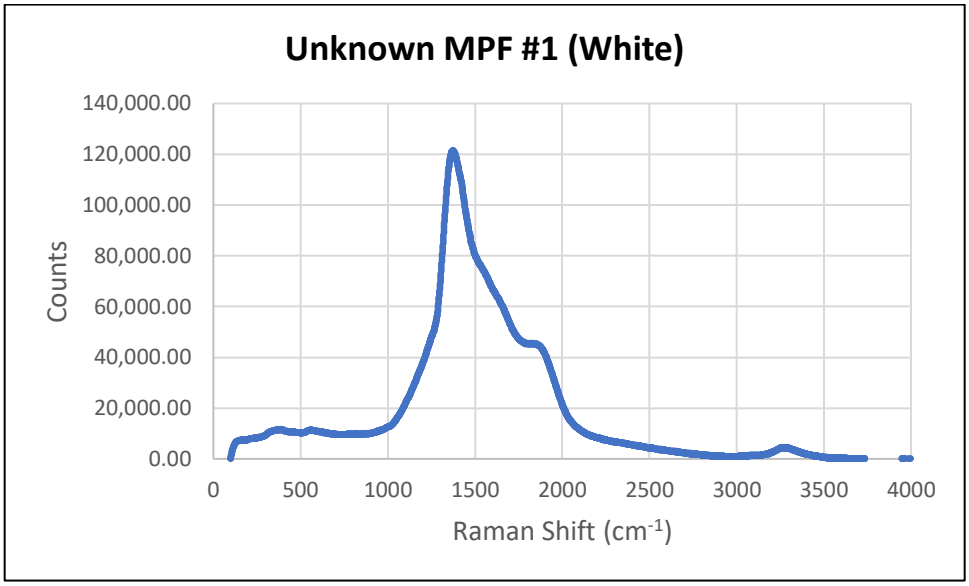

Figure B1. Shows the Raman spectra of a MPF, unknown in its composition, with a white birefringent color.

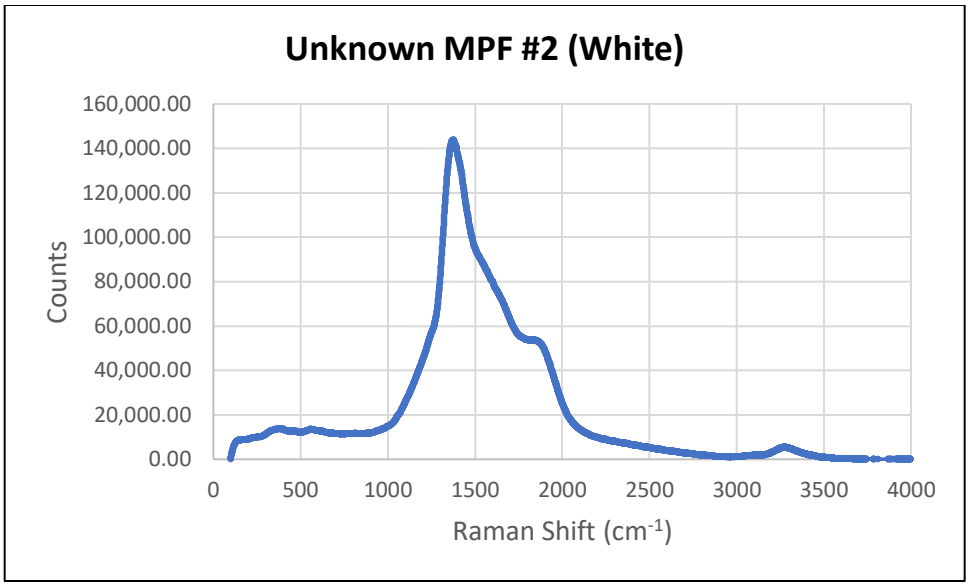

Figure B2. Shows the Raman spectra of a MPF, unknown in its composition, with a white birefringent color.

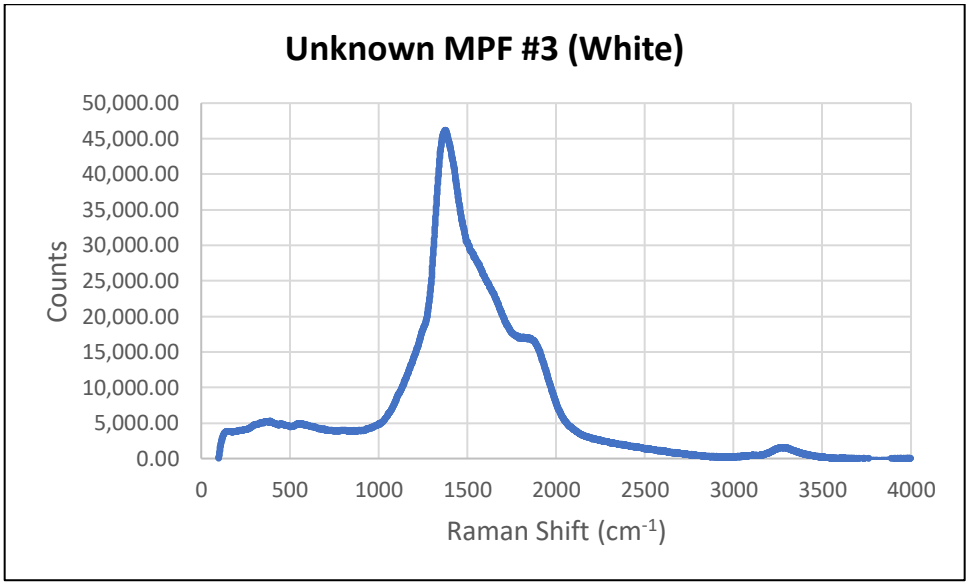

Figure B3. Shows the Raman spectra of a MPF, unknown in its composition, with a white birefringent color.

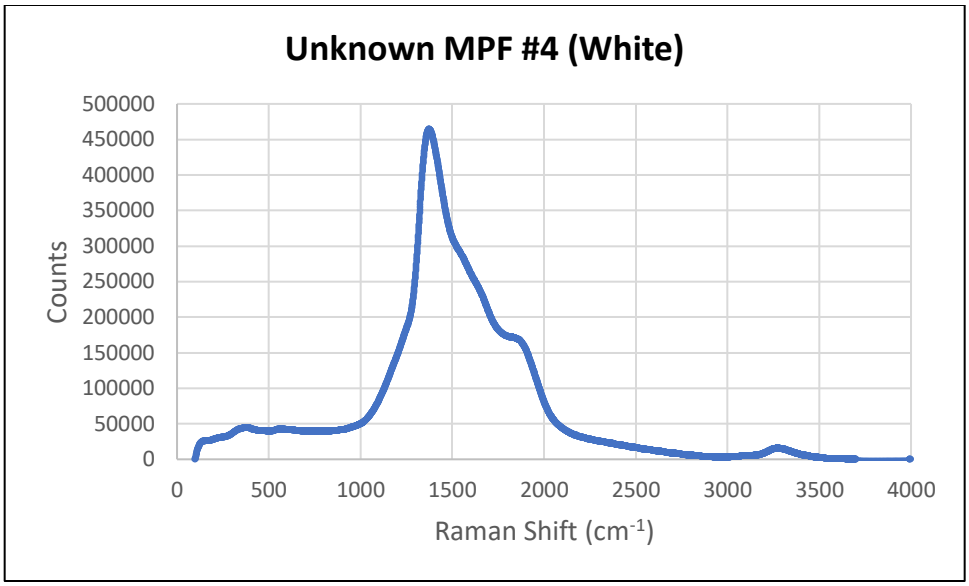

Figure B4. Shows the Raman spectra of a MPF, unknown in its composition, with a white birefringent color.

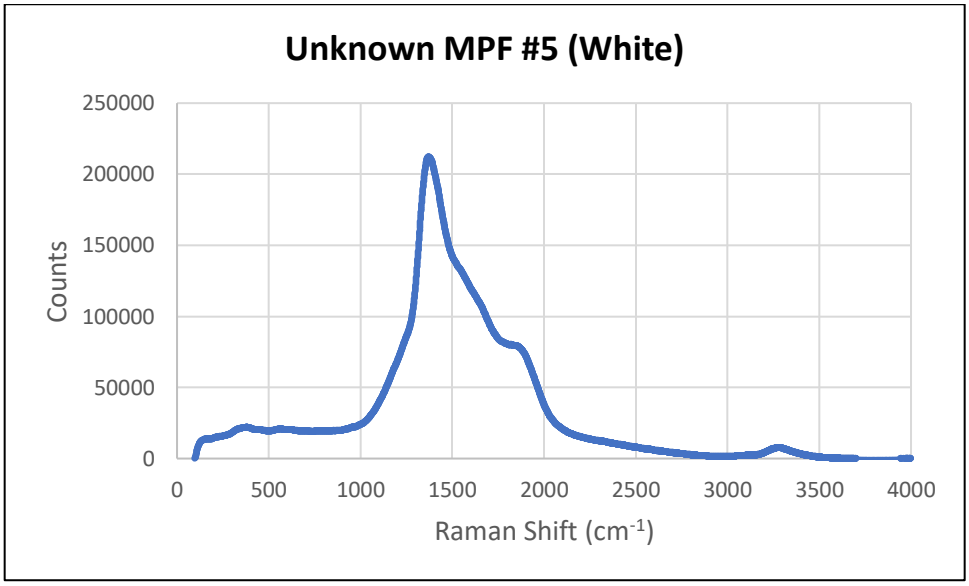

Figure B5. Shows the Raman spectra of a MPF, unknown in its composition, with a white birefringent color.

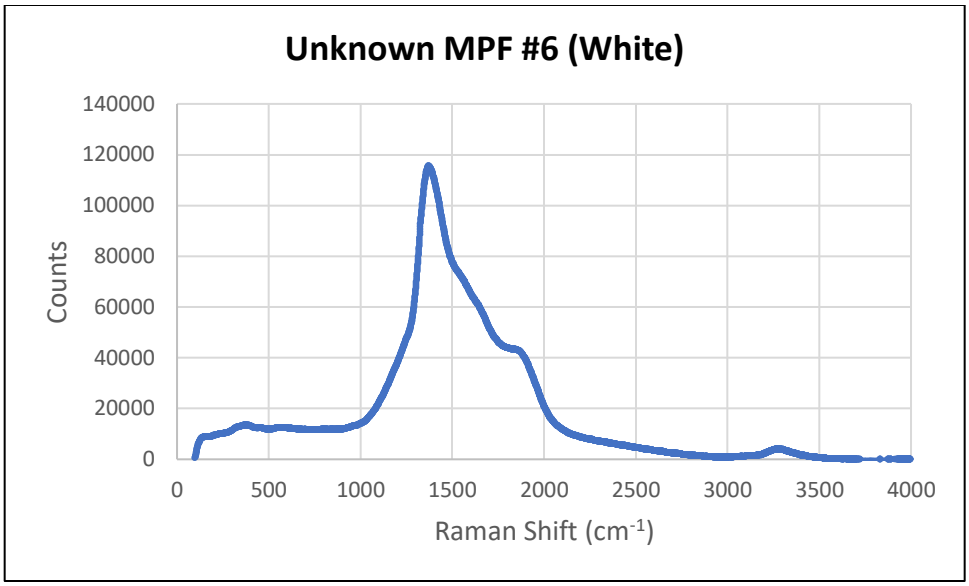

Figure B6. Shows the Raman spectra of a MPF, unknown in its composition, with a white birefringent color.

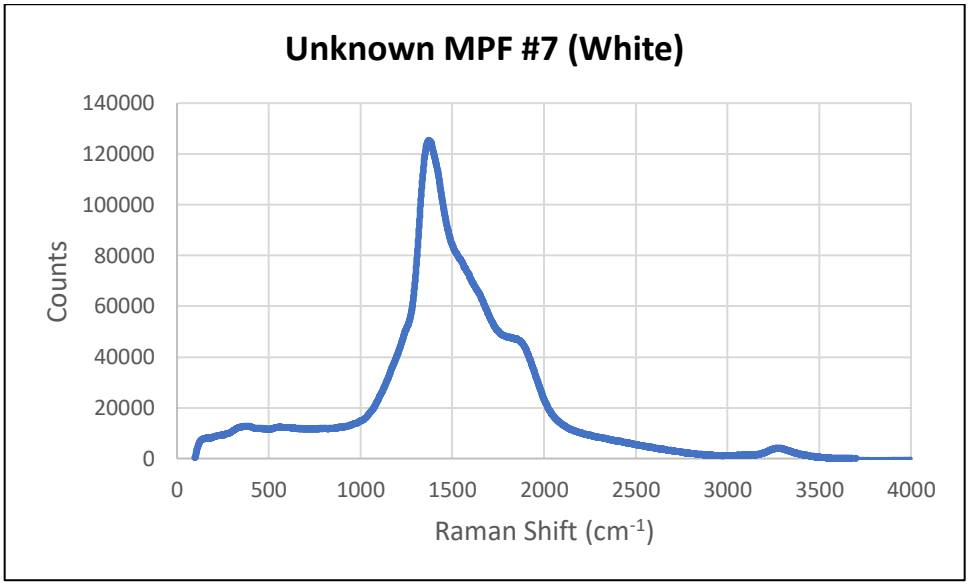

Figure B7. Shows the Raman spectra of a MPF, unknown in its composition, with a white birefringent color.

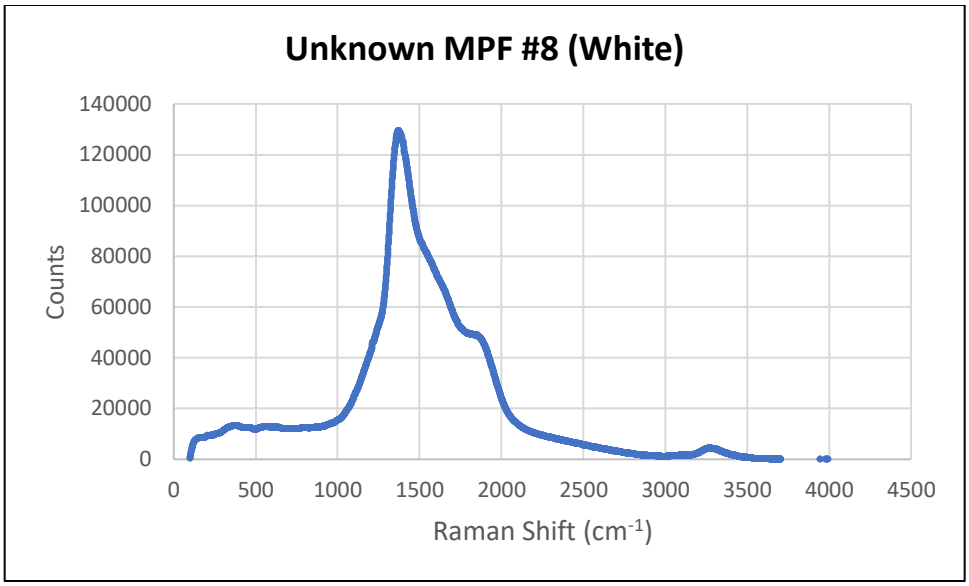

Figure B8. Shows the Raman spectra of a MPF, unknown in its composition, with a white birefringent color.

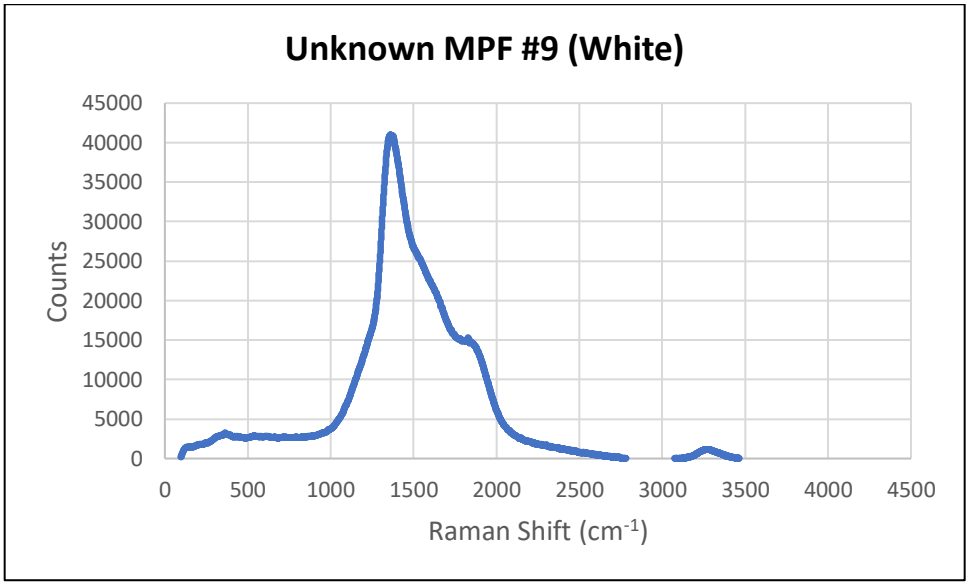

Figure B9. Shows the Raman spectra of a MPF, unknown in its composition, with a white birefringent color.

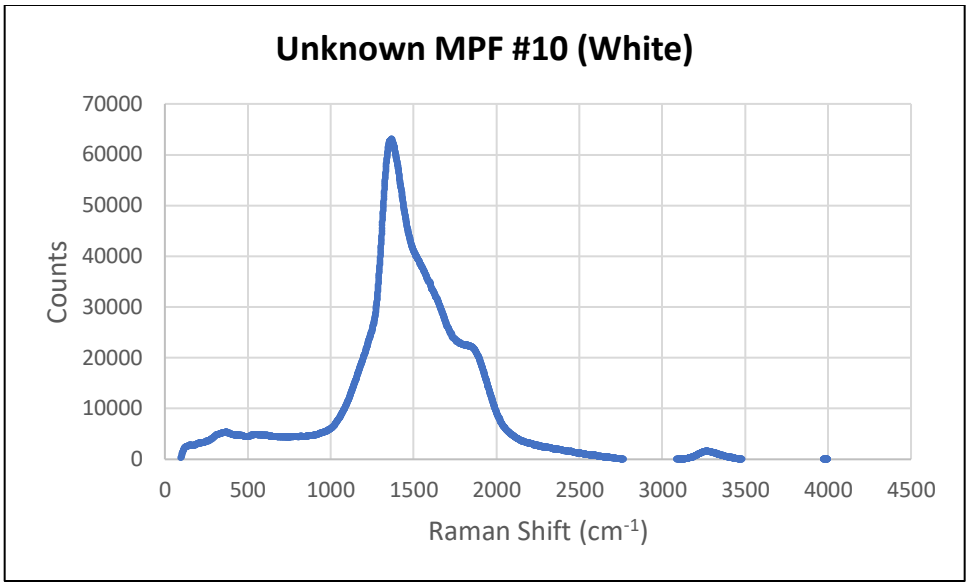

Figure B10. Shows the Raman spectra of a MPF, unknown in its composition, with a white birefringent color.

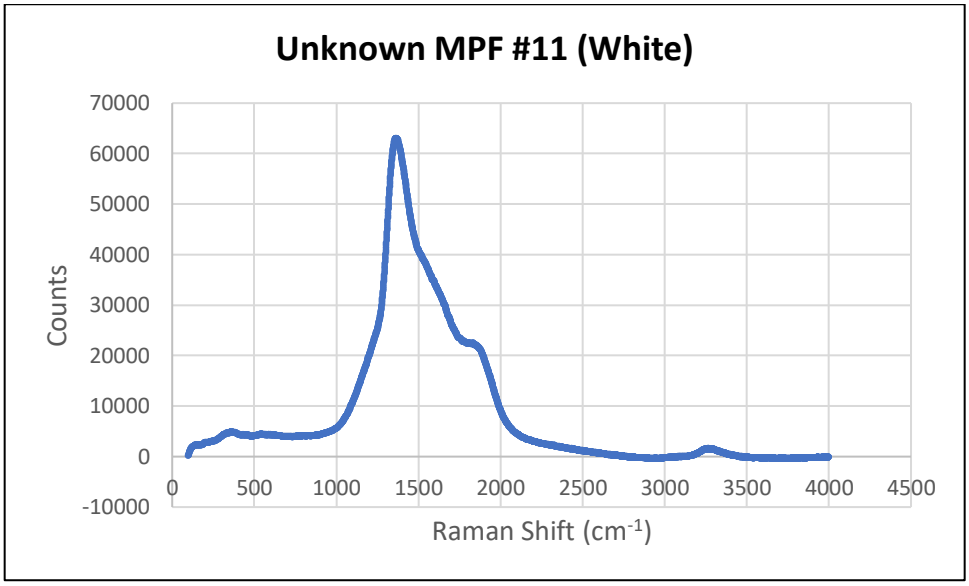

Figure B11. Shows the Raman spectra of a MPF, unknown in its composition, with a white birefringent color.

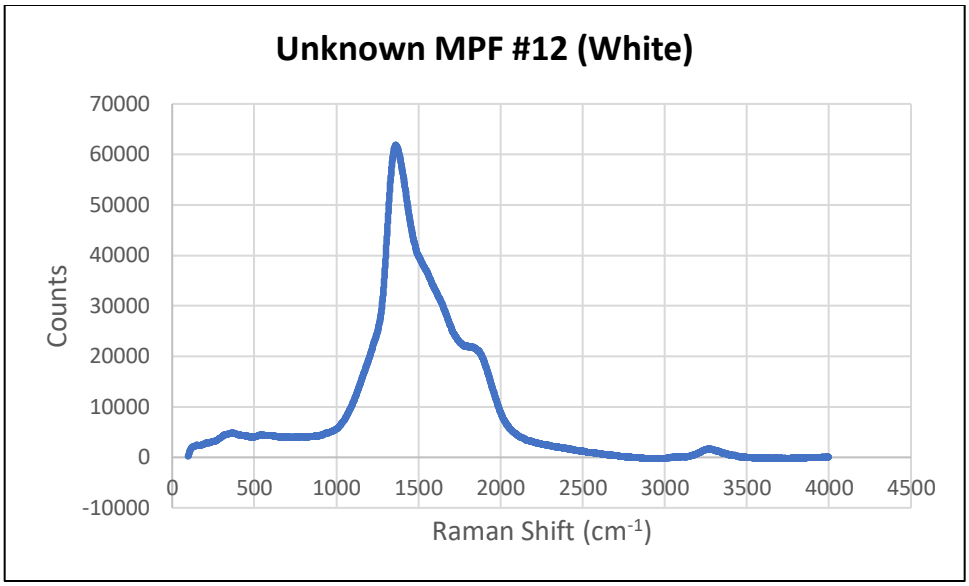

Figure B12. Shows the Raman spectra of a MPF, unknown in its composition, with a white birefringent color.

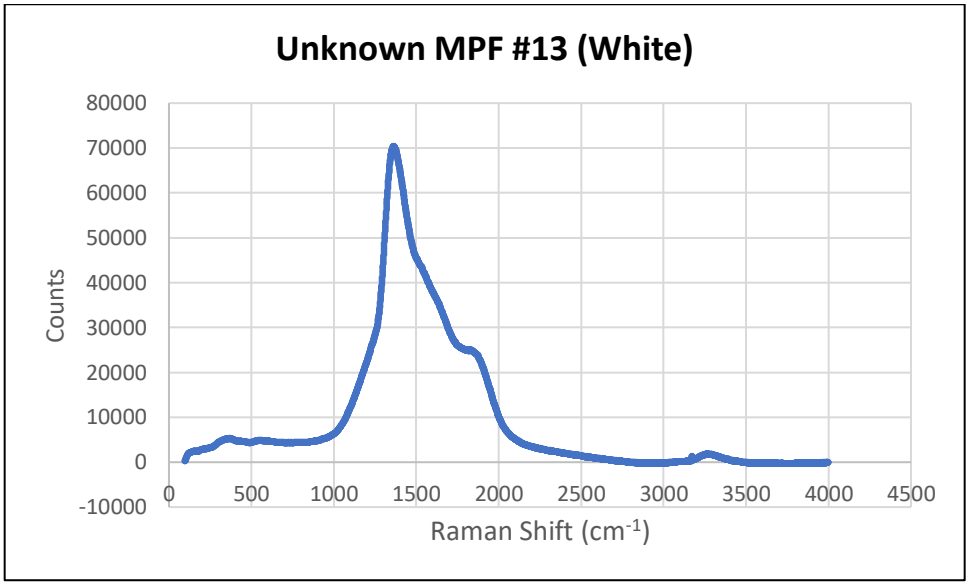

Figure B13. Shows the Raman spectra of a MPF, unknown in its composition, with a white birefringent color.

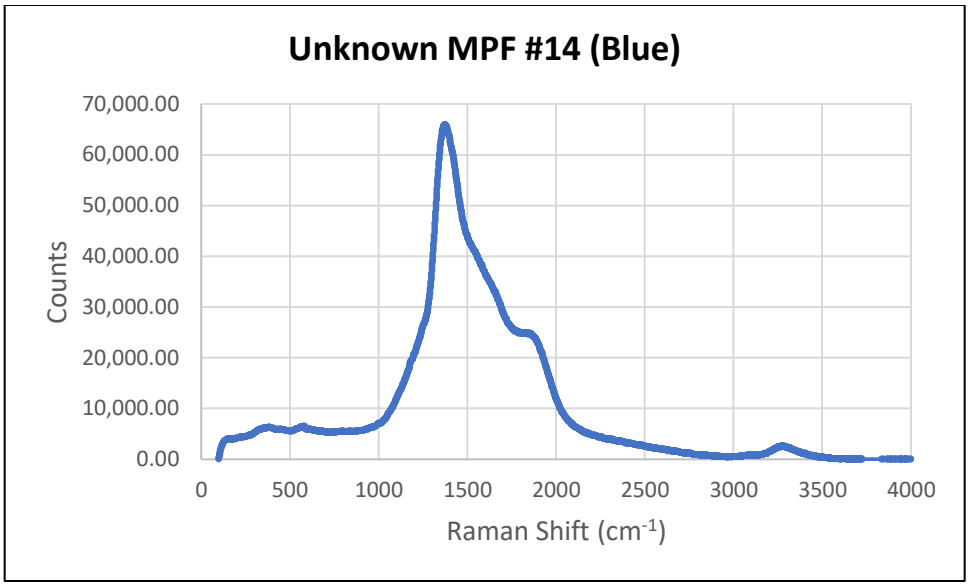

Figure B14. Shows the Raman spectra of a MPF, unknown in its composition, with a blue birefringent color.

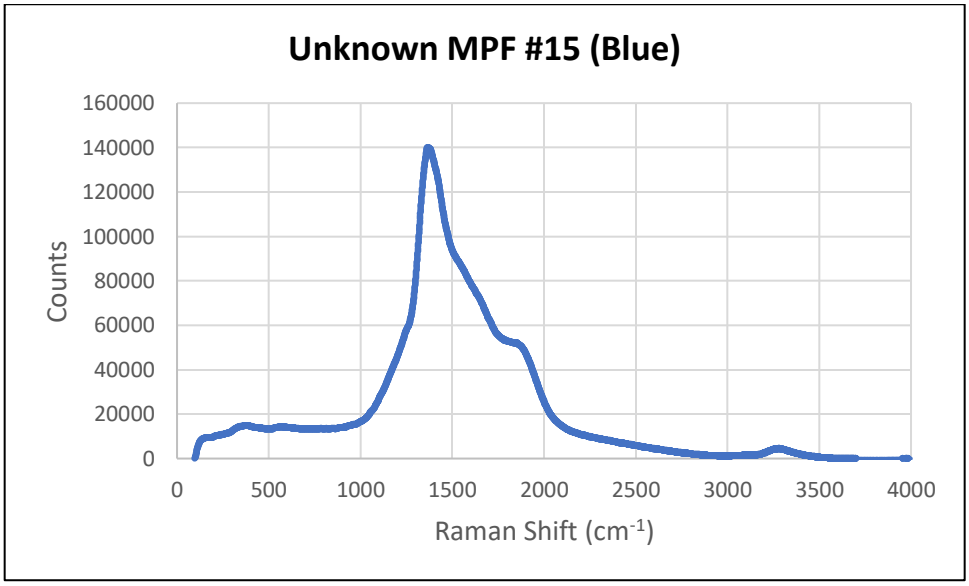

Figure B15. Shows the Raman spectra of a MPF, unknown in its composition, with a blue birefringent color.

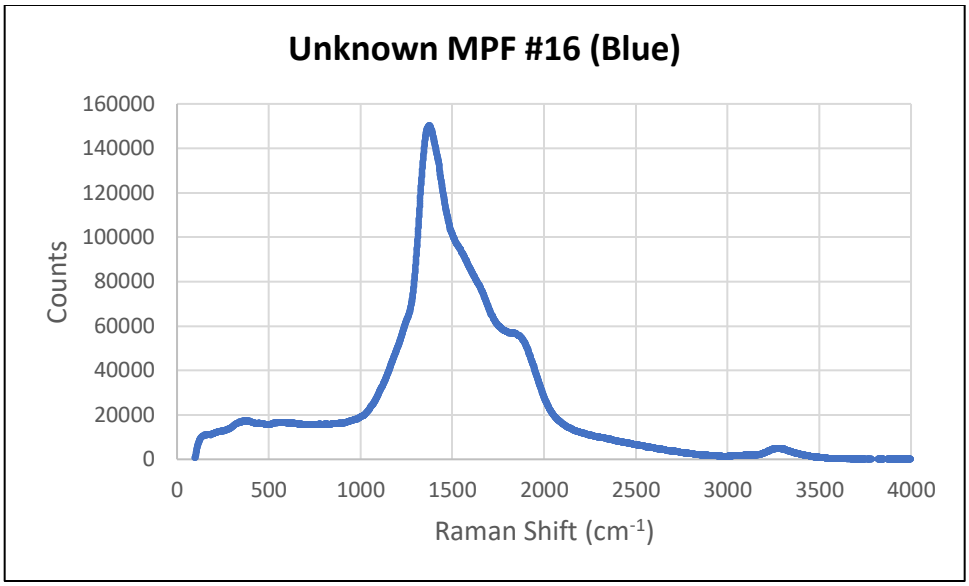

Figure B16. Shows the Raman spectra of a MPF, unknown in its composition, with a blue birefringent color.

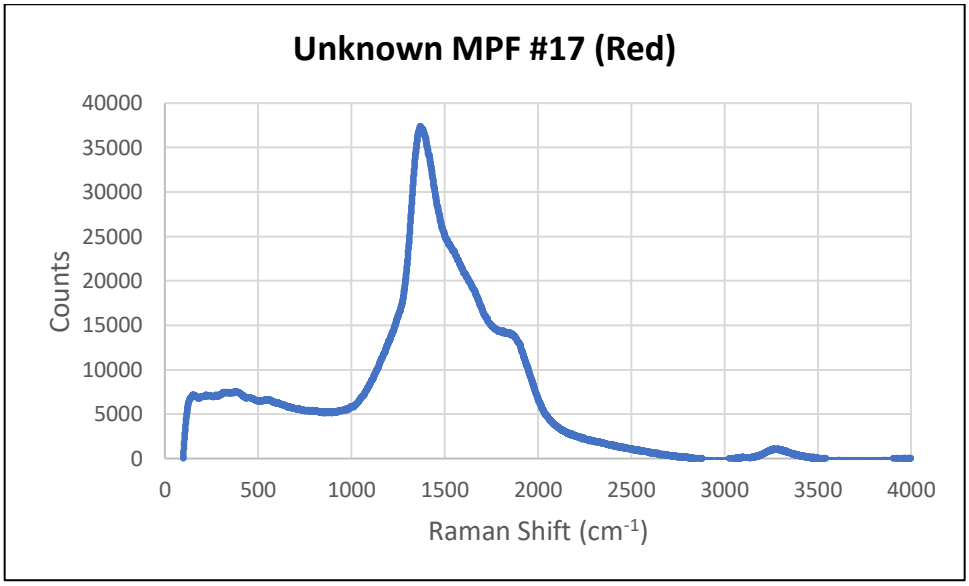

Figure B17. Shows the Raman spectra of a MPF, unknown in its composition, with a red birefringent color.

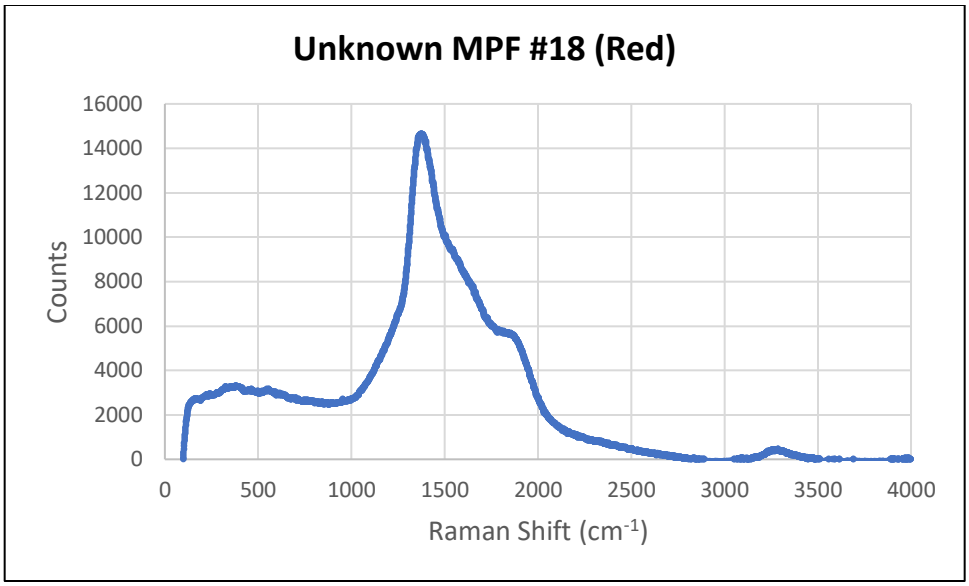

Figure B18. Shows the Raman spectra of a MPF, unknown in its composition, with a red birefringent color.

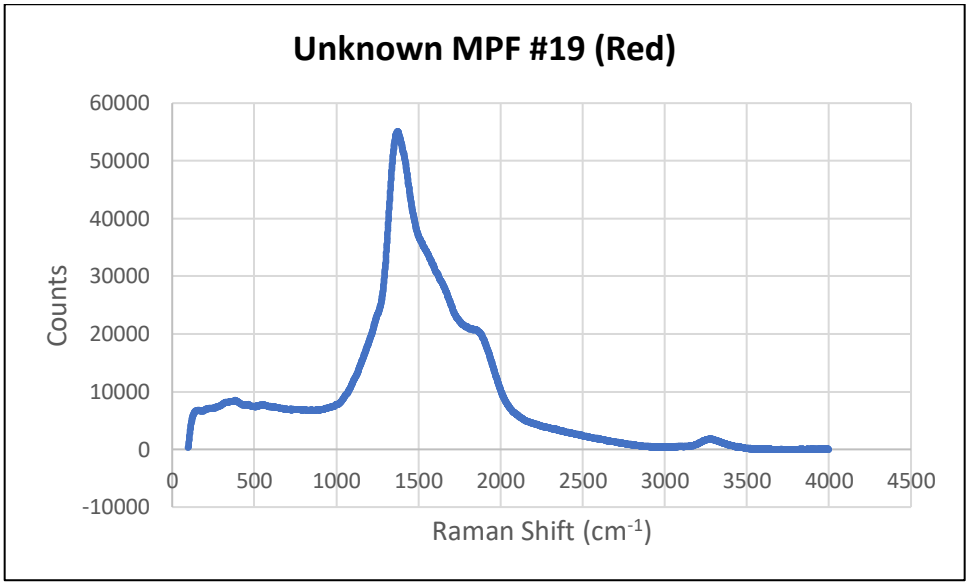

Figure B19. Shows the Raman spectra of a MPF, unknown in its composition, with a red birefringent color.

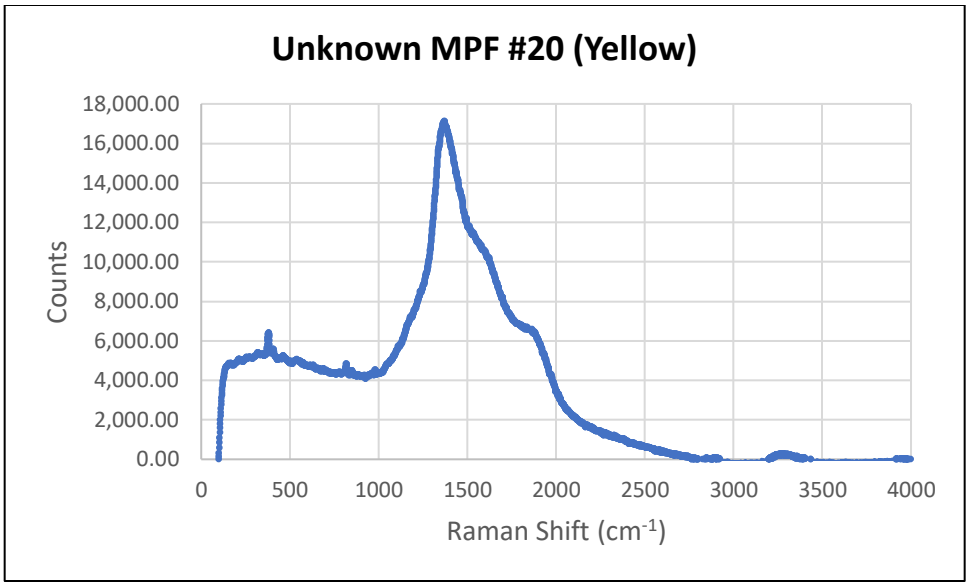

Figure B20. Shows the Raman spectra of a MPF, unknown in its composition, with a yellow birefringent color.

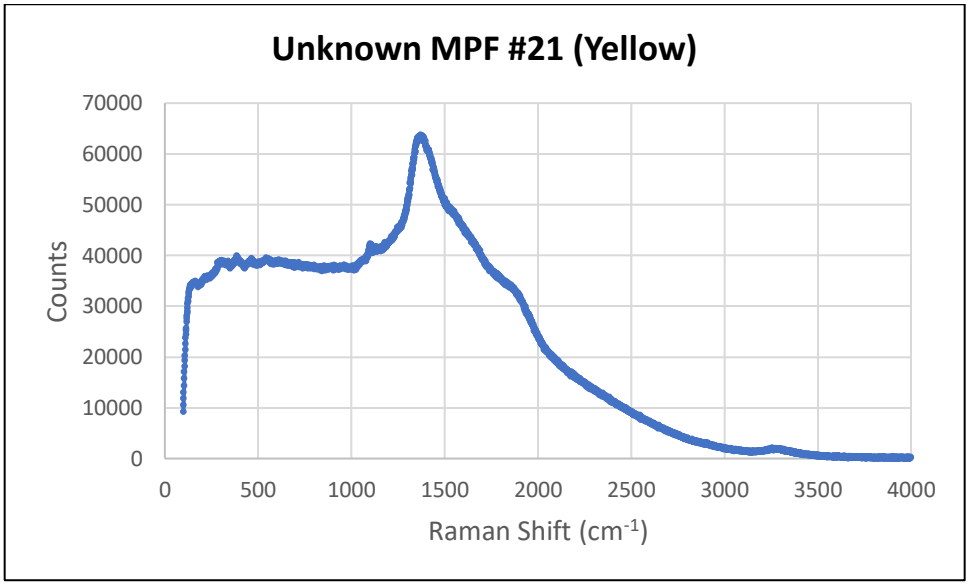

Figure B21. Shows the Raman spectra of a MPF, unknown in its composition, with a yellow birefringent color.

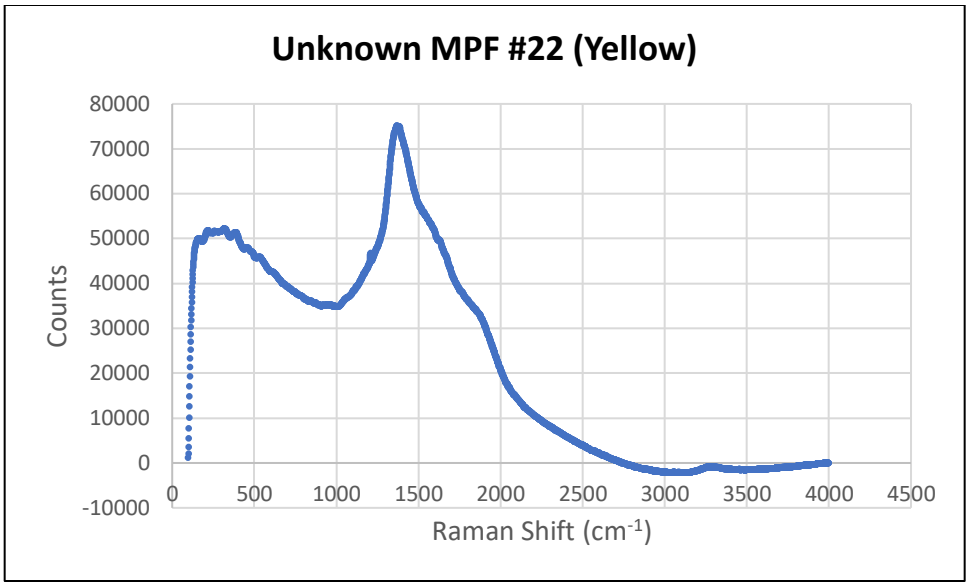

Figure B22. Shows the Raman spectra of a MPF, unknown in its composition, with a yellow birefringent color.

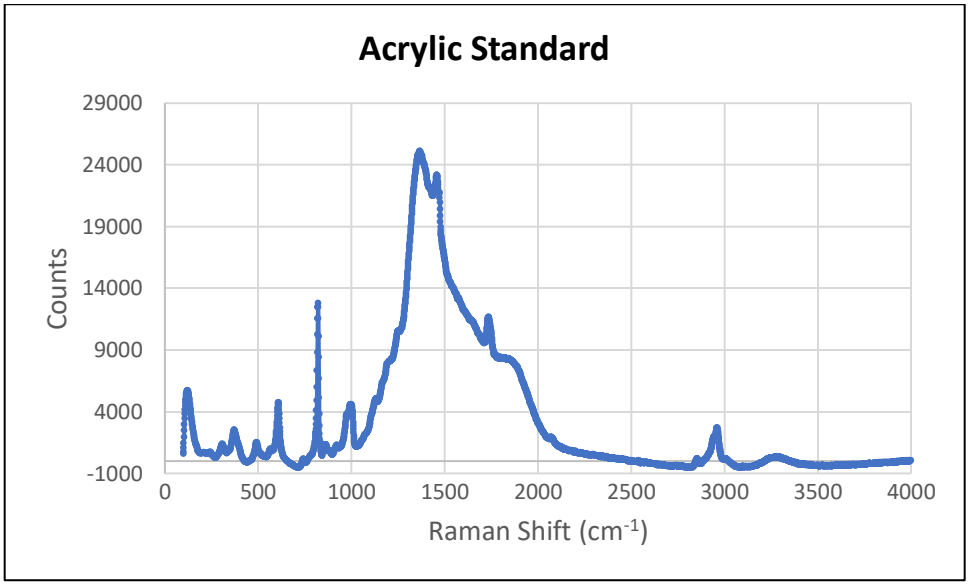

Figure B23. Shows the Raman spectra obtained from a 1/8-inch diameter acrylic bead (U.S. Plastics).

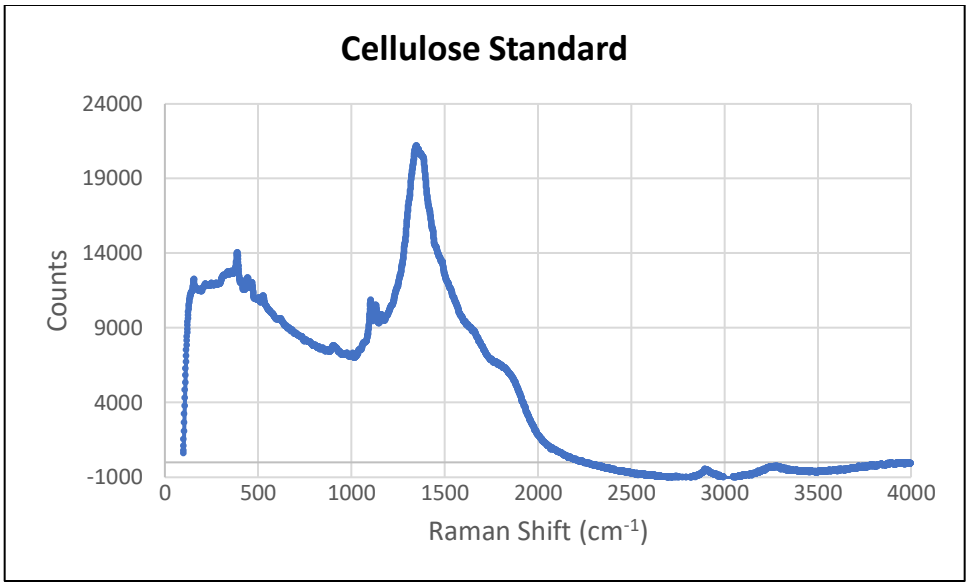

Figure B24. Shows the Raman spectra obtained from a Cellulose microcrystalline powder (Arcos Organics).

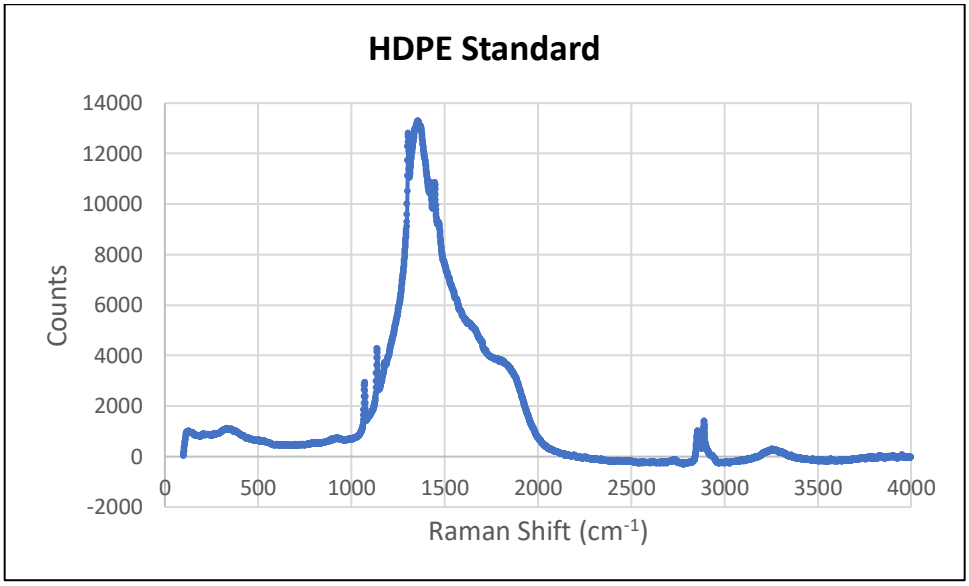

Figure B25. Shows the Raman spectra obtained from a 1/8-inch diameter HDPE bead (U.S. Plastics).

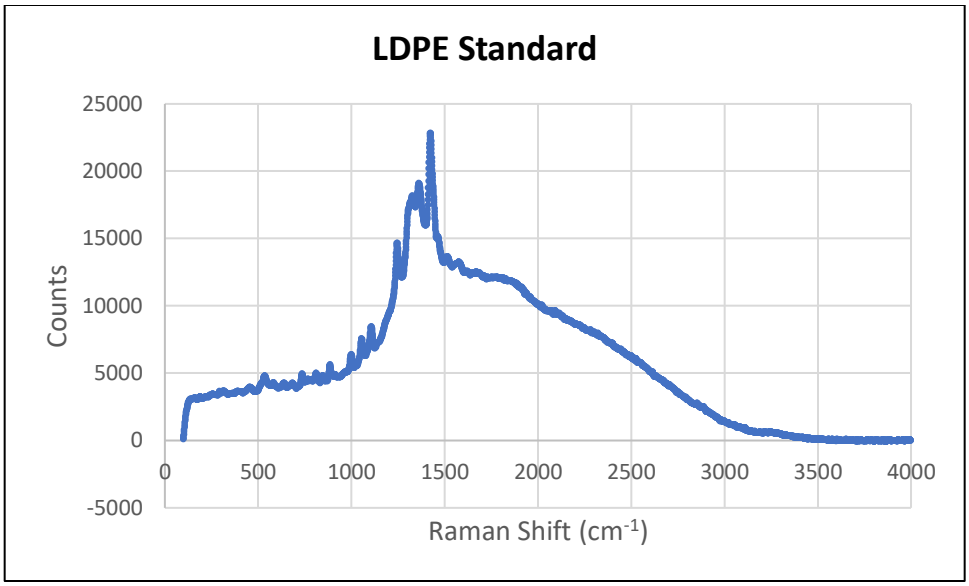

Figure B26. Shows the Raman spectra obtained from a LDPE film (U.S. Plastics).

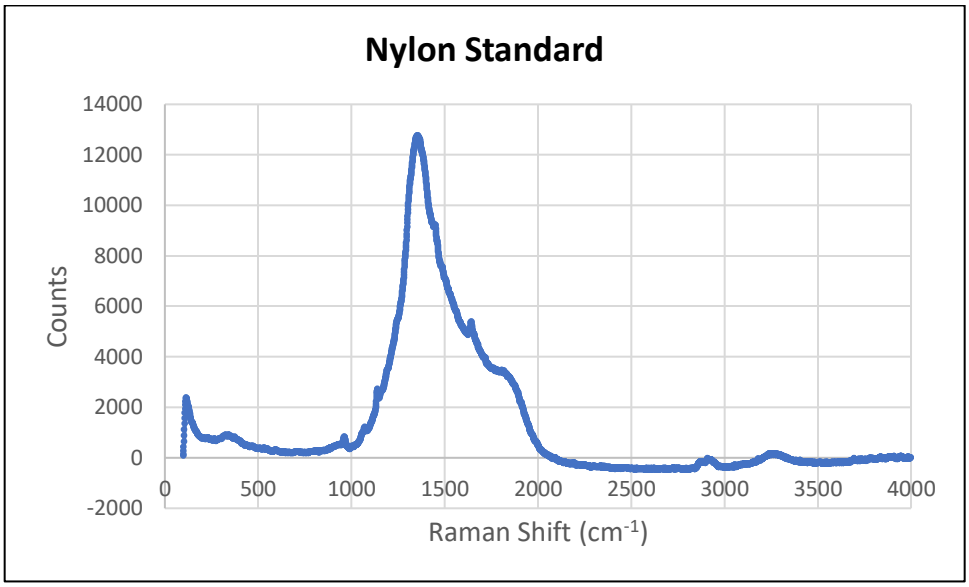

Figure B27. Shows the Raman spectra obtained from a 1/8-inch diameter Nylon bead (U.S. Plastics).

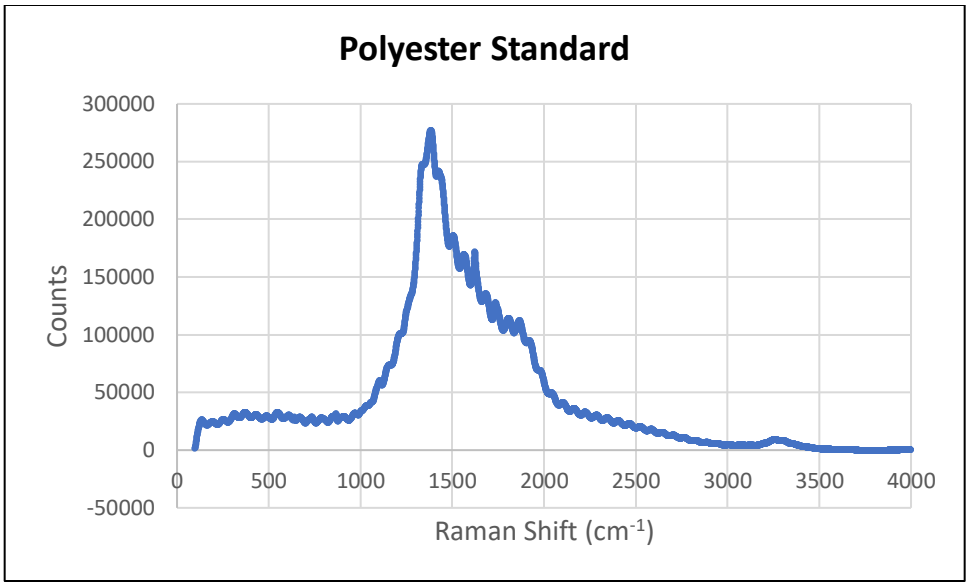

Figure B28. Shows the Raman spectra obtained from a Polyester film (U.S. Plastics).

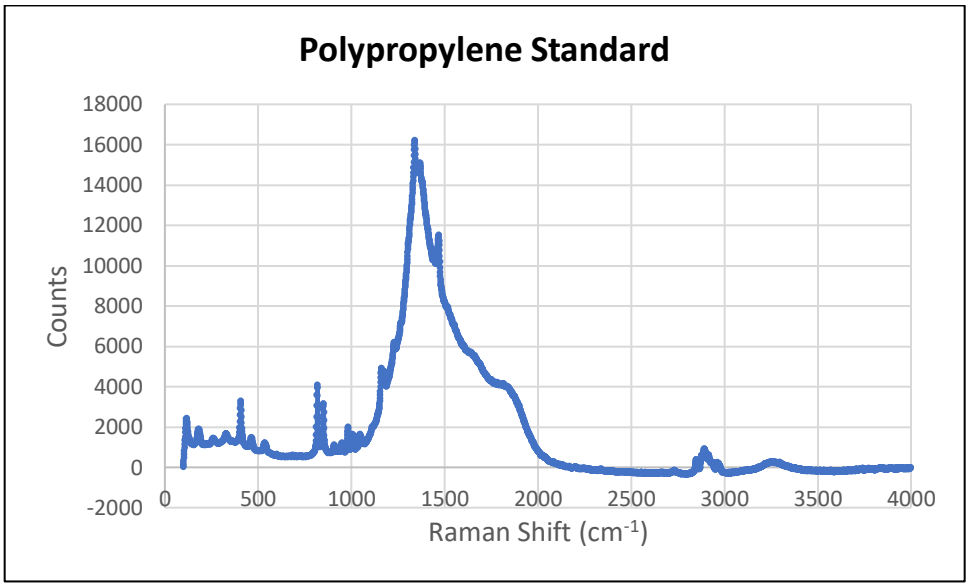

Figure B29. Shows the Raman spectra obtained from a 1/8-inch diameter Polypropylene bead (U.S. Plastics).

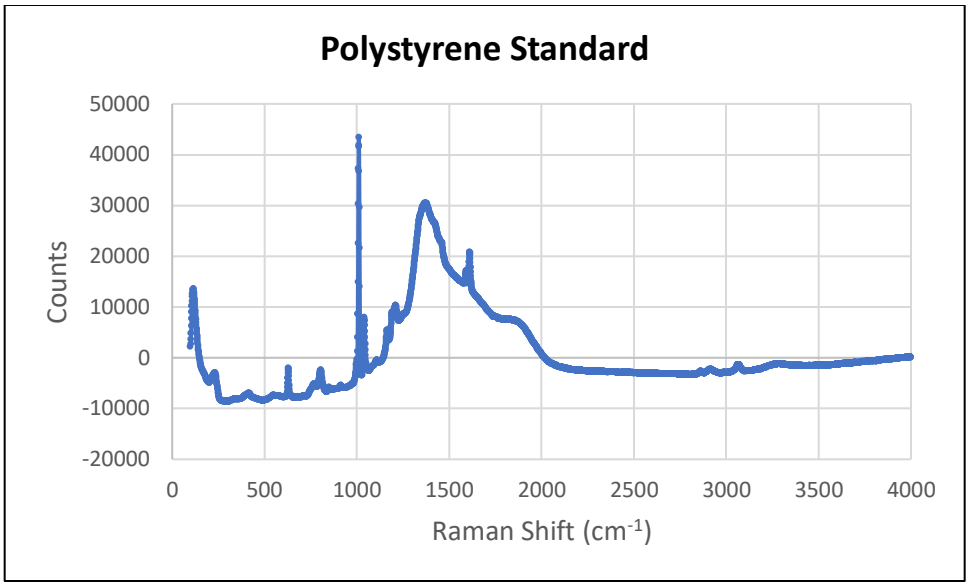

Figure B30. Shows the Raman spectra obtained from a Polystyrene microparticle (Sigma Aldrich).

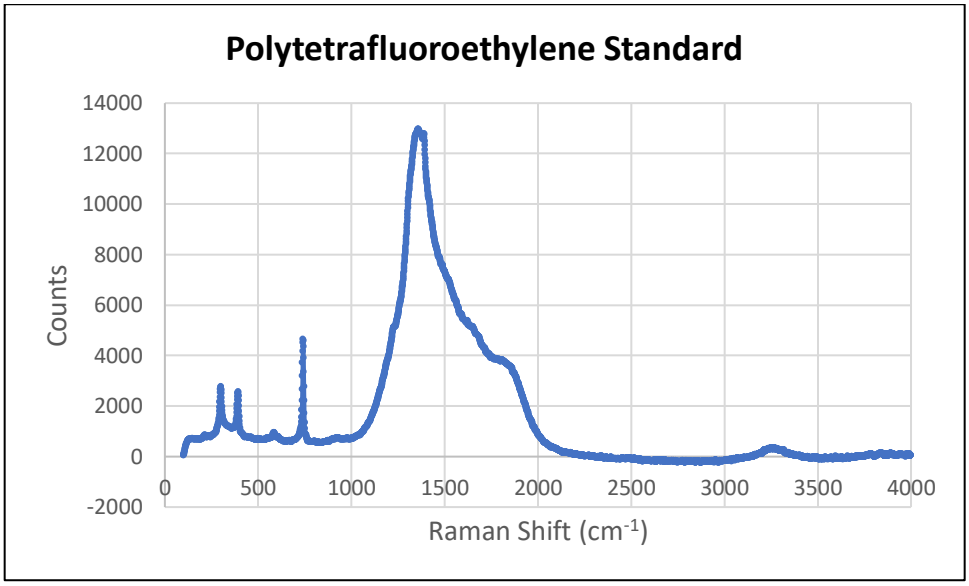

Figure B31. Shows the Raman spectra obtained from a 1/8-inch diameter Polytetrafluoroethylene bead (U.S. Plastics).

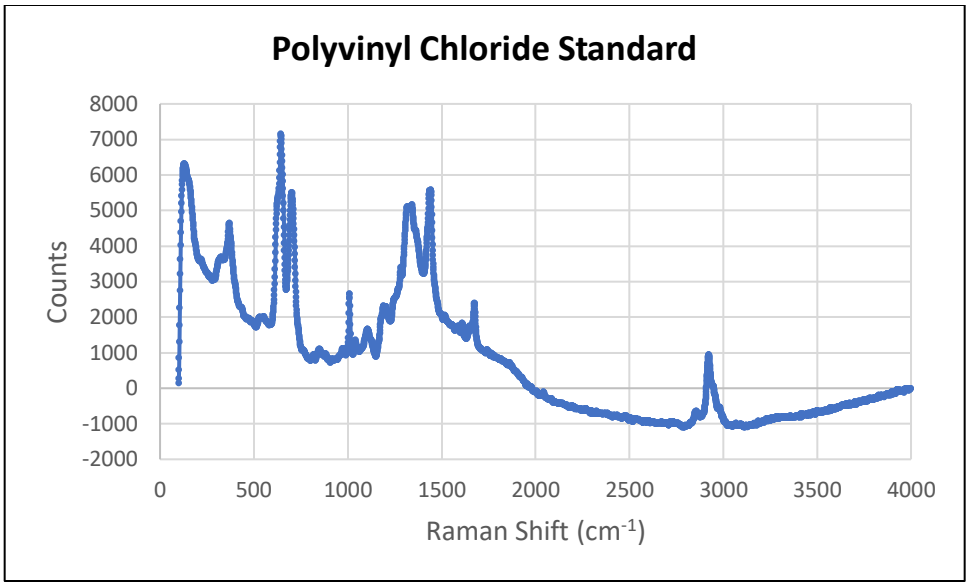

Figure B32. Shows the Raman spectra obtained from a 1.5-inch diameter section cut from the same clear PVC tubing used to construct to SMIUs.

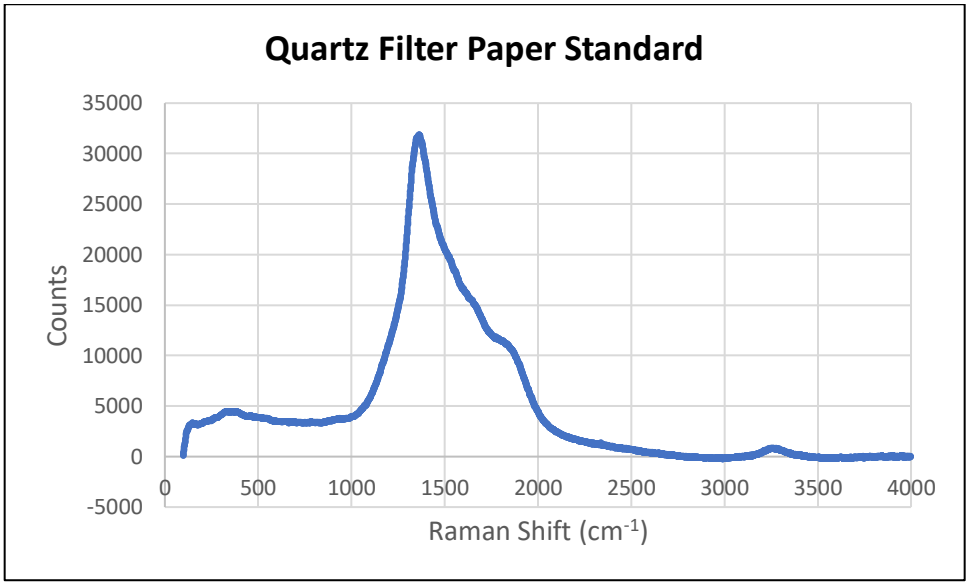

Figure B33. Shows the Raman spectra obtained from a quartz filter used to vacuum filter samples (Whatman).

APPENDIX C. MACROS

This appendix shows the macros used within ImageJ to automatically count microplastic fibers (MPFs). The utilized ImageJ MPF macro was adapted from a study conducted by Cho et al. (2011) where this macro was used to count asbestos fibers. A similar macro, known as the ImageJ MPP macro, was adapted from the ImageJ MPF macro to count microplastic particles (MPPs).

ImageJ MPF Macro

```
run("Invert");
run("Subtract Background...", "rolling=50 light");
run("8-bit");
run("Auto Local Threshold...", "method=Phansalkar radius=10
parameter_1=0 parameter_2=0 white");
setOption("BlackBackground", false);
run("Dilate");
run("Analyze Particles...", "size=50-5000 circularity=0.00-0.33 display
clear summarize add");
```

Figure C1. Shows the ImageJ MPF macro.

ImageJ MPP Macro

```
run("8-bit");
run("Auto Threshold...", "method=MaxEntropy white");
run("Analyze Particles...", "  circularity=0.00-0.28 display clear summarize
add");
```

Figure C2. Shows the ImageJ MPP macro.

APPENDIX D. FIELD AND LABORATORY EQUIPMENT

This appendix shows the devices used to collect and process samples. The construction of the sediment microplastic isolation unit (SMIU) was done in-house (Figure D1). The 2-liter horizontal water sampler is shown in the closed position with the attached rope and traveling weight (Figure D2).

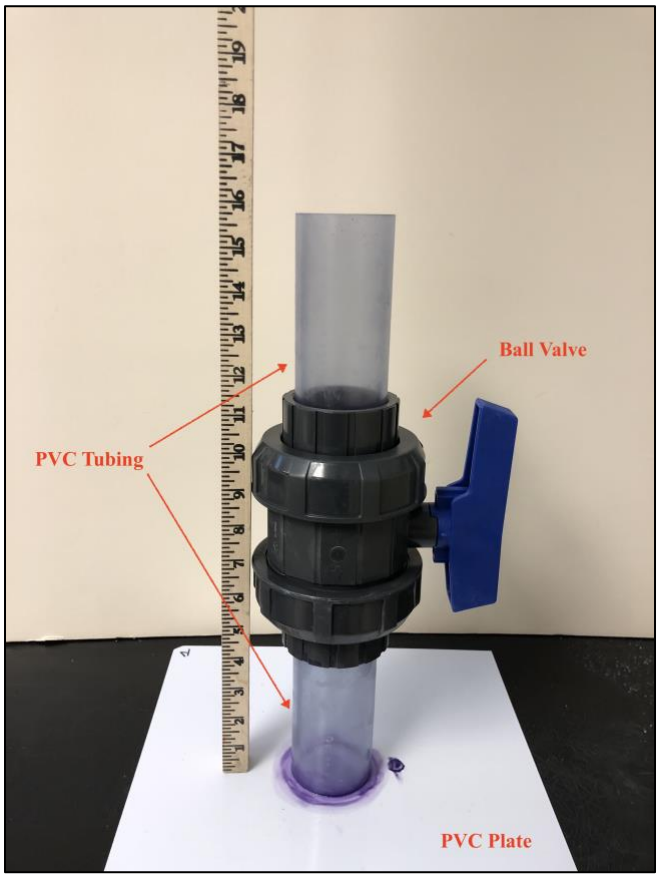

Figure D1. Shows a profile of the sediment microplastic isolation unit (SMIU) used to facilitate density separation. A measuring stick, showing units of inches, is incorporated into the figure for reference.

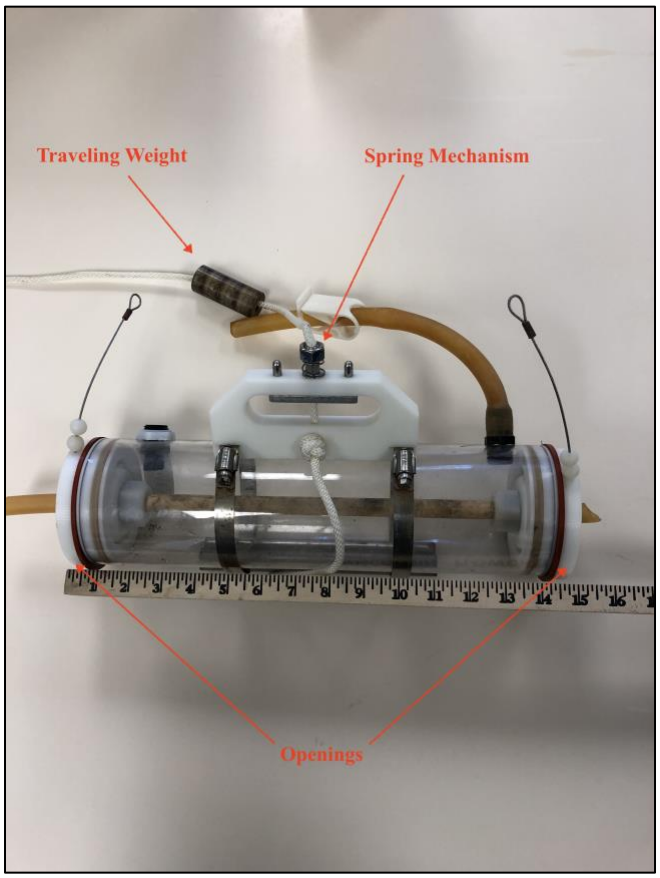

Figure D2. Shows the 2-liter horizontal water sampler (in the closed position) used to collect grab samples from the bottommost portion of combined sewer overflow outfalls. A measuring stick, showing units of inches, is incorporated into the figure for reference.

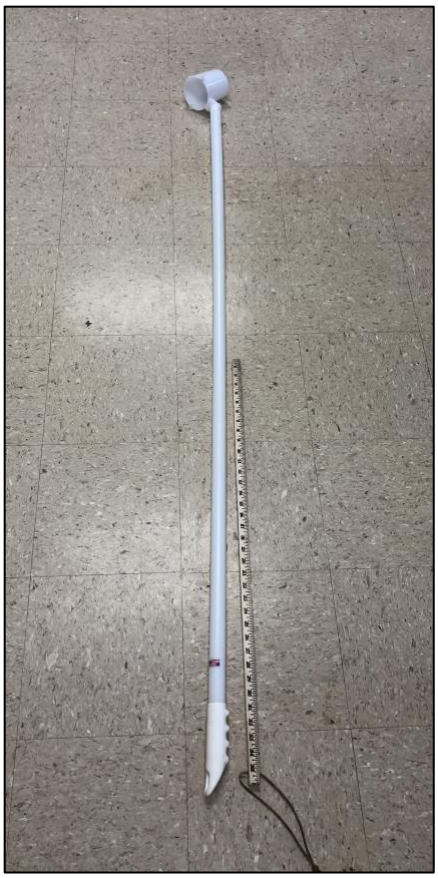

Figure D3. Shows the long-arm sample dipper used to collect grab samples from the surface of combined sewer overflow outfalls. A 36-inch measuring stick is incorporated into the picture for reference.